

THE GROWTH OF BAINITE

- By

Gilbert R. Speich

BS, Illinois Institute of Technology

1950

MS, University of Wisconsin

1951

Submitted in Partial Fulfillment of the

Requirements for the Degree of

DOCTOR OF SCIENCE

at the

Massachusetts Institute of Technology

1958

**Signature of Author
Department of Metallurgy
May 19, 1958**

**Signature of Professor
in Charge of Research**

**Signature of Chairman
Department Committee
on Graduate Research**

Morris Cohen

John J. Watson

ABSTRACT

THE GROWTH OF BAINITE

Gilbert R. Speich

Submitted to the Department of Metallurgy on May 19, 1958, in Partial
Fulfillment of the Requirements for the Degree of Doctor of Science

The influence of time, temperature, and composition on the growth rates of bainite has been studied in a series of high-purity iron-carbon alloys and in a iron-carbon-chromium and iron-carbon-nickel alloy both of the same carbon content. A special hot-stage designed for rapid quenching was used in this work. It has been established that the plates grow in length at a rate independent of time but dependent on temperature. The temperature dependence of the growth rate for the length of the plate can be expressed by the equation:

$$\dot{l} = B \exp (-Q_l/RT)$$

where Q_l has a value between 14000 - 18000 cal/mol. At lower temperatures, where the plates are lens shaped, two characteristic growth rates are present, one for the length and one for the width of the plate. The growth rates are markedly decreased by increasing the carbon content or by adding chromium or nickel at a constant carbon level.

The experimental data is compared with the Krisement-Wever and Fisher growth models. The predictions of the Krisement-Wever theory are not confirmed. The calculated growth rates from the Fisher growth model agree with the observed growth rates in the width direction of the bainite plates. A modified Fisher growth model is proposed to explain the surface upheavals accompanying the formation of bainite.

The bainitic structures formed in these high-purity alloys have been studied by electron microscopy and electron diffraction. The electron microscope work indicates that there is no carbide precipitation within the austenite and that at all times the carbide phase is surrounded by a ferrite sheath. The electron diffraction work indicates the possibility of the formation of ϵ -carbide in bainitic structures formed at low temperatures.

Thesis Supervisor: Morris Cohen
Professor of Physical Metallurgy

TABLE OF CONTENTS

<u>Chapter Number</u>		<u>Page Number</u>
	List of Figures	
	List of Tables	
	Acknowledgments	
1	Introduction	1
2	Previous Work	2
	2.1 Definition of Bainitic Structures	2
	2.2 Carbide Distribution	4
	2.3 Nature of the Carbide Phase	7
	2.4 Distribution of Carbon and Alloying Elements	8
	2.4.1 Carbon Content of the Austenite	8
	2.4.2 Carbon Content of the Ferrite	13
	2.4.3 Distribution of Alloying Elements ..	15
	2.5 Crystallographic Relationships	15
	2.6 Other Characteristics	17
	2.7 Theories	22
	2.7.1 Davenport and Bain (1930)	22
	2.7.2 Zener (1946)	22
	2.7.3 Hultgren	24
	2.7.4 Fisher (1949)	25

<u>Chapter Number</u>		<u>Page Number</u>
	2.7.5 Ko and Cottrell (1952)	30
	2.7.6 Krisement and Wever (1955)	31
	2.8 Summary	36
3	Experimental Procedure	39
	3.1 Alloys	39
	3.2 Hot Stage Design	40
	3.2.1 General Description	40
	3.2.2 Heating Unit, Shutter, and Sample Design	46
	3.2.3 Vacuum System	51
	3.2.4 Quenching Procedure	51
	3.2.5 Optical System	53
	3.2.6 Typical Run	57
	3.3 Length Measurements	60
	3.4 Light Microscopy	60
	3.5 Electron Microscopy	60
	3.6 Electron Diffraction	61
4	Experimental Results	62
	4.1 Growth Rates	62
	4.1.1 Measurements of Growth Rate	62
	4.1.2 Scatter in Growth Rates	65

<u>Chapter Number</u>		<u>Page Number</u>
	4.1.3 Activation Energies for Growth	75
	4.1.4 Effect of Composition on Growth Rate	75
	4.1.5 Width Measurements	83
	4.1.6 Hot-Stage Lengths Compared to Metal- lographic Lengths	84
	4.2 M_s Measurements	88
	4.3 Light Metallography	92
	4.3.1 Chemically Etched Structures	92
	4.3.2 Thermally Etched Structures	98
	4.3.3 Effect of the Free Surface	100
	4.4 Electron Metallography	100
	4.5 Electron Diffraction	102
5	Discussion of Results	108
	5.1 Volume Growth Rates	108
	5.2 Comparison of Experimental Data with the Krisement -Wever Theory	110
	5.3 Comparison of Experimental Data with the Fisher Growth Model	113
	5.4 Modified Fisher Model	129
	5.5 Electron Diffraction and Electron Microscopy	132
	5.6 Summary	135

<u>Chapter Number</u>		<u>Page Number</u>
6	Conclusions	137
7	Suggestions for Future Work	139
	Bibliography	140
	Biographical Sketch	146

LIST OF TABLES

<u>Table Number</u>		<u>Page Number</u>
I	Alloy Compositions	39
II	Values of Q_f and B	81
III	Alloy M_s Temperatures	88
IV	Electron Diffraction Results	106
V	Activation Energy for Carbon Diffusion in Austenite	111
VI	Overall Activation Energies for Bainite	112
VII	Overall Activation Energies	112
VIII	Intercarbide Spacing	121
IX	Calculation of $C_{\alpha\gamma}$	122
X	Values of $C_{\alpha c}$ and $C_{\alpha\gamma}$	124
XI	Calculated Values of σ^2	125
XII	Values of $\frac{dx}{dt}$	127

LIST OF FIGURES

<u>Figure Number</u>		<u>Page Number</u>
1	Lattice parameter of austenite in kx versus time of holding in hours in the bainite range	11
2	Lattice parameter of retained austenite and the amount of retained austenite as a function of tempera- ture for a 0.25 - 0.35 percent carbon, Cr-Mn-Si structural steel. after Pevzner et al	12
3	Lattice parameter of retained austenite versus the amount of bainite formed, after Pevzner, for a 0.25 - 0.35 percent carbon, Cr-Mn-Si structural steel	12
4	Composition of the carbide phase for different annealing temperatures for a 0.5 percent carbon, 4.97 percent nickel steel. from Hultgren	16
5	Habit Planes of Bainite	18
6	Temperature dependence of total dilatometric expansion (amount of bainite formed) in a series of 3% chromium steels of different carbon contents. from Lyman and Troiano	20
7	Effect of stress on isothermal transformation of austenite in a 1085 steel at 535° F (279° C). from Bhattacharyya and Kehl	20

<u>Figure Number</u>		<u>Page Number</u>
8	Effect of partial reaction at 938° F (501° C) on progress of transformation at 800° F (426° C) in a 4340 steel. from Hehemann and Troiano	21
9	Equilibrium relations in iron-carbon system. from Zener	23
10	The T_o ($\Delta F = 0$), B_s and M_s temperatures versus carbon content for 3 percent chromium steels. from Fisher	26
11	Quasi-Equilibrium Diagram of the Bainite Reaction. from Krisement and Wever	32
12	Side view of stage	42
13	Front view of stage	43
14	Supporting ring and sample support tube, heating unit, inner radiation shield, and outer radiation shield,...	45
15	Cover plate, O-rings, quartz window, shutter support, and iron foil shutter	47
16	Specimen design	48
17	Hot-stage sample with its two retaining rings	49
18	Hot-stage with heating unit, sample, radiation shields, and thermocouple in place.....	50
19	Completely assembled hot-stage	52

<u>Figure Number</u>		<u>Page Number</u>
20	Arrangement of hot-stage equipment	54
21	Reflecting objective	55
22	Optical system	56
23	Power-temperature-pressure relationships.....	59
24	1.12% C, 5.28% Ni Alloy; 30 min. 1060° C/1180 min. 196° C	63
25	1.12% C, 5.28% Ni Alloy; 30 min. 1060° C/1567 min. 196° C	63
26	1.12% C, 5.28% Ni Alloy; 30 min. 1060° C/1947 min. 196° C	64
27	1.12% C, 5.28% Ni Alloy; 30 min. 1060° C/2210 min. 196° C	64
28	Plate length versus time for a 1.16% C, iron-carbon alloy	66
29	Growth rates for a 0.96% C, iron-carbon alloy	67
30	Growth rates for a 1.16% C, iron-carbon alloy	68
31	Growth rates for a 1.43% C, iron-carbon alloy	69
32	Growth rates for a 1.14% C, 2.71% Cr, iron-carbon- chromium alloy	70
33	Growth rates for a 1.12% C, 5.28% Ni, iron-carbon- nickel alloy	71

<u>Figure Number</u>		<u>Page Number</u>
34	Bainite plate in space	73
35	Variation of \dot{l}/\dot{R} with l and S	74
36	Average growth rates for a 0.96% C, iron-carbon alloy	76
37	Average growth rates for a 1.16% C, iron-carbon alloy	77
38	Average growth rates of a 1.43% C, iron-carbon alloy	78
39	Average growth rates for a 1.14% C, 2.71% Cr, iron-carbon-chromium alloy	79
40	Average growth rates for 1.12% C, 5.28% Ni, iron-carbon-nickel alloys	80
41	The effect of carbon on bainitic growth rates in high-purity iron-carbon alloys	82
42	Length-width ratios of bainitic areas	85
43	1.14% C, 2.71% Cr Alloy; 30 min. 1060° C/180 min. 260° C.....	86
44	1.14% C, 2.71% Cr Alloy; 30 min. 1060° C/180 min. 260° C.....	86
45	Comparison of hot-stage and etched lengths.....	87
46	1.14% C, 2.71% Cr alloy; 30 min. 1060° C/91° C (above M_s)	89

<u>Figure Number</u>		<u>Page Number</u>
47	1.14% C, 2.71% Cr Alloy; 30 min. 1060° C/83° C (below M_s)	89
48	1.14% C, 2.71% Cr alloy 30 min. 1060° C/74° C (below M_s)	90
49	M_s temperatures for iron-carbon alloys	91
50	1.43% C iron-carbon alloy; 30 min. 1060° C/366 min. 181° C	94
51	1.43% C iron-carbon alloy; 30 min. 1060° C/43 min. 238° C	94
52	1.43% C iron-carbon alloy; 30 min. 1060° C/366 min. 181° C	95
53	1.14% C, 2.71% Cr alloy; 30 min. 1060° C/652 min. 215.7° C	96
54	1.14% C, 2.71% Cr alloy; 30 min. 1060° C/180 min. 263° C	96
55	1.14% C, 2.71% Cr alloy; 30 min. 1060° C/43 min. 307° C	97
56	1.14% C, 2.71% Cr alloy; 30 min. 1060° C/38 min. 328° C	97
57	0.96% C iron-carbon alloy; 30 min. 1060° C/40 min. 237° C	99
58	0.96% C iron-carbon alloy; 30 min. 1060° C/40 min. 237° C	99

<u>Figure Number</u>		<u>Page Number</u>
59	1.16% C iron-carbon alloy; 30 min. 1060° C/23 min. 253° C	101
60	1.16% C iron-carbon alloy. 30 min. 1060° C/34 min. 30 sec. 270° C	103
61	1.43% C iron-carbon alloy. 30 min. 1060° C/366 min. 181° C	103
62	1.43% C iron-carbon alloy 30 min. 1060° C/43 min. 237.7° C	103
63	1.14% C, 2.71% Cr alloy; 30 min. 1060° C/3017 min. 180° C	104
64	1.14% C, 2.71% Cr alloy; 30 min. 1060° C/180 min. 263° C	104
65	1.14% C, 2.71% Cr alloy; 30 min. 1060° C/38 min. 328° C	104
66	Growth Model for Bainite	115
67	Schematic Growth Process for Bainite	118
68	Schematic Picture of Carbide Distribution in Upper and Lower Bainite	120
69	Variation of σ^2 with Temperature	126
70	Height of the Surface Upheavals Versus Transformation Temperature after Tsuya ⁽²⁰⁾ .	133

<u>Figure Number</u>		<u>Page Number</u>
71	(a) Length of relief markings versus time for a 0.76% C Ni-Cr-Mo die steel from Tsuya ⁽¹⁹⁾	134
	(b) Log growth rate versus $\frac{1}{T}$ plot for growth rates given in Figure 71(a) after Tsuya ⁽¹⁹⁾	134

ACKNOWLEDGMENTS

The author would like to express his appreciation to Professor Morris Cohen for his invaluable advice and guidance during the course of this work. He would also like to thank Dr. S. V. Radcliffe for his encouragement and advice on experimental problems, Professor Nicholas J. Grant for the loan of the reflecting objective used in this work, and the Union Carbide Corporation for the Fellowship Grant which made this work possible.

1. INTRODUCTION

The subject of bainite has been studied extensively by a large number of investigators since its discovery in 1930 by Davenport and Bain⁽¹⁾. It has been established that bainite has characteristics intermediate between those of martensite and pearlite. For instance, bainite exhibits both stabilization, surface relief, and in some composition ranges, the amount of bainite formed is a function of the temperature; in these aspects, bainite resembles martensite. On the other hand, bainite forms as a ferrite-carbide aggregate and exhibits slow growth; in these aspects, it resembles pearlite. It is this intermediate nature of bainite which makes it such an interesting and rewarding subject for study.

In 1952, Ko and Cottrell⁽²⁾ showed that the formation of bainite is accompanied by surface upheavals. By observing these surface relief effects with a hot-stage microscope, it is possible to measure the growth rates of individual bainite plates. The present work was undertaken to study systematically by such a technique the effects of time, temperature, and composition on the growth rate of bainite. The nature and distribution of the carbide particles were also studied using electron diffraction and electron microscopy. It was felt that with this information, one might better understand the factors controlling the growth of bainite and thus be able to set up a reasonable growth model for the transformation.

2. PREVIOUS WORK

No attempt has been made here to make an exhaustive review of the literature on bainite, since a number of literature reviews are available (3, 4, 5). Only the more recent results which seem important to an understanding of the reaction mechanism(s) are discussed in detail.

2.1 Definition of Bainitic Structures

Many investigators have studied the metallographic features of the structures formed in steels in the temperature range intermediate between that of pearlite formation and martensite formation. The variety of structures that form in this temperature range can usually be separated into three main groups:

(1) Lower bainite is the product formed at temperatures near M_s and has a dark-etching acicular appearance much like that of tempered martensite. In general, the nucleation of lower bainite does not occur preferentially at the grain boundaries.

(2) Upper bainite occurs at higher temperatures in the bainite range and shows several metallographic variants; the classical upper bainite structure is a feathery ferrite-carbide aggregate which nucleates at the grain boundaries and grows into the center of the grains.

(3) Pro-bainitic ferrite is an essentially carbide-free, acicular ferrite that forms in low-carbon steels at higher temperatures in the bainite range. It is also called acicular ferrite and the α -constituent. Maltgren⁽⁶⁾ prefers not to call this bainite, since he reserves this

term for a ferrite-carbide aggregate. However, since it forms in the bainite temperature range, it is listed here as one possible group of bainitic structures.

More recently, Habraken⁽⁵⁾ has made an exhaustive review of bainitic structures formed in a number of different steels, both upon isothermal and aisoothermal treatment. He prefers to separate the bainitic structures into two groups: (1) acicular structures, and (2) granular structures. The acicular structures are further subdivided into three types: (1) acicular ferrite, (2) upper bainite, and (3) lower bainite. These structures are the same ones discussed previously and are the most commonly observed. They occur in many types of steels and are most easily obtained by isothermal transformation.

The granular structures of Habraken appear in the upper zones of the bainite transformation and particularly in steels where the pearlite and bainite reactions are clearly separated. They are most clearly seen when the sample is air cooled. The structure consists of plates of ferrite containing nodules of enriched, retained austenite. In some cases, the nodules of enriched austenite may decompose into an agglomeration of ferrite plus carbide. These enriched nodules of austenite arise from the carbon heterogeneity of the parent austenite. This structure is the same as the para-ferrite or pre-bainitic ferrite

of Hultgren⁽⁸⁾ according to Habraken, although this would seem questionable. Hultgren's definition of pro-bainitic ferrite does not include the case of nodules of retained austenite occurring within the ferrite.

It must be strongly emphasized that these classifications are based mainly on differences in metallographic appearance. The divisions between the different structures are not sharp and the basic differences in the reaction mechanisms, if any, are not yet clearly understood.

2.2 Carbide Distribution

Since the carbides in bainitic structures are not resolvable by light metallography, only the overall shapes of the bainitic regions can be revealed by this technique. With the introduction of the electron microscope as a research tool, considerable advances were made in understanding the nature of the carbide distribution^(5, 9, 10, 11, 12).

On the basis of their study of plain-carbon eutectoid steel, the ASTM Subcommittee XI on Electron Microstructure of Steel^(9, 10) has concluded:

"The transition from lower to upper bainite is characterized by two distinct changes in the microstructure. First, the size, shape and orientation of the carbide particles change from extremely small platelets arranged in a parallel array at an angle of approximately 55° with respect to the axis of the bainite needles, to larger carbide particles

and stringers arranged more nearly parallel, lengthwise. Second, the needles of ferrite which account for the marked acicular nature of lower bainite disappear. In their place appear small irregularly-spaced areas in which the carbide particles and stringers are arranged in parallel fashion, with their length in the direction of the longer dimension of the area."

Modin and Modin⁽¹²⁾ have also recently completed an electron microscope study of the pearlite and bainite structures formed in a plain-carbon eutectoid steel. Their results are similar to those of the ASTM Committee XI, however, they also studied the shape of extracted carbides. They state that the carbide particles formed at 400° C have a two-dimensional set of branches; the growth in the third dimension is limited since the carbide forms in the austenite between the growing ferrite plates.

Whether or not the carbide phase precipitates within the ferrite, within the austenite, or both, still seems to be a point of dispute. Habraken⁽⁵⁾ assumes that at low-temperatures carbide precipitation occurs within the ferrite; however, at higher temperatures carbide precipitation can and does occur within the austenite.

Hultgren⁽⁸⁾ assumes that carbide precipitation occurs during the growth of the bainite unit to full size; the carbide nuclei probably form at the austenite/ferrite interface as it migrates, but whether or not

nucleation occurs within the ferrite or austenite remains an open question.

Recent work by Kaufman, Pound, and Aaranson⁽¹¹⁾ indicates that carbide precipitation occurs both within the ferrite and austenite. Modin and Modin⁽¹²⁾ assume that above 350° C carbide precipitation occurs within the austenite; they state that the fineness of the carbide distribution below 350° C makes it difficult to determine the site of carbide precipitation.

Krisement and Wever⁽¹⁰⁾ assume that carbide precipitation occurs within the austenite in high-carbon steels. In fact, the rate of nucleation of carbide in the austenite, according to their theory, is the rate controlling process in the formation of bainite in high-carbon steels.

It is rather unfortunate that this question of the sites for carbide nucleation is not completely settled, since it is fundamental to any theory of the formation of bainite. The main difficulty is that one can only examine the end-product of the bainite reaction by electron microscopy, and one must extrapolate backwards to obtain information on the site of carbide nucleation. This has probably led to the wide diversity of opinions. Since most of the published electron micrographs of bainitic structures^(9, 10, 12) indicate that the carbide particles are surrounded by a ferrite sheath, regardless of temperature of formation, the most reasonable assumption to make is that

carbon removal from the austenite is occurring by carbon diffusion through the ferrite to carbide particles precipitating within the ferrite. However, it is also possible to argue that the formation of bainitic ferrite occurs in a martensitic fashion. In this case, carbide precipitation in the austenite would be followed by a very rapid formation of ferrite engulfing the carbide particles. Thus it would not be possible to see carbides precipitated in the austenite without the accompanying ferrite. The end product of both these models is the same - carbide particles surrounded by a ferrite sheath.

2.3 Nature of the Carbide Phase

Several investigators^(14, 15, 23) have shown the existence of cementite by x-ray diffraction in steels transformed into bainite at temperatures above 400° C. No x-ray diffraction work seems to have been done at lower temperatures probably because of the difficulty encountered with particle-size broadening. The formation of alloy carbides does not seem to occur in bainitic structures due to the low transformation temperatures where the diffusion of alloying elements is severely restricted^(15, 23). At higher temperatures in the pearlite range, the formation of alloy carbides can occur^(14, 15).

The problem of particle-size broadening can be improved by using electron diffraction, since the wavelengths of the electrons normally used is only about 0.05 Å. Austin and Schwartz⁽¹⁶⁾ have used electron diffraction techniques to study the structure of the carbide phase formed

in bainite in a eutectoid plain carbon steel. At 750° F (399° C) cementite was the only carbide phase present, but at 550° F (288° C) and 500° F (260° C) there is evidence for the formation of both cementite and ϵ -carbide. The ϵ -carbide lines agree with those reported by Jack⁽⁴⁰⁾ for the tempering of martensite at 120° C.

2.4 Distribution of Carbon and Alloying Elements

2.4.1 Carbon Content of the Austenite

There has been considerable controversy as to whether or not the carbon content of the austenite is raised during partial transformation into bainite. Klier and Lyman⁽¹⁵⁾ report the retention of austenite and the splitting of the (110) line of the martensite formed on quenching after partial transformation into bainite at 500° C in a 0.38 percent carbon, 2.98 percent chromium steel. The c/a ratio of 1.020 obtained for martensite indicates a carbon content of the austenite of 0.5 to 0.6 percent carbon. The above authors conclude that both the retention of austenite and the splitting of the martensite line indicate carbon enrichment of the austenite. Lyman and Troiano⁽¹⁴⁾, however, found little or no carbon enrichment of austenite in hyper-eutectoid steels and claim that the retention of austenite in the low-carbon steel of Klier and Lyman was due to stabilization.

Hohemann and Troiano⁽⁴⁾ claim that the carbon enrichment in hypo-eutectoid steels is extremely localized around the bainite plate, and that in either hypoeutectoid or hypereutectoid steels large regions of non-

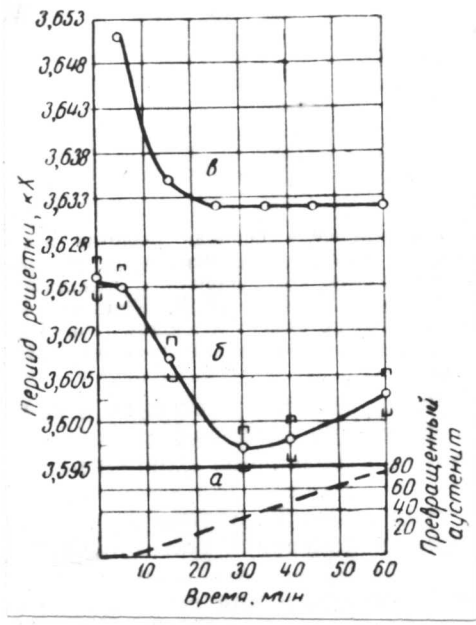
enriched austenite exist after the end of the bainite transformation. Thus carbon enrichment of the austenite cannot be offered as a reason for the self-stopping nature of the reaction, according to Hehemann and Treiano.

Considerable work has been done recently in Russia by Estin and his co-workers on this problem^(38, 39). These investigators have determined the lattice parameter of the austenite as a function of time and temperature of holding in the bainite range. The carbon content of the austenite could be determined from the value of the lattice parameter. Their results on a number of widely different steels, of both high and low carbon content, indicate that the problem is quite complex as both carbon enrichment, carbon depletion, or no change in the carbon content of the austenite can occur depending on the composition of the steel. For instance, in the case of a 1.44 percent carbon, 3.45 percent chromium steel a decrease in lattice spacing of the austenite (decrease in carbon content) was found on holding at 400° C and 300° C (see Figure 1a); for a 0.98 percent carbon, 3.15 percent chromium steel no change in the lattice spacing of the austenite was found on holding at 250 - 350° C; and for a 0.54 percent carbon, 3.54 percent chromium steel an increase in lattice spacing (increase in carbon content) of the austenite was found on holding at 350° C. In general, steels of low carbon content (0.3 - 0.6 percent carbon) showed carbon enrichment of the austenite (see Figure 1b), steels of medium

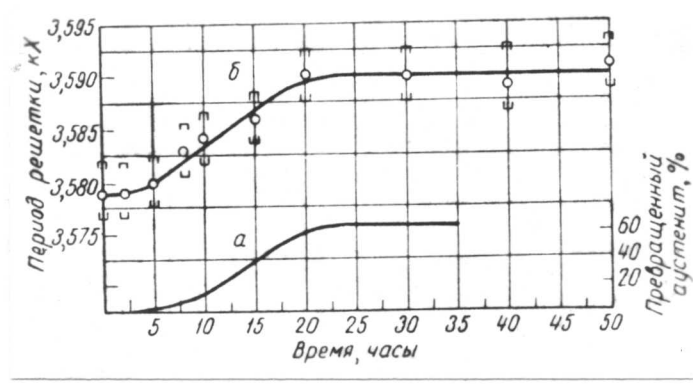
carbon content (0.7 - 1.0 percent carbon) showed no change in carbon content and steels of high carbon content (above 1 percent carbon) showed carbon depletion of the austenite. This seemed to be true regardless of alloy additions except for the case of silicon. Steels containing silicon, even of high carbon content, invariably showed carbon enrichment of the austenite. The degree of enrichment or depletion always increased with increasing temperature of transformation and was roughly proportional to the percent of bainite formed. These results explain the discrepancies between the results of Lyman and Troiano and Klier and Lyman.

The work of Pevzner et al⁽²¹⁾, also in Russia, have shown that carbon enrichment of the austenite occurs in a hypoeutectoid steel (0.25 - 0.35 percent carbon, Cr-Mn-Si structural steel) in agreement with the results of Satin. The technique used was the same as that of Satin. In addition, the amount of retained austenite was determined and found to first increase and then decrease with decreasing temperature of transformation. In interpreting the retained austenite results, it must be appreciated that as the temperature of transformation decreases the amount of untransformed austenite remaining at the transformation temperature also decreases. The results of Pevzner are shown in Figures 2 and 3.

It should be mentioned that the microstructures accompanying the Russian work have not been reported. Since there are possibilities for



(a) 1.44 percent carbon, 3.45 percent chromium steel, β is the lattice parameter of the austenite determined at temperature, δ is the lattice parameter of the retained austenite, and the dashed curve is the percent transformation. The transformation temperature is 400° C.



(b) 0.48 percent carbon, 4.33 percent manganese steel. δ is the lattice parameter of the retained austenite and a is the percent transformation. The transformation temperature is 275° C.

FIGURE 1. Lattice parameter of austenite in Å (left hand ordinate) versus time of holding in hours (abscissa) in the bainite range. The percent transformation is given in the right hand ordinate. Data from Kogan and Entin⁽³⁹⁾.

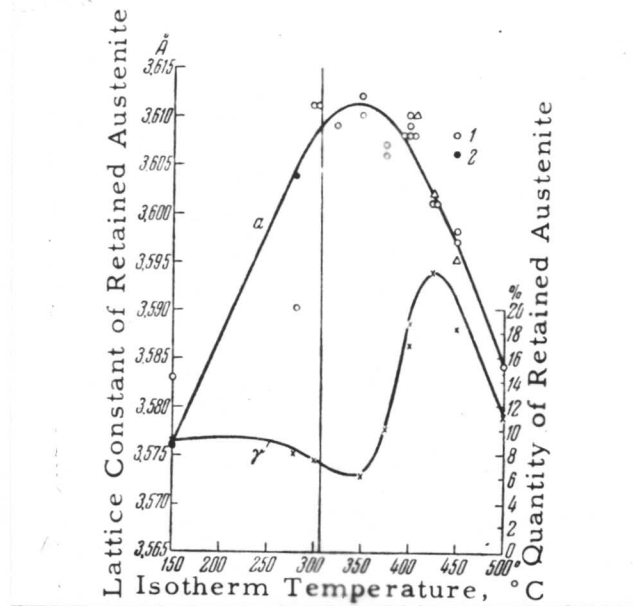


FIGURE 2. Lattice parameter of retained austenite and the amount of retained austenite as a function of temperature for a 0.25 - 0.35 percent carbon, Cr -Mn-Si structural steel, after Pevzner et al(21)
 1. Holding time 15 minutes 2. Holding time 5 hours
 Triangular points are for the back reflection method.

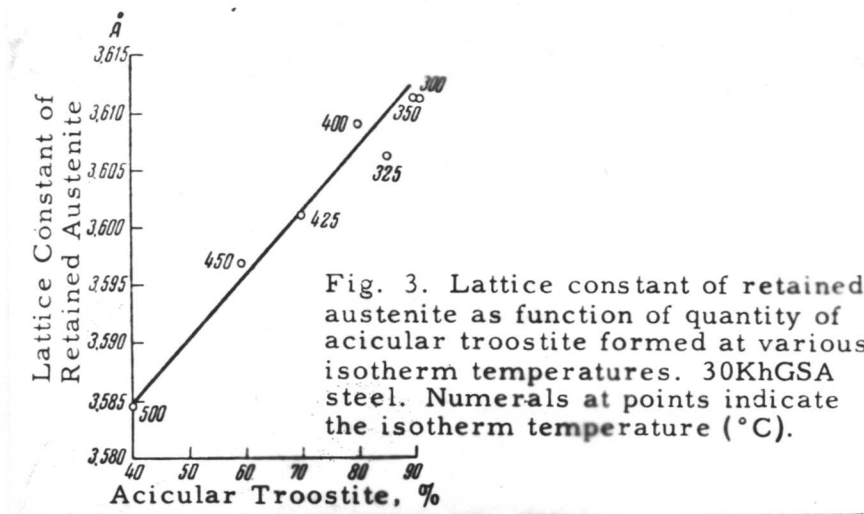


FIGURE 3. Lattice parameter of retained austenite versus the amount of bainite formed after Pevzner(21) for a 0.25 - 0.35 percent carbon, Cr-Mn-Si structural steel (30 KhGSA steel).

separate carbide and bainite reactions occurring in high-carbon steels⁽¹⁴⁾ as well as for the formation of pro-bainitic ferrite (carbide free) in low-carbon steels, it would seem important to have this information. We should know whether the carbon enrichment or depletion of the austenite is due solely to the formation of bainite or due to complicating side reactions.

2.4.2 Carbon Content of the Ferrite

In 1951, Kurdjumov and Perkas⁽⁴¹⁾ determined the c/a ratio of the ferrite in samples of a 1.0 percent carbon, 1.43 percent chromium steel and a 1.2 percent carbon, 2.0 percent molybdenum steel transformed at 250 - 300° C. The c/a ratios were determined by the method of Kurdjumov and Lyssak⁽³³⁾ using single crystals of austenite. The alloyed steels were used by Kurdjumov because he states that above 250° C, plain-carbon steels gave a c/a ratio of unity within the experimental error. The addition of chromium and molybdenum slowed down the tempering process. The results for both steels indicate a c/a ratio of 1.006 - 1.008 and thus a carbon content of 0.12 - 0.17 percent carbon. This is essentially the same value obtained for samples of martensite tempered in the same temperature range. Kurdjumov and Perkas therefore conclude that the martensite reaction must be an intermediate stage in the formation of bainite such as in the "delayed martensite" theory where the bainite

plate forms instantaneously as martensite and then tempers to a ferrite-carbide aggregate.

More recently, Werner, Averbach and Cohen⁽²²⁾ have made similar c/a ratio measurements on a 1.43 percent carbon high-purity iron-carbon alloy transformed at 210° C. Their results indicate that the c/a ratio is unity within the experimental error. However, martensite tempered at the same temperature still retained c/a ratio of 1.005. The above authors conclude that there is no tetragonal phase formed in the decomposition of austenite in the bainite range and that bainite forms from austenite as a body-centered cubic phase.

The disagreement in the results of Kurdjumov and Perkas and Werner et al cannot be explained as Kurdjumov suggests⁽⁴²⁾ by the differences in compositions. Addition of alloying elements does slow down the tempering process and allow measureable c/a ratios to be found at higher temperatures for tempered martensite structures⁽⁴¹⁾. However, even for a plain-carbon steel, a measureable c/a ratio for tempered martensite is found after tempering at 210° C as Werner reports. Since Werner finds no tetragonality in the case of the ferrite phase of bainite, it does not seem that the formation of bainite involves a tetragonal martensite as suggested by Kurdjumov. This still does not explain Kurdjumov's results and more work along this line would be welcome.

2.4.3 Distribution of Alloying Elements

Hultgren⁽⁸⁾ has made a study of the compositions of the bainitic carbides formed in a number of low/alloy steels. In general, the iron/alloy mol ratio of the carbide is the same as the iron/alloy mol ratio of the parent austenite. The resulting carbide composition is called the paracomposition. As the holding time in the bainite range is increased, the alloy content of the carbide approaches the equilibrium value. Some of the results of Hultgren are shown in Figure 4.

These results indicate that no diffusion of alloying elements occur during the formation of bainite. Similar results have been obtained by Entin⁽²³⁾ and there seems to be general agreement on this point.

2.5 Crystallographic Relationships

Greninger and Troiano⁽⁶⁾ have determined the habit planes for bainite in a 0.92 percent carbon and a 1.78 percent carbon plain-carbon steel. The habits were determined by a two-surface analysis with the austenite grain orientation being derived from the retained austenite or by a twin-band vestige method. Trace normals were also determined and were shown to pass through the poles established by the two-surface analysis.

The habit plane for the 0.92 percent carbon steel (see Figure 5a) was found to be almost octahedral at 450° C and gradually moved along a (134) great circle as the reaction temperature was lowered. The

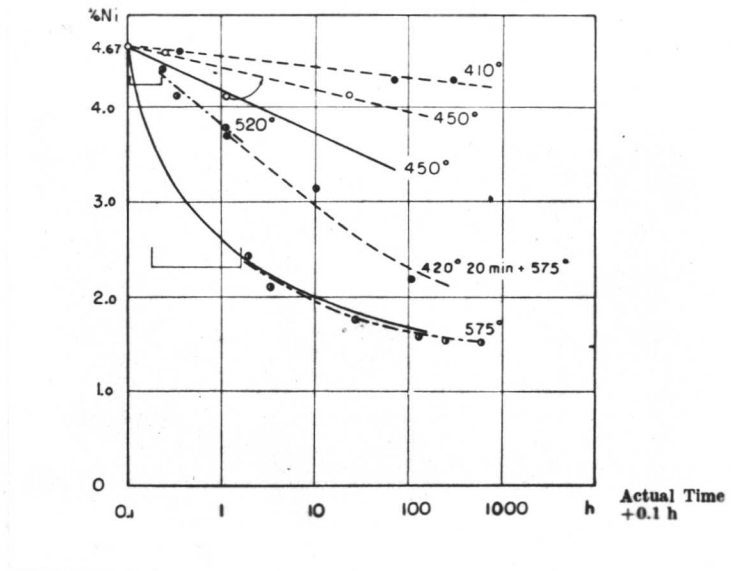


FIGURE 4. Composition of the carbide phase for different annealing temperatures for a 0.5 percent carbon, 4.97 percent nickel steel from Maltgren⁽⁸⁾. Tempering of martensite (—), annealing of bainite (-----) and pearlite (- - - -).

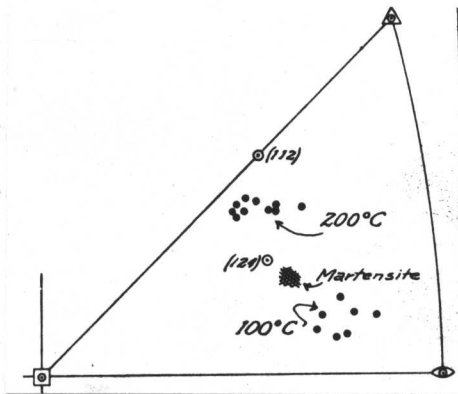
habit plane was different from that of martensite at all temperatures. The habit plane for the 1.78 percent carbon steel was also found to be different from that of martensite, and it also changed with temperature (see Figure 5b).

Smith and Mehl⁽⁷⁾ have determined the habit plane for bainite formed in a 0.78 percent carbon plain-carbon steel by using a single-surface analysis with the orientation of the original austenite being measured by the twin-band vestige method. The results, shown in Figure 5c, are similar to those found by Greninger and Troiano for the 0.96 percent plain-carbon steel.

The orientation relationships of the ferrite phase in bainite have also been determined by Smith and Mehl⁽⁷⁾ for the 0.78 percent plain-carbon steel. Using a pole-figure analysis, they found that the ferrite obeyed the Nishiyama relations, $(111)_A \parallel (110)_F$ and $\langle 211 \rangle_A \parallel \langle 011 \rangle_F$ at 450° C and 350° C, but obeyed the Kurdjumov-Sachs relationships, $(111)_A \parallel (110)_F$ and $\langle 110 \rangle_A \parallel \langle 111 \rangle_F$, at 250° C.

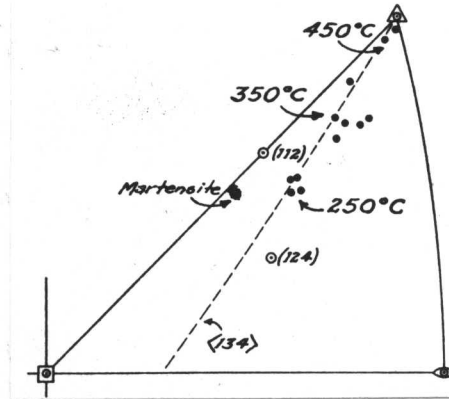
2.6 Other Characteristics

Many investigators^(14, 15, 21, 25) have found that the amount of bainite formed varies with temperature, lower temperatures favoring the formation of more bainite. The results of Lyman and Troiano⁽¹⁴⁾ for 3 percent chromium steels are shown in Figure 6. These B-T curves closely resemble martensite range curves, with more and



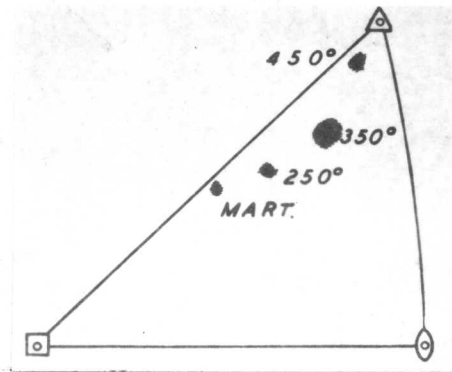
(a) 1.78% C

Greninger and Troiano⁽⁶⁾



(b) 0.92% C

Greninger and Troiano⁽⁶⁾



(c) 0.78% C

Smith and Mehl⁽⁷⁾

FIGURE 5. Habit Planes of Bainite.

more bainite being formed as the temperature is lowered. This self-stopping nature of the bainite reaction has not been adequately explained, although carbon enrichment of the austenite⁽²⁴⁾ and the exhaustion of critical size nuclei⁽²⁵⁾ have been suggested as possible causes.

It has been shown by Bhattacharyya and Kehl⁽²⁶⁾ that the bainite reaction is markedly accelerated by an applied tensile stress in 1045, 1085, and 4340 steels. It was observed that the amount of transformation increased rapidly over a certain critical stress range, which was found to agree with the yield stress range for unstable austenite. The effect of an applied tensile stress on the bainite transformation at 535° F (279° C) in 1085 steel is shown in Figure 7.

Hehemann and Troiano⁽²⁵⁾ have shown that partial transformation to bainite at one temperature increases the induction period and stabilizes part of the austenite against further transformation at some lower temperature. This is similar to the case of martensite. Some results of Hehemann and Troiano for a 4340 steel are shown in Figure 8.

Ko and Cottrell⁽²⁾ have shown that a surface upheaval accompanies the formation of bainite. This is similar to the case of martensite, except that the plates were observed to grow slowly under a hot-stage microscope.

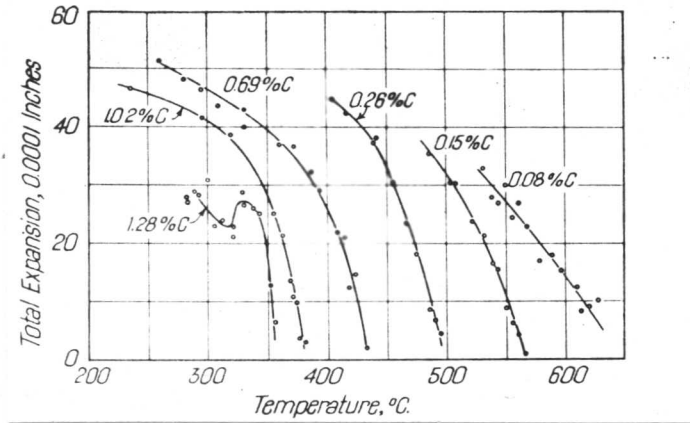


FIGURE 6. Temperature dependence of total dilatometric expansion (amount of bainite formed) in a series of 3% chromium steels of different carbon contents from Lyman and Troiano(14).

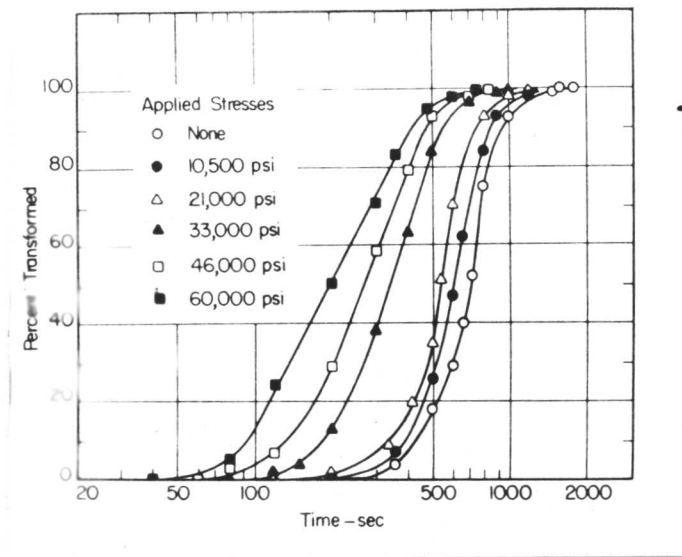


FIGURE 7. Effect of stress on isothermal transformation of austenite in a 1085 steel at 535° F (279° C) from Bhattacharyya and Kehl(26).

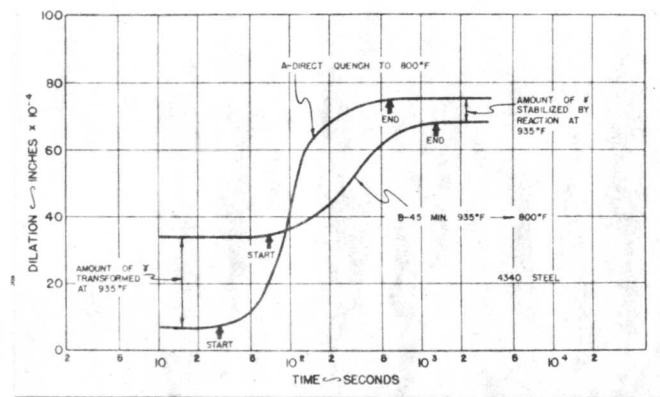


FIGURE 8. Effect of partial reaction at 938° F (501° C) on progress of transformation at 800° F (426° C) in a 4340 steel from Hehemann and Troiano(25).

2.7 Theories

A large number of theories have been presented to explain the formation of bainite. Not all the proposed theories have been reviewed here in order to treat the more important ones in some detail. The theories are reviewed in chronological order.

2.7.1 Davenport and Bain (1930)

The early theories for the formation of bainite postulated that the formation of bainite was similar to that of martensite. However, an incubation period was required before the formation of any plates and in addition the plates precipitated carbide almost immediately after their formation. The term "delayed martensite" was used to describe this growth process. This idea was formulated by Davenport and Bain⁽¹⁾ at the time of the discovery of bainite and probably arose from the similar appearance of low-temperature bainite and tempered martensite.

2.7.2 Zener (1946)

This "delayed martensite" theory was further extended by Zener⁽²⁴⁾. He suggested that the criterion for the formation of bainite should be based on thermodynamic grounds and calculated the temperatures at which the free energy of austenite and ferrite of the same composition are equal. These results are shown in Figure 9. The $\Delta F = 0$ curve seems to agree qualitatively with the upper limit for the formation of bainite. An order to differentiate between bainite and

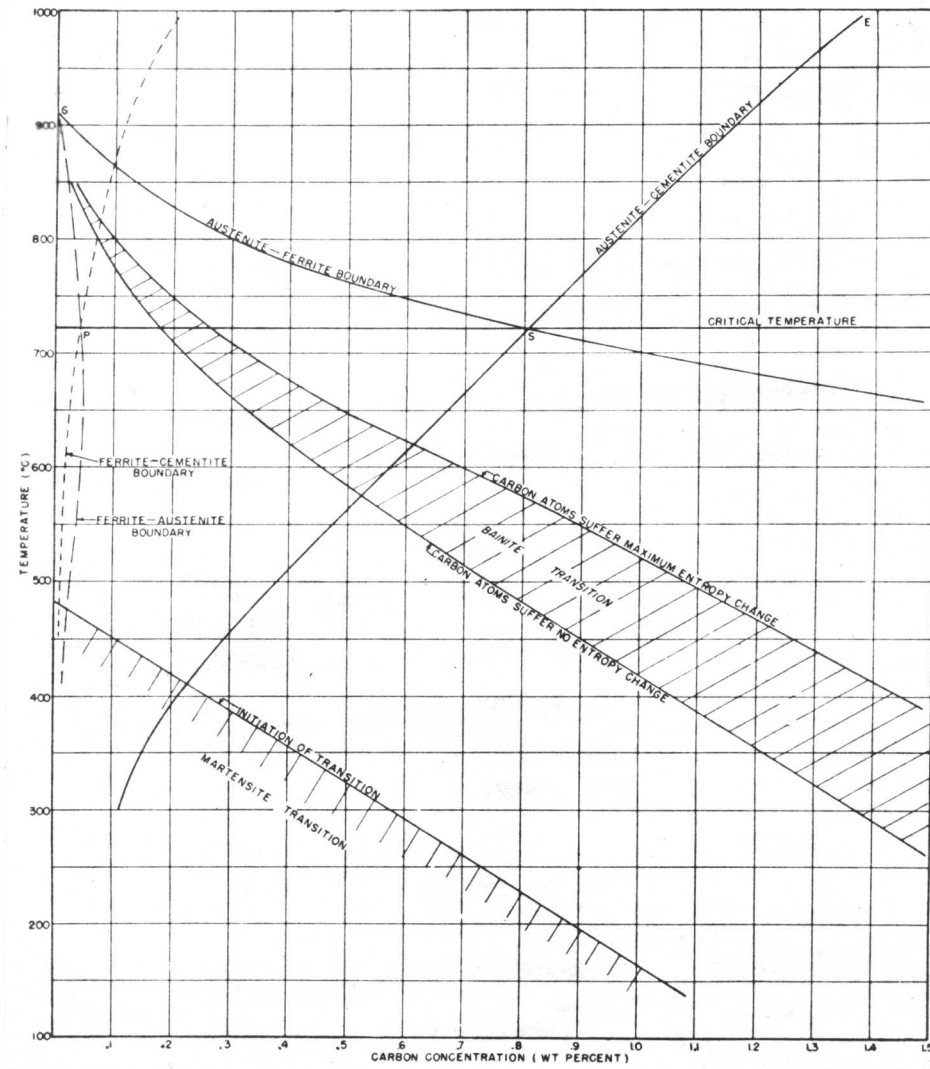


FIGURE 9. Equilibrium relations in iron-carbon system from Zener⁽²⁴⁾.

martensite, it was necessary for Zener to postulate that the formation of martensite severely strains the austenite so that additional free energy is needed to supply the strain energy. Thus, the formation of martensite must occur at lower temperatures than bainite in order to supply this additional free energy. The self-stopping nature of the bainite transformation was explained by carbon enrichment of the austenite or by carbide precipitation at the austenite/ferrite interface.

2.7.3 Hultgren (1947)

According to Hultgren⁽²⁷⁾ bainite forms directly from austenite as a ferrite-carbide aggregate. He assumes that ferrite nucleates the reaction and that ferrite grows into the austenite with carbon diffusing away into the austenite. When the austenite surrounding the ferrite plate has been sufficiently enriched in carbon, carbide precipitation occurs in the austenite.

During the bainite transformation, no diffusion of alloying elements occurs, with the exception of carbon. As a result, the carbide and ferrite phases inherit the same iron/alloy mol ratio as that of the parent austenite. Of course, diffusion of carbon occurs and the carbon content of the ferrite and carbide phases are markedly different. The ferrite and carbide phases that inherit the alloy content of the austenite are called paracarbide and para-ferrite. Those phases which have the equilibrium alloy content are called orthocarbide and orthoferrite.

Hultgren postulates that the difference between bainite and pearlite is that pearlite contains orthoferrite and orthocarbide whereas bainite contains paraferriite and paracarbide. In order to differentiate between pearlite and bainite in plain-carbon steels, Hultgren assumes that in the case of pearlite the carbide has a primary lattice relationship to the parent austenite, whereas the succeeding ferrite has a so-called secondary relation. In the case of bainite, the ferrite first formed has a primary relation to the austenite, whereas the succeeding carbide has a secondary relationship to the austenite. Thus, according to Hultgren, the formation of pearlite requires both the diffusion of carbon and alloying elements; the formation of bainite requires only the diffusion of carbon; and the formation of martensite requires neither the diffusion of carbon nor alloying elements.

2.7.4 Fisher (1949)

Fisher⁽²⁸⁾ has also presented a thermodynamic treatment of the bainite reaction. He shows that the B_s temperature for a series of chromium steels agree well with the $\Delta F = 0$ curve if the values are shifted about 0.4 percent carbon to higher carbon contents. The B_s , M_s and $\Delta F = 0$ curves are shown in Figure 10. From this observation, Fisher suggests that the local carbon concentration in the austenite surrounding the bainite plate may be 0.4 percent higher than the average carbon content of the austenite. This increase in carbon content could be associated with the dislocations spaced along the interface

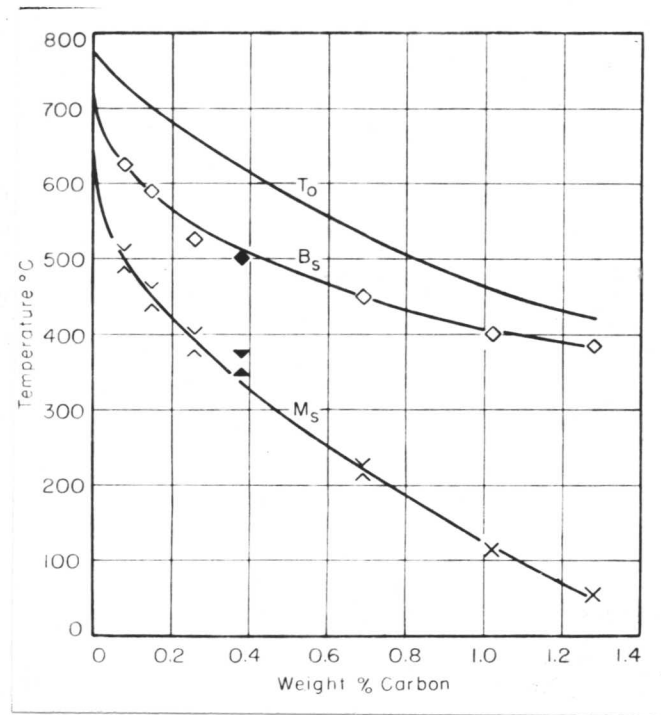


FIGURE 10. The T_0 ($\Delta F = 0$), B_s , and M_s temperatures versus carbon content for 3 percent chromium steels from Fisher⁽²⁸⁾.

or with carbon pile-up in the austenite ahead of the growing ferrite phase. Fisher then assumes that the criterion for the B_s temperature is that $\Delta F' = 0$, where $\Delta F'$ is the free energy change for the transformation of austenite to ferrite of the same composition in the region enriched in carbon. The amount of carbon adsorbed at the interface is determined from the Langmuir's adsorption equation, determining the unknown constants by use of the experimentally determined B_s values.

The nucleation sites for bainite, according to Fisher, are small regions of low-carbon content in the austenite which are retained on quenching from the austenitizing temperature. During the quench, these regions transform into ferrite. Those regions, not large enough to nucleate martensite at the transformation temperature, may grow slowly by diffusion of carbon; when they reach the critical size for coherent martensitic growth, they shear over into martensite. The dependence of the amount of bainite formed on the reaction temperature is due to the decrease in critical embryo size with temperature. The self-stopping nature of the transformation may be either due to exhaustion of available nuclei or to carbon enrichment of the austenite.

Fisher considers that the mode of growth can be either martensitic or some type of slow growth. If it grows in a martensitic fashion, it is "delayed martensite." If it grows slowly three possibilities arise:

(1) growth as supersaturated ferrite, (2) growth as pro-eutectoid ferrite, carbon diffusing away in the austenite, and (3) grow as ferrite and cementite, with carbon diffusing from austenite to cementite through the ferrite. Due to the high rate of diffusion of carbon in ferrite, the possibility of slow growth as supersaturated ferrite is discarded. If bainite grows by one of the other two mechanisms, the criterion, that the B_s is the temperature above which transformation to supersaturated ferrite becomes impossible, must be discarded since the bainite is not supersaturated with respect to carbon. Fisher suggests that a new criterion for the B_s might be that above B_s partitioning of alloying elements occur, while below it no partitioning occurs. This is identical with Hultgren's proposal.

Using a plane front model, Fisher gives the following equation for growth of bainite when controlled by carbon diffusion through the ferrite:

$$\dot{X} = \frac{D_c^f \Delta C}{C_o L} \quad (1)$$

where \dot{X} is the velocity of growth, D_c^f is the diffusion coefficient for diffusion of carbon in ferrite, ΔC is the carbon gradient in the ferrite, C_o is the original carbon content of the austenite, and L is the diffusion path distance in the ferrite.

Fisher obtains an approximate value of L from the interlamellar spacing formula of pearlite extrapolated to the bainite temperature

range. D_c^{δ} and C_o are known, and ΔC is equated to C_o^* , the carbon content of the ferrite at the austenite/ferrite interface. This is derived from the extrapolated austenite/ferrite boundary of Zener⁽³²⁾. The thickness of a bainite plate is then given by:

$$\delta = \frac{2D_c^{\delta} \Delta C t}{C_o L} \quad (2)$$

where δ is the thickness of the plate and t is the time. Using the beginning times of transformation for a series of chromium steels, Fisher shows that the calculated sizes of bainite plates from equation (2) are much larger than the limiting size of visibility.

If bainite grows as proeutectoid ferrite with carbon diffusing away into the austenite, Fisher offers the following equation:

$$\delta = 2 \left(\frac{C^*}{C_o} \right)^{1/2} (D_c^{\gamma} t)^{1/2} \quad (3)$$

where C^* is the carbon concentration of austenite adjacent to the ferrite, and D_c^{γ} is the diffusion coefficient for the diffusion of carbon in austenite. The calculated value of δ from equation (3) for the beginning times of the transformation for chromium steels gives plate sizes which are close to the limiting size of visibility.

Fisher concludes that growth of bainite probably occurs as "delayed martensite" or as proeutectoid ferrite with carbon diffusing away into the austenite.

2.7.5 Ko and Cottrell (1952)

In 1952 Ko and Cottrell⁽²⁾ showed that a surface relief accompanies the formation of bainite, similar to the case of martensite. Through use of a hot stage, they were also able to demonstrate that the plates grow slowly, unlike martensite. Thus, the idea of "delayed martensite" can be discarded (at least on a macroscopic scale).

Ko and Cottrell offer the following explanation for the slow growth of bainite:

"It is suggested that the free energy difference between austenite and supersaturated ferrite is not sufficiently large to allow the formation of martensite due to adverse strain. Nevertheless, coherent growth can take place when the strain due to the density change is relieved, and the driving force for the transformation is increased if the amount of carbon dissolved in the bainite is reduced. This can be achieved either by carbon diffusion from bainite into the austenite, or by precipitation as carbide within the bainite plates or by a combination of both."

Ko and Cottrell suggest that at high temperatures the carbon is removed mainly by carbon diffusion in the austenite, so that here the growth rate should be controlled by the rate of carbon diffusion in the austenite. At lower temperatures, the carbon is precipitated in the form of carbides within the ferrite, and the rate of growth

is then controlled by the rate of nucleation of carbides within the ferrite and the rate of carbon diffusion in ferrite.

2.7.6 Krisement and Wever (1955)

Krisement and Wever^(29, 30) have proposed a theory based on the law of growth for coupled precipitates⁽³¹⁾. They suggest that the iron-carbon diagram can be separated into three regions which are shown in Figure 11. The Z curve represents the upper limit for the formation of bainitic ferrite; it may correspond to the $\Delta F = 0$ or a slightly different relation. The other boundary is the extrapolated austenite/cementite boundary.

In region I, the formation of pro-bainitic ferrite is possible. Austenite quenched into region III, on the other hand, will initiate the bainite reaction by precipitation of carbide. However, once carbide forms, the composition of the austenite adjacent to the carbide falls to the extrapolated austenite/cementite boundary. Since the composition of the austenite would then lie to the left of the Z curve, the formation of bainitic ferrite becomes possible. This bainitic ferrite is formed by an "unklapp" or martensitic mechanism; carbon immediately diffuses out of the ferrite into the austenite due to the high rate of diffusion of carbon in ferrite and the lower chemical potential of carbon in the austenite. This raises the carbon level of the austenite adjacent to the ferrite until carbide precipitation occurs again. The

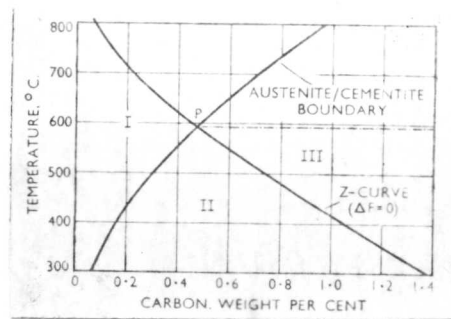


FIGURE 11. Quasi-Equilibrium Diagram of the Bainite Reaction from Krisement and Wever⁽³⁰⁾.

process is then repeated.

This process is called the "double-growth" mechanism with the carbide forming by a diffusion controlled process and the ferrite forming by an "umklapp" or diffusionless mechanism.

Austenite quenched into region II may either form pro-bainitic ferrite or two-phase aggregates. To the left of region II, the formation of pro-bainitic ferrite is favored, while to the right of this region, the double-growth mechanism is favored.

The rate of nucleation of such two-phase aggregates is controlled by the rate of nucleation of carbide within the austenite. The growth rate of this two-phase region is determined by the rate of growth of the carbide and of the ferrite. From the law of growth for two-phase aggregates⁽³¹⁾, Krisement and Wever derive the following growth equation:

$$\dot{X} = \beta \exp \left(- \frac{\bar{A}}{RT} \right) \quad (4)$$

where \dot{X} is the rate of surface displacement of a two-phase aggregate, β is a constant depending on the geometry and concentration, and \bar{A} is the activation energy for growth. For the present case, that of a double-reaction mechanism, the value of \bar{A} is an average of the activation energy for carbon diffusion in austenite (A_c^Y) and the activation energy for coherent growth of ferrite (A_{coh}), i.e. $A_{coh} \leq \bar{A} \leq A_c^Y$.

The value of \bar{A} depends on carbon content. In the low-carbon

range (Region I of Figure 11), no double-reaction occurs and $\bar{A} = A_{\text{coh}}$, while for high-carbon contents, $\bar{A} \sim A_c^Y$.

In order to compare the overall activation energy for the bainitic transformation with the activation energy for this growth mechanism, it is necessary to make some assumptions about the nucleation process. Krisement and Wever assume that the nucleation rate of the double-growth process is controlled by the nucleation rate of carbide which is given by:

$$I = \alpha' D_c^Y = \alpha \exp\left(-\frac{A_c^Y}{RT}\right) \quad \text{exp}\left(-\frac{A_c^Y}{RT}\right) \quad (5)$$

where I is the nucleation rate of carbide, D_c^Y is the diffusion coefficient for diffusion of carbon in austenite, α' and α are constants which vary little with temperature, and A_c^Y is the activation energy for carbon diffusion in austenite.

The empirical formula for the volume fraction transformed $W(t)$ is:

$$W(t) = 1 - \exp\left(-\left(\frac{t}{\tau}\right)^{s+1}\right) \quad (6)$$

where s is a constant approximately equal to 3. The quantity τ is a time constant and is given by the Boltzmann formula:

$$\tau = c \cdot \exp\left(\frac{Q}{RT}\right) \quad (7)$$

For short times t , the transformation rate from equation (6) is:

$$\dot{W}(t) = \frac{s+1}{\tau^{s+1}} \cdot t^s \quad (8)$$

It can also be shown that:

$$\dot{W}(t) = I \cdot V(t) \quad (9)$$

where I is the nucleation rate of carbide, and $V(t)$ is the bainite volume at any given time which is given by:

$$V(t) = \gamma (X t)^3 \quad (10)$$

γ is a constant depending on geometry and X is given by equation (4).

Using equations (4), (5) and (10), it can be shown that:

$$\dot{W}(t) = \gamma' \cdot \exp \left[- \frac{A_c^Y + 3\bar{A}}{RT} \right] \cdot t^3 \quad (11)$$

Krisement and Wever take $s = 3$, and thus from equations (7) and (8):

$$\tau = c \cdot \exp \left[\frac{\frac{1}{4} (A_c^Y + 3\bar{A})}{RT} \right] \quad (12)$$

Thus, the overall activation energy for bainite transformation, Q , should be related to A_c^Y and \bar{A} by the relation:

$$Q = \frac{1}{4} (A_c^Y + 3\bar{A}) \quad (13)$$

Equation (13) predicts that, since \bar{A} is always less than A_c^Y , the overall activation energy Q must be less than A_c^Y ; in addition, since \bar{A} is expected to increase with carbon content, Q will also increase with carbon content. Krisement and Wever calculate activation energies from a number of TTT diagrams and find that both these predictions are confirmed.

In further support of their theory, Krisement and Wever, show that B_s temperatures should remain constant at about 590° C for carbon contents above 0.5 percent carbon. This is because the upper limit of region III in Figure 10 is given by a horizontal line passing through P. In addition, since pro-bainitic ferrite only occurs in region I, steels with carbon contents greater than 0.5 percent carbon should not contain pro-bainitic ferrite. Krisement and Wever present data for a number of steels which seem to confirm these predictions.

2.8 Summary

This review of previous work has summarized the existing information on bainite. The general fields of agreement and ~~disagreement~~ have been pointed out and the most important theories have been presented. The theories which seem worthwhile considering on the basis of present knowledge are those of Fisher, Ko and Cottrell, and Krisement and Wever.

Fisher's theory has the advantage of using one of the most reasonable growth models, that of carbon diffusion through ferrite, and presenting quantitative predictions of the growth rate. It suffers from the disadvantage of not explaining the surface upheavals accompanying the transformation since it was suggested before the work of Ko and Cottrell.

The theory of Ko and Cottrell offers an explanation of the difference between the growth of martensite and bainite on the basis of the strain energy due to the density change. However, it is not clear that the

strain energy due to the density change is the strain energy which is most important. The shear strain energy in the austenite which must accompany the formation of bainite would seem to be more important, and it is not clear how carbide precipitation in the ferrite will affect this strain energy. In addition, Ko and Cottrell's theory is based on qualitative arguments, so that quantitative comparisons with experimental data are not possible.

The main drawback of the theory of Krisement and Wever is that it assumes carbide precipitation in austenite to be the controlling process at higher carbon levels. It is not clear from the evidence available that this is correct. Certainly, in the case of lower bainite it is not correct. However, the theory of Krisement and Wever does focus attention on changes in chemistry of the austenite at the ferrite/austenite or carbide/austenite interface. This is what the theory of Ko and Cottrell does not do and would seem to be very important. Krisement and Wever also furnish a number of predictions which can be quantitatively checked.

Since surface upheavals accompany the formation of bainite, the austenite to ferrite transformation must occur in a martensitic fashion. However, since slow growth of the bainite plates is observed, the formation of martensitic ferrite can only occur on a microscale or in some continuous shearing fashion. The explanation of this

continuous shearing mechanism is the main stumbling block of most theories and has only been treated adequately by Krisement and Wever. Unfortunately, carbide precipitation in the austenite is basic to the Krisement-Wever theory, and this is not necessarily supported by the experimental information.

The purpose of the present work was to supply the necessary experimental information to prove or disprove the existing theories and if necessary develop a new theory based on the more reasonable growth model of carbide precipitation in ferrite.

3. EXPERIMENTAL PROCEDURE

3.1 Alloys

The compositions of the five high-purity iron-base alloys used in this investigation are given in Table I.

TABLE I
Alloy Compositions

<u>Alloy No.</u>	<u>% C</u>	<u>% Cr</u>	<u>% Ni</u>	<u>% Mn</u>	<u>% Si</u>
126	0.96	*	*	*	**
127	1.16	*	*	*	**
127C	1.14	2.71	**	<0.005	0.02
127N	1.12	**	5.28	0.006	0.01
128	1.43	*	*	*	**
* <0.001%			** <0.01%		

Other trace elements determined were Al, Co, Cu, Mg, Sn, Ti, and V. These were found to be less than 0.005 percent for the Fe-C-Cr and Fe-C-Ni alloys and less than 0.001 percent for the iron-carbon alloys.

The iron-carbon alloys (126, 127, and 128) were selected to study the influence of carbon on the bainitic growth rates. Some work was attempted with lower carbon content alloys, but due to the high rates of transformation it was not possible to make growth rate measurements

in iron-carbon alloys with a carbon content less than 0.96 percent carbon. The iron-carbon-chromium and iron-carbon-nickel alloys were selected to study the influence of nickel and chromium on the bainitic growth rates at a constant carbon level of about 1.2 percent carbon and to allow the extension of the growth rate measurements to higher temperatures. The particular values of nickel and chromium were selected because TTT diagrams were available in the literature^(14, 43) for compositions close to those given in Table I.

The iron-carbon alloys were available from the work of C. S. Roberts et al⁽³⁴⁾ and were in the form of dilatometer samples (0.400 inch diameter by 4 inches long). To facilitate machining of the iron-carbon alloys, they were annealed for four hours at 1450° F (788° C) in evacuated Vycor capsules, and then furnace cooled.

The Fe-C-Cr and Fe-C-Ni alloys were vacuum melted and cast by National Research Corporation in the form of tapered two-pound ingots. These were forged at 2000° F (1093° C) to 5/8-inch diameter rods and subsequently homogenized for 20 hours at 1100° C in evacuated Vycor capsules and air cooled. They were then tempered at 1200° F (649° C) for three hours.

3.2 Hot Stage Design

3.2.1 General Description

A hot stage is simply a device that allows one to examine microscopically the metallographically polished surface of a sample

while it is at temperature. Either a vacuum or a protective atmosphere is used to prevent oxidation of the surface of the sample. The sample may be heated by its own resistance or by a heating coil. To allow observation of the sample, a quartz window is placed on the top of the stage and appropriately sealed.

For most hot-stage work, a long working distance objective is needed to prevent damage to the objective from the heat radiated by the sample. Two types of objectives are used at present: (1) a reflecting objective⁽³⁵⁾ and (2) a special long distance refracting objective⁽³⁶⁾. In the present work, a reflecting objective was employed.

The design of the present stage is somewhat similar to other stages described in the literature^(18, 36, 37). The novel feature of the present stage is that it allows the sample to be quenched rapidly with a helium blast from the austenitizing temperature to some lower (transformation) temperature. This high quenching rate is needed to prevent the formation of carbide or pearlite in the alloys studied here.

Side and front views of the stage are shown in Figures 12 and 13. The numbered parts of the stage shown in Figure 12 are given below.

- (1) Supporting ring (Lava)
- (2) Sample support tube (Incoel)
- (3) Resistance heating element (Platinum)
- (4) Radiation shield (Tantalum)

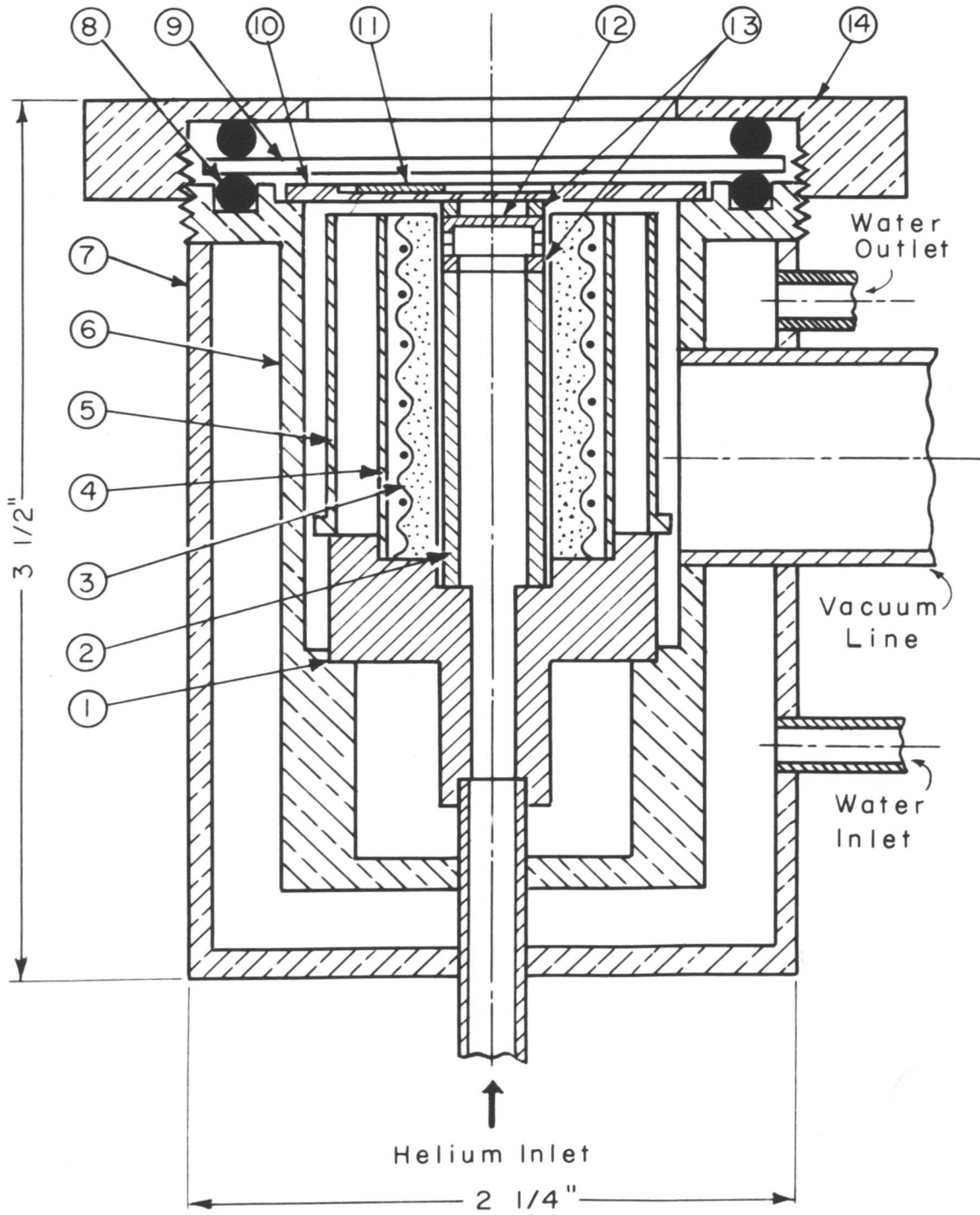


FIG.12 SIDE VIEW OF STAGE

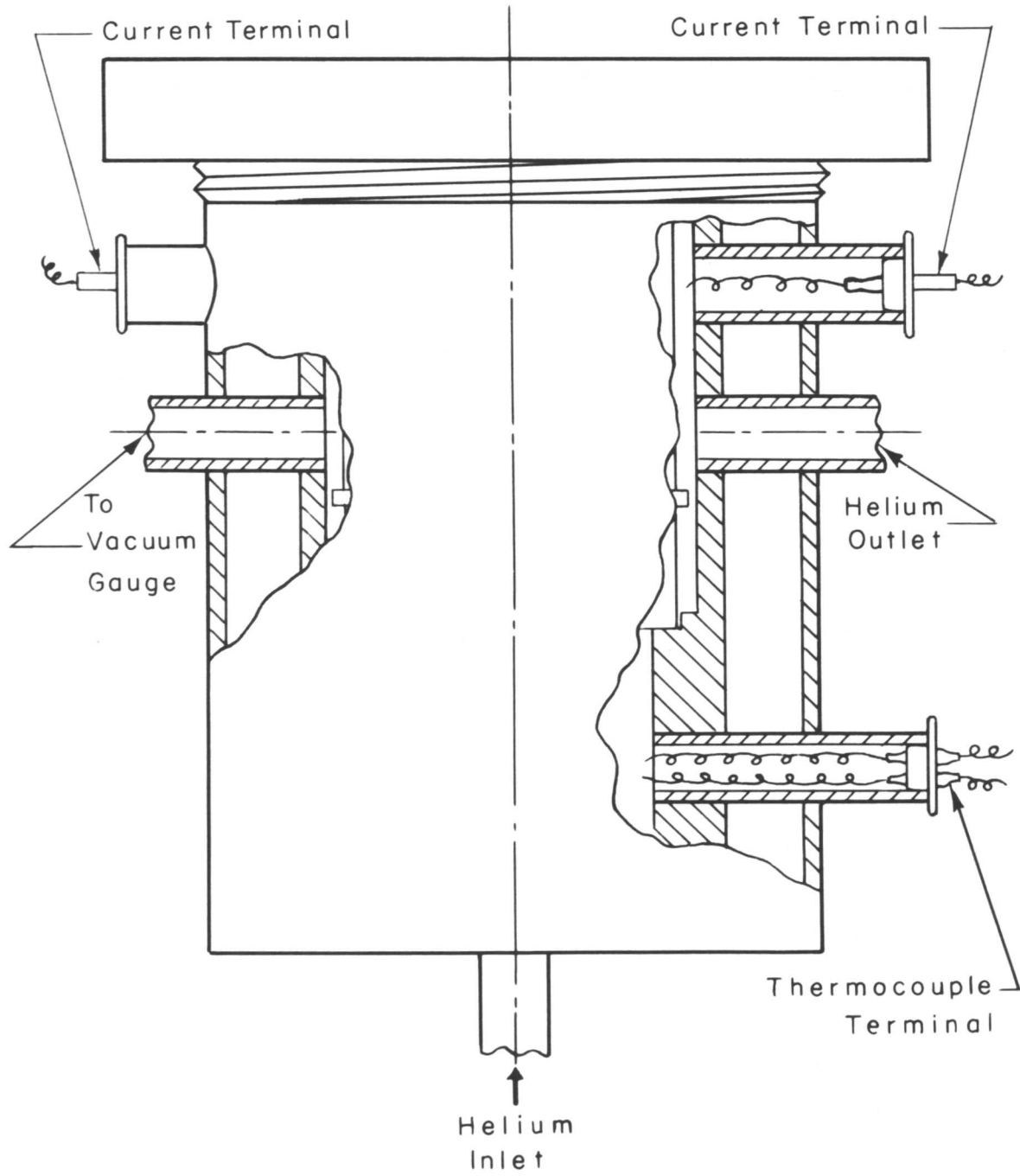


FIG.13 FRONT VIEW OF STAGE

- (5) Radiation shield (Stainless Steel)
- (6) Inner brass shell (water cooled)
- (7) Outer brass shell
- (8) O-ring seal
- (9) Quartz window
- (10) Shutter support
- (11) Shutter (Iron foil)
- (12) Specimen
- (13) Retaining rings (Lava)
- (14) Cover Plate (Brass)

3.2.2 Heating Unit, Shutter, and Sample Design

The heating element of the stage consisted of six feet of 0.020 inch platinum wire wound in the form of a tight helix. This was then cemented with alundum cement to a grooved alundum core. The power input to the coil was controlled by a variac with a stabilized voltage source. The heating element was supported by a Lava ring (see Part I, Figure 12). Two radiation shields surrounded the heating coil, with the outer radiation shield being split to make it easier to replace the heating coil. The sample support tube was fitted within the heating element and cemented with Sauereisen cement to the supporting ring. The supporting ring, sample support tube, heating element, and radiation shields are shown in Figure 14.

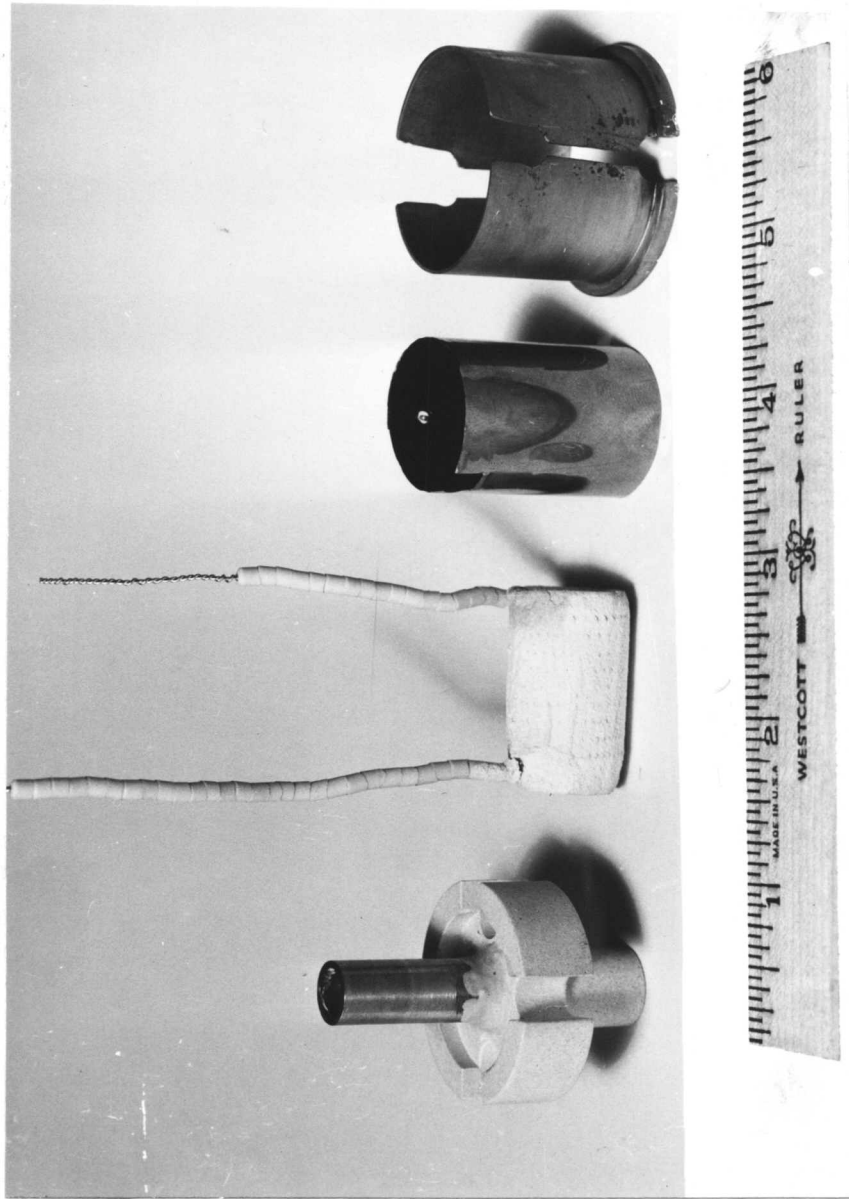


FIGURE 14. Supporting ring and sample support tube, heating unit, inner radiation shield, and outer radiation shield, reading from left to right.

In order to prevent deposition of metal vapor on the quartz window, it was found necessary to install a shutter arrangement. This consisted of a stainless steel support and an iron foil shutter which could be moved back and forth in the groove in the shutter support with a magnet. The window was a polished quartz disc (0.080inch thick) which fitted directly over the shutter and made a vacuum seal to the main chamber through the use of an O-ring. At the higher temperatures, the shutter was moved to cover the hole in the shutter support and prevent "fogging" of the quartz window; at the lower temperatures, it was moved away to allow observation of the specimen surface. A brass cover plate was screwed down on the quartz window to prevent it from blowing off when helium was blasted into the stage. The O-ring between the window and cover plate was used to apply more uniform pressure on the quartz window. The details of this arrangement are shown in Figure 15.

The form of sample used for all the hot-stage microscopy is shown in Figure 16. The thin section (0.010 - 0.020 inch) permitted a high quenching rate. A platinum, platinum - 10 percent rhodium thermocouple (0.010 inch diameter wires) was spot welded to the top face of the sample using an arc-discharge method. Two lava retaining rings were placed above and below the sample. The lower one prevented welding of the sample to the support tube, while the upper one fitted snugly against the shutter support. (See Figure 12, part 13). This prevented the sample from being dislodged when helium was blasted

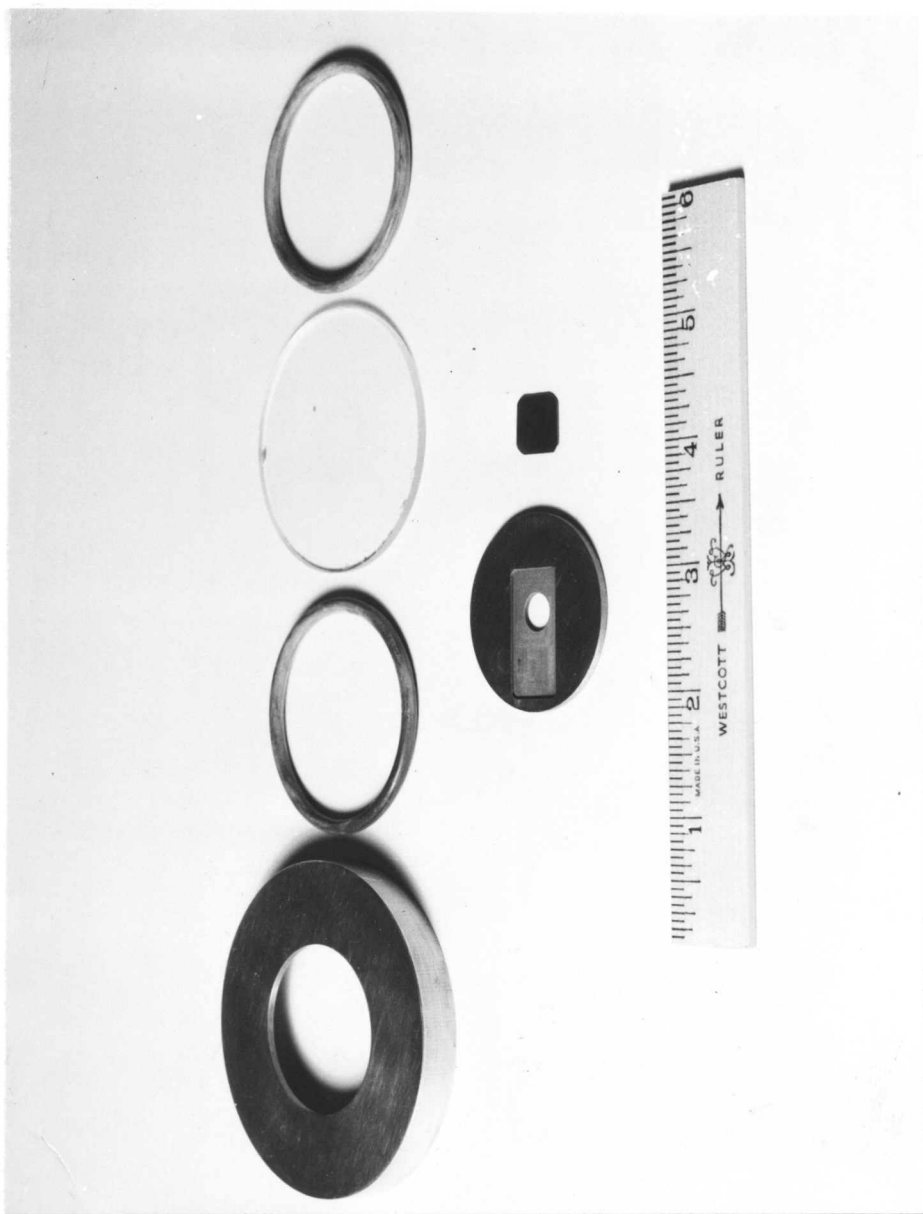


FIGURE 15. Cover plate, O-rings, quartz window, shutter support, and iron foil shutter.

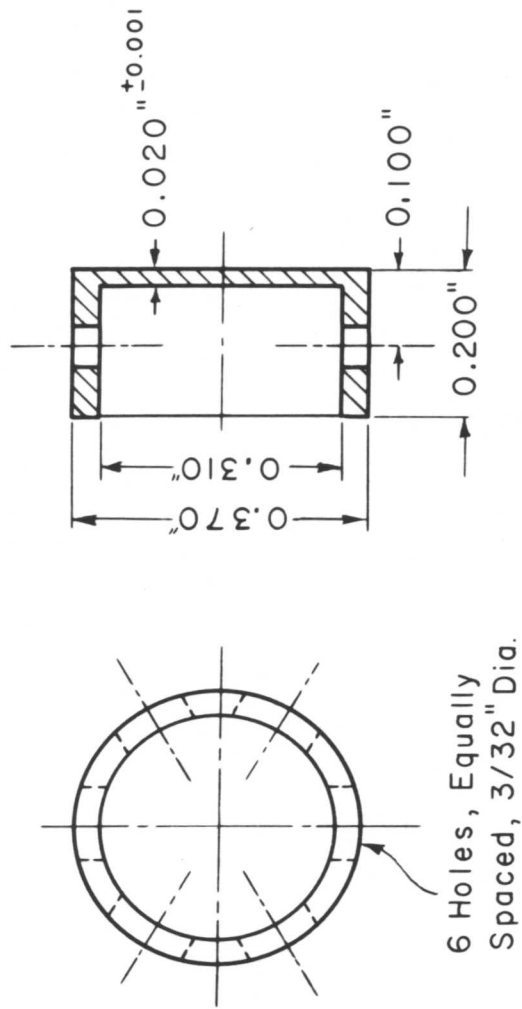


FIG. 16 SPECIMEN DESIGN

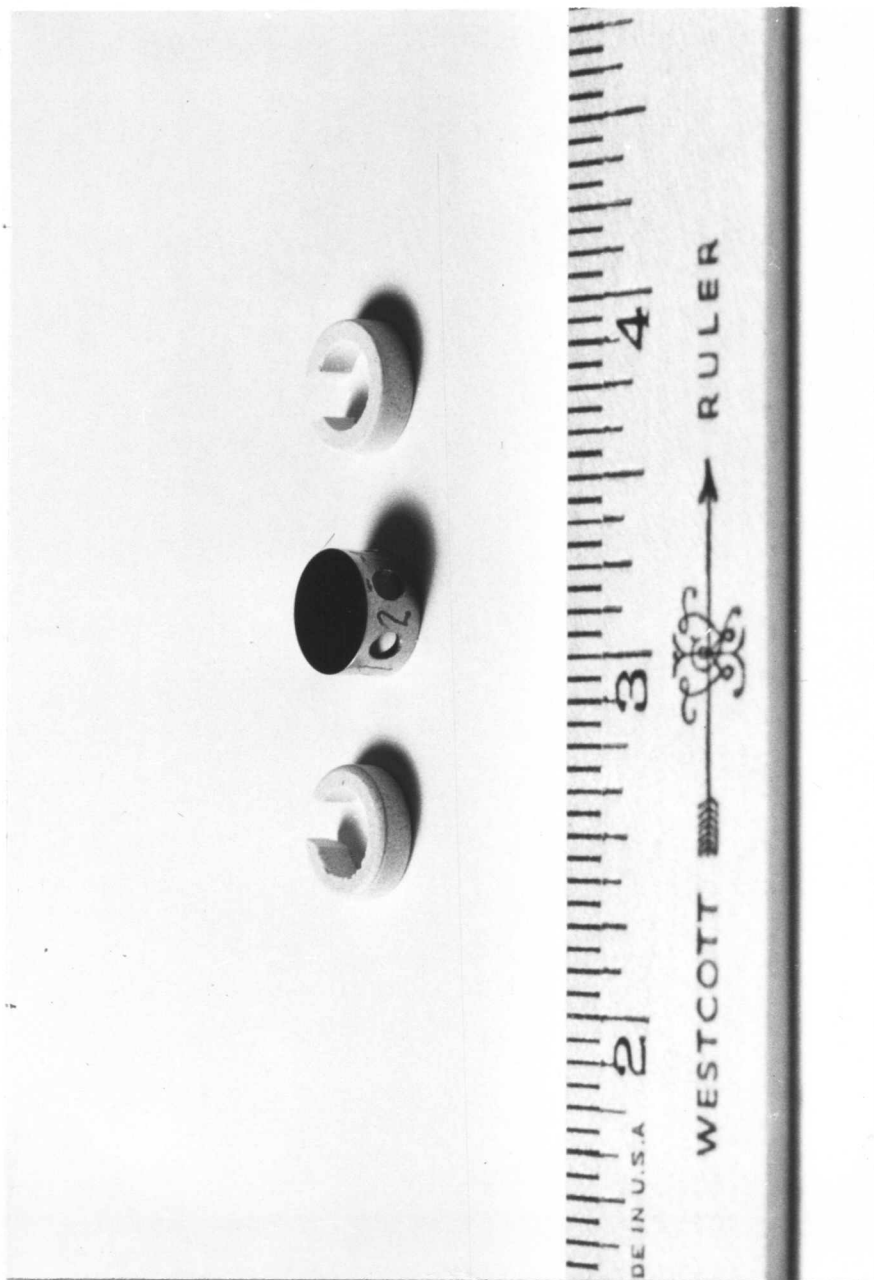


FIGURE 17. Hot-stage sample with its two retaining rings.

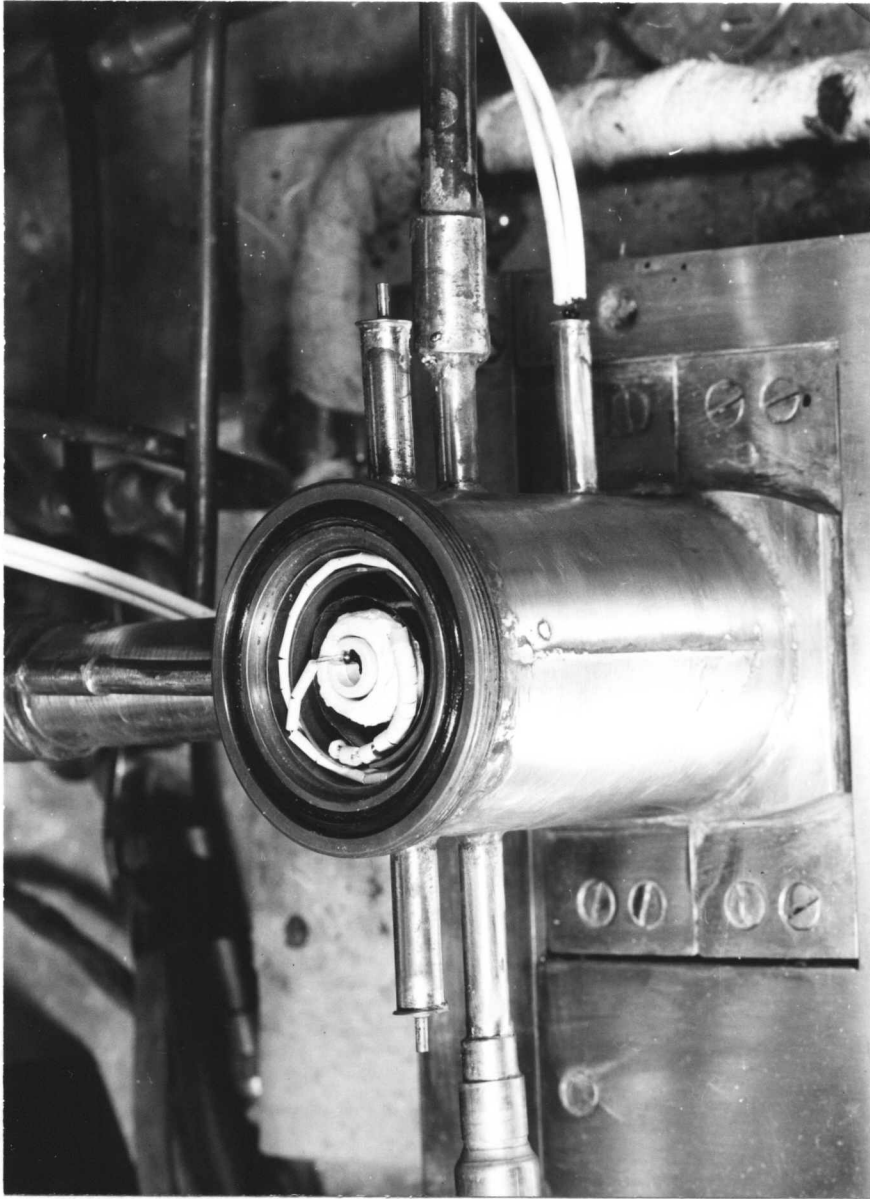


FIGURE 18. Hot-stage with heating unit, sample, radiation shield, and thermocouple in place.

into the stage.

The sample and its two retaining rings are shown in Figure 17. The partially assembled stage is shown in Figure 18, with the heating element, radiation shields, sample, retaining rings, and thermocouple in place. The completely assembled stage, with the shutter assembly, quartz window, and cover plate in position is shown in Figure 19.

3.2.3 Vacuum System

To prevent the sample from oxidation or decarburization at high temperatures, the sample chamber was evacuated. The vacuum system consisted of a 20 liter/second oil diffusion pump backed by a rotary mechanical pump. This gave a vacuum of 0.01 - 0.1 μ in the sample chamber during the austenitizing treatment. Considerable degassing occurred from the refractory material during the heating cycle; however, by slowly heating the stage, the degassing was virtually complete by the time the stage reached temperature.

Two vacuum gauges were used: a Pirani gauge was placed near the diffusion pump, and a cold-cathode Phillips gauge inserted at the farthest point from the diffusion pump. The combination of these two gauges allowed the pressure to be read from 1 mm to 0.01 μ .

3.2.4 Quenching Procedure

In order to avoid the formation of pearlite in the plain-carbon iron-carbon alloys, it was necessary to quench the samples rapidly from the austenitizing temperature. This was accomplished

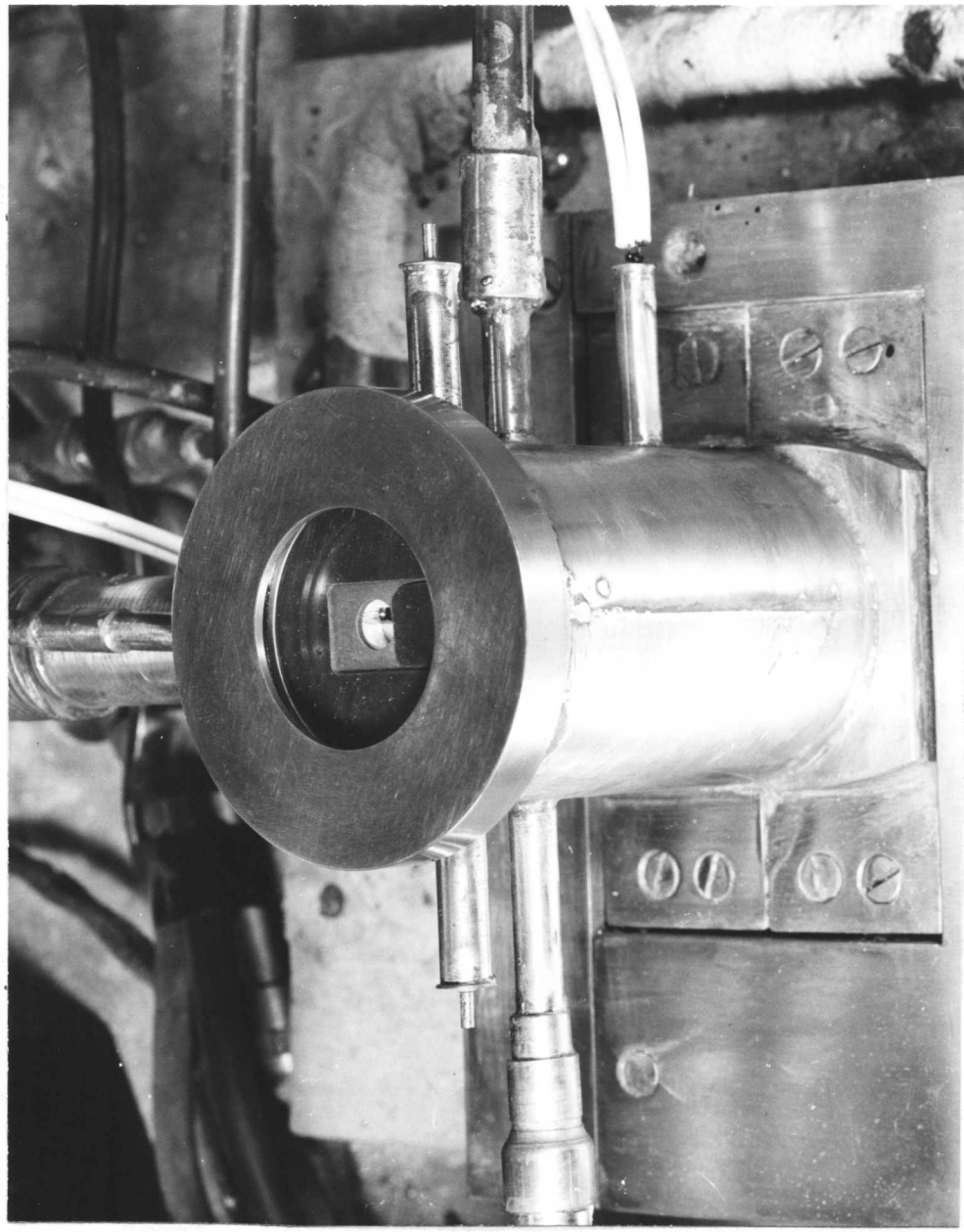


FIGURE 19. Completely assembled hot-stage.

by breaking the vacuum with a helium blast which was directed at the bottom of the sample. Considerable trouble was experienced at first with oxidation of the sample by contaminants in the tank helium. A calcium-turnings trap was installed in the helium line to remove this difficulty. The trap consisted of an iron tube, filled with calcium turnings, and heated to 1200° F.

It was also found advisable to install a double bubble-trap on the helium outlet line to prevent back diffusion of air into the system. Diffusion pump oil was used in the bubble trap because of its low vapor pressure. A double trap was used instead of a single one to avoid the possibility of oil being sucked back into the hot-stage. The final arrangement of the equipment is shown in Figure 20.

3.2.5 Optical System

As mentioned earlier, a long-working-distance reflecting-objective was used in this work. It was kindly supplied by Professor N. J. Grant of the Metallurgy Department at MIT. The objective had been made by Bausch and Lomb and had a working distance of 14 mm, a magnification of 20x, and a numerical aperture of 0.40. A picture of the objective is shown in Figure 21 and a diagram of the components is shown in Figure 22. This objective was used with a Bausch and Lomb table microscope equipped with a Leitz micro-ipse attachment for taking 35 mm. pictures. The hot-stage fitted directly between the

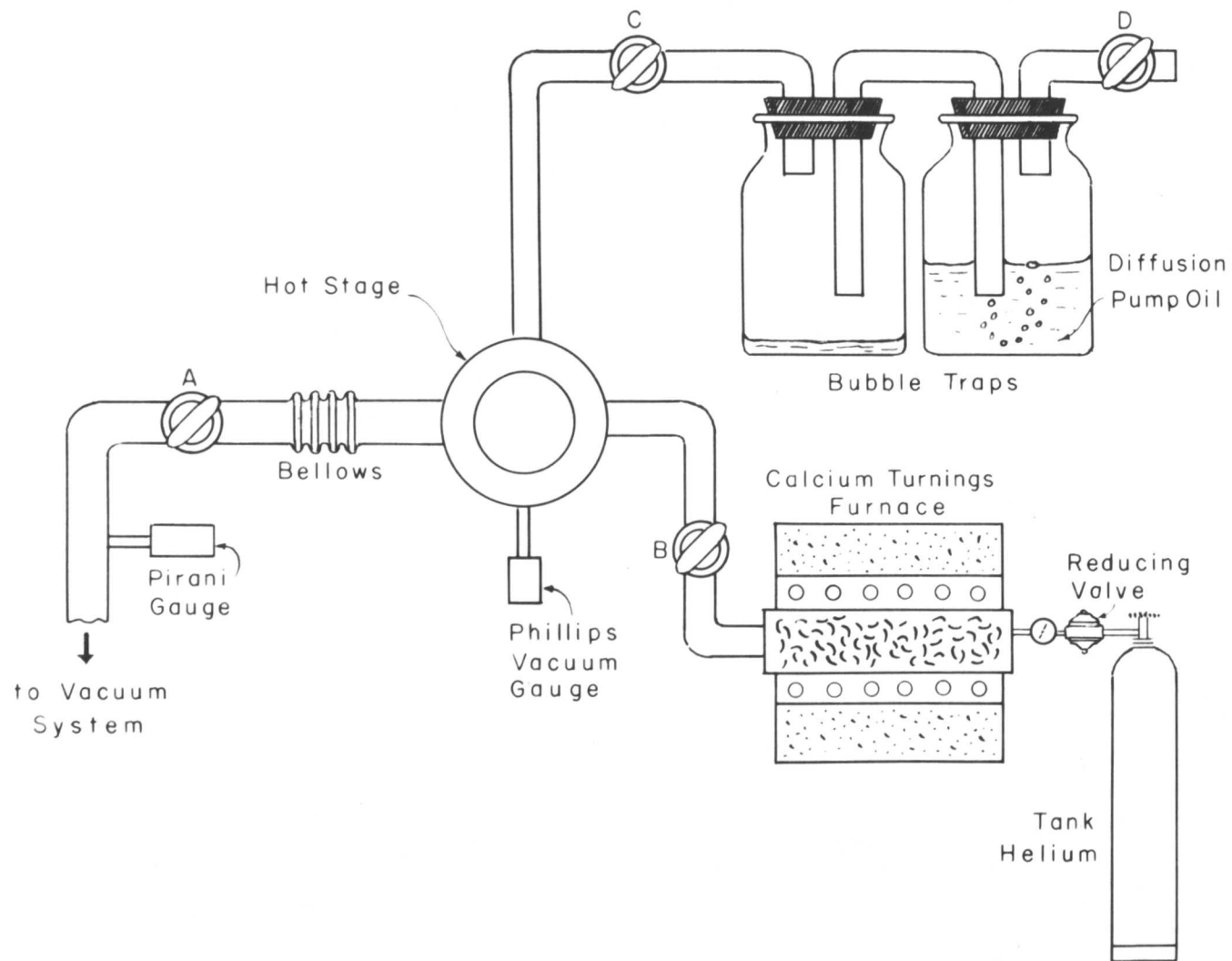


FIG. 20 ARRANGEMENT OF HOT-STAGE EQUIPMENT



FIGURE 21. Reflecting Objective

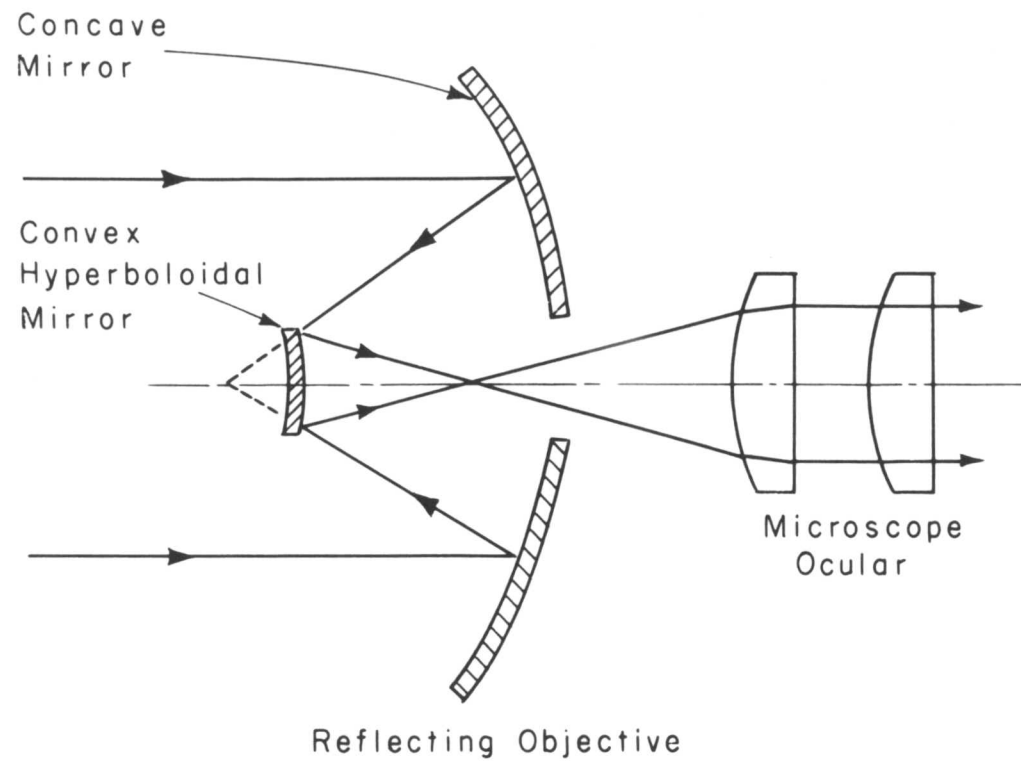


FIG.22 OPTICAL SYSTEM

legs of the bench microscope after the normal stage had been removed. An external tungsten filament lamp was used with the normal vertical illuminator.

3.2.6 Typical Run

To give a better understanding of the operation of the stage, a typical run will be described in detail.

The sample is metallographically polished and degreased in ether. The Pt, Pt - 10% Rh thermocouple is spotwelded to the top surface of the sample, and the sample is placed on the support tube. The retaining ring is placed on top of the sample, and the shutter support, iron foil shutter, quartz window, O-ring, and brass cover plate are placed in position.

The helium line, bubble traps, and stage are pumped down to about 100μ with valves A, B and C open, and valves D and the reducing valve closed (Figure 20). The system is flushed with helium once by closing valve A and opening the reducing valve; valves B and C are now closed, and A and D are opened. This seals the stage from the bubble traps and the helium line. The stage is then pumped down again to 100μ , and the diffusion pump and cooling water turned on. When the pressure in the stage has reached 0.1μ , the heating cycle is begun and the power input gradually increased until the austenitizing temperature is reached. Some outgassing occurs during the heating cycle, but with sufficiently slow heating, the pressure rise in the system can be kept to a low

level. The power input and pressure at different temperatures is shown in Figure 23.

After the austenitizing treatment, the sample is quenched rapidly to the transformation temperature with a blast of helium by closing valve A and opening first valve B and then valve C; the power input to the heating coil is simultaneously reduced to some predetermined value which maintains the sample at the desired transformation temperature. The emf output from the thermocouple is fed into a Leeds and Northrup high-speed millivolt recorder (sweep time for full-scale deflection is 2 seconds). During the quench, the high-speed recorder gives a continuous record of the temperature of the sample so that the quench can be stopped at the desired temperature.

When the desired temperature is reached, the helium flow rate is reduced by partially closing valve B. Continual adjustment of the helium flow rate is necessary to keep the sample at an approximately constant temperature while the heating coil cools down to the transformation temperature. The rate of quenching of the sample is estimated to be $500^{\circ}\text{C}/\text{second}$; however, it requires several minutes for the heating coil to cool down. Once the heating coil reaches the transformation temperature, the rate of helium flow is reduced further, and the sample transforms isothermally in the helium atmosphere. When thermal equilibrium is reached, the temperature remains very constant.

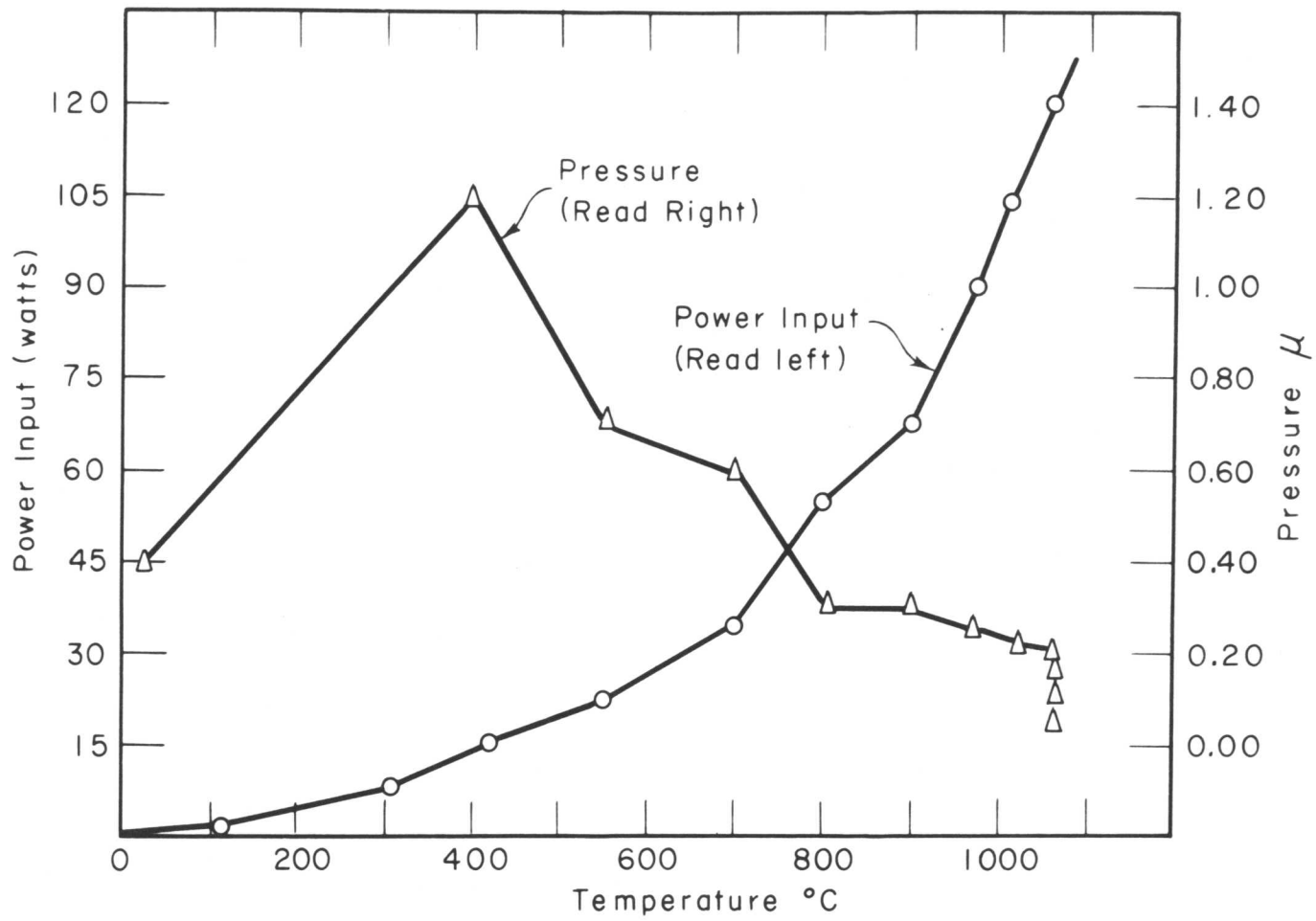


FIG. 23 POWER-TEMPERATURE-PRESSURE RELATIONSHIPS

Normally, the sample is transformed only to about 50 percent bainite. The sample is then quenched to room temperature by increasing the rate of helium flow and turning off the power.

3.3 Length Measurements

In order to measure the bainite plate length as a function of time, a series of 35 mm. pictures were taken of the surface during transformation. Prints were made of the frames at an enlargement of about 6x; an exposure of a ruled grating was enlarged with each series of prints to obtain the exact degree of enlargement. The lengths of individual plates were then measured directly on the prints, using vernier calipers with an accuracy of ± 0.01 cm.

3.4 Light Microscopy

Many of the hot-stage samples were examined after transformation by normal light microscopy. The surface relief accompanying the formation of bainite or martensite was removed by lightly abrading the sample on No. 600A Behr-Manning emery paper. The sample was then polished through No. 9 diamond powder, using kerosene as a lubricant; a final polish was performed with Cr_2O_3 .

The etchant found most satisfactory was 1 percent nital. The above polishing technique was also used to prepare the samples for the hot-stage, except they were not etched.

3.5 Electron Microscopy

In order to determine the distribution of carbide particles within

the ferritic matrix of the bainite, a number of samples were examined by electron microscopy. An RCA (EMB-4) electron microscope was used for this purpose.

The samples were metallographically polished and etched in modified 4 percent picral consisting of:

Solution A - 25 cc 4 percent picral

Solution B - To ISCC ethyl alcohol add 0.1 cc HCl

Add 1 cc of solution B to solution A.

Replicas were made of the surface using 1.5 percent Parlodian in n-butyl acetate; the replicas were rotary shadowed with chromium at an angle of 27°. Electron micrographs were made at magnifications of 8000 \times and 14000 \times .

3.6 Electron Diffraction

In order to determine the nature of the carbide phase forming in the ferritic matrix of the bainite, a number of samples were examined by electron diffraction. The RCA EMB-4 electron microscope was also used for the electron diffraction work and was calibrated using an iron standard.

Since the reflection electron diffraction technique was employed, it was necessary to etch the sample to make the carbide phase stand in relief. The etchant used for this purpose was 1 percent nital. Etching times of about two minutes were necessary to obtain good diffraction patterns. The samples were rinsed with alcohol after etching.

4. EXPERIMENTAL RESULTS

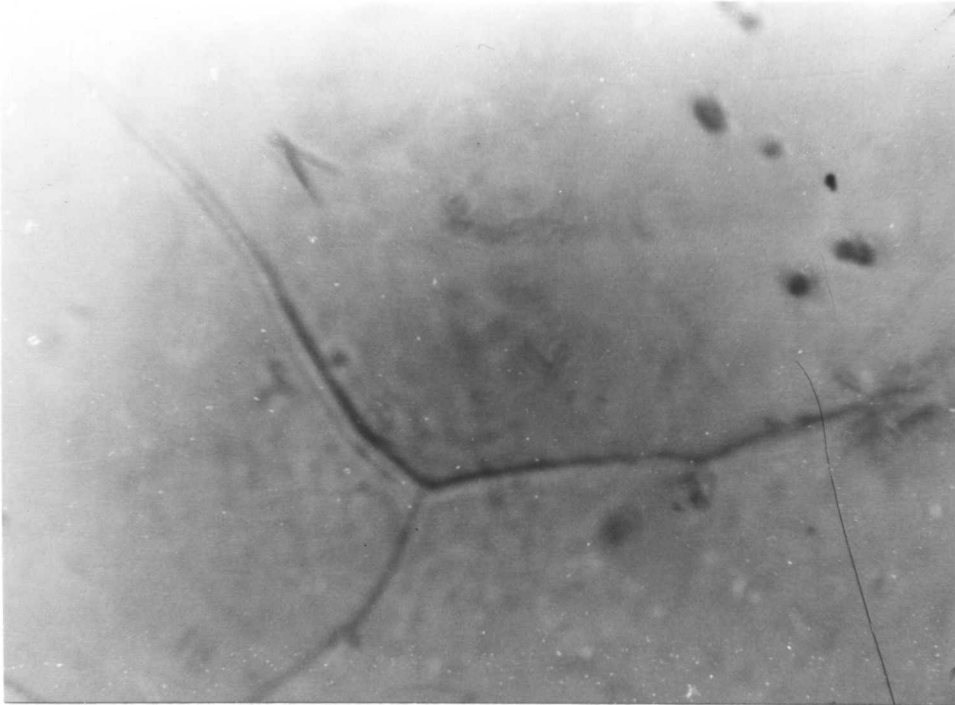
4.1 Growth Rates

4.1.1 Measurements of Growth Rate

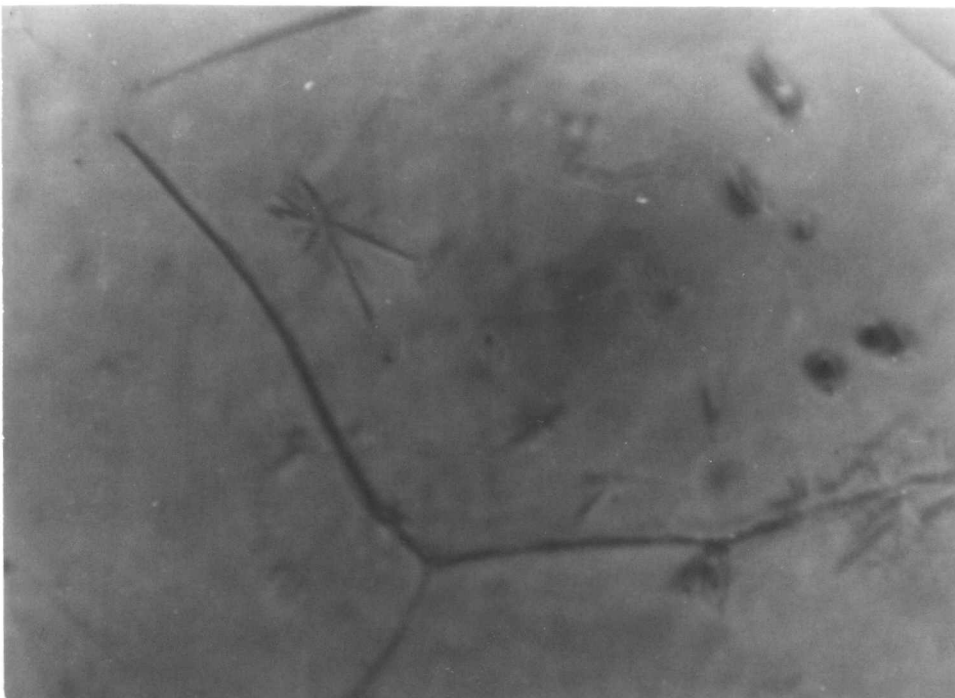
In order to determine the plate lengths as a function of time, a series of 35 mm pictures were taken of the surface during transformation on the hot stage. The plate lengths were measured directly on enlargements of the 35 mm film. Some hot-stage pictures for the 1.12 percent carbon, 5.28 percent nickel alloy are shown in Figures 24 - 27. This alloy was austenitized on the hot stage for 30 minutes at 1060° C and then quenched to 196° C, and isothermally transformed.

In Figures 24 - 27, the austenite grain boundaries are apparent because of thermal etching at the austenitizing temperature. The gradual growth of existing plates and the formation of new plates is clearly evident in this sequence of pictures. The bainite plates are visible only because of the surface upheaval accompanying their formation.

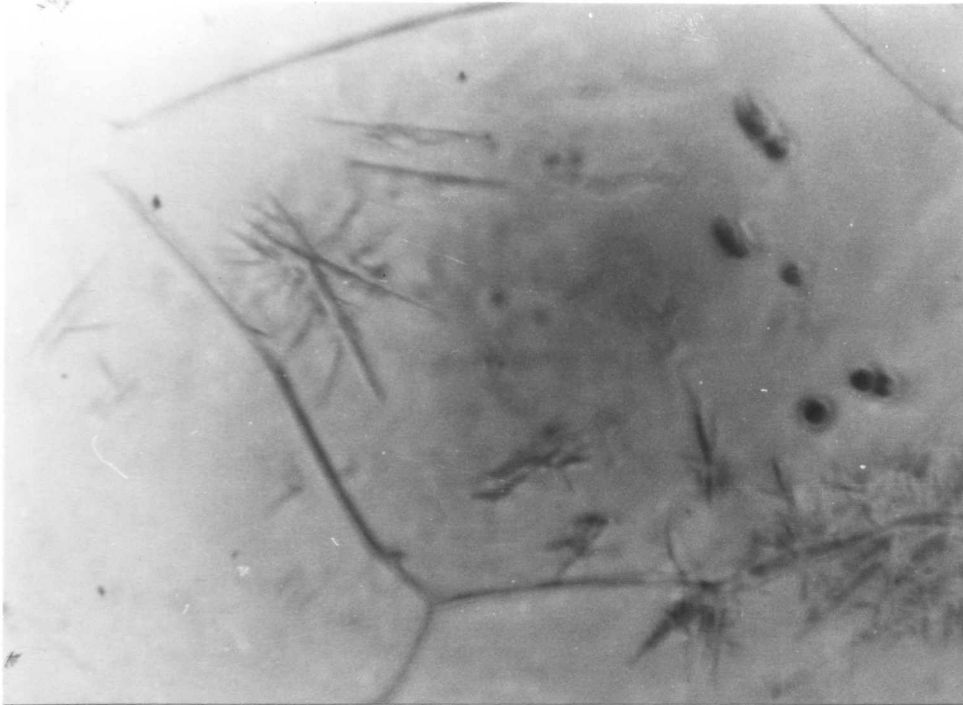
From such a series of photographs, it was possible to determine the length of the plates as a function of time. Some results for the 1.16 percent carbon alloy are shown in Figure 28. The length versus time plots result in straight lines. The growth rate, \dot{l} , is equal to the slope of this straight line. The value of \dot{l} can be seen from Figure 28 to be markedly dependent on temperature. Similar results were found for all the alloys.



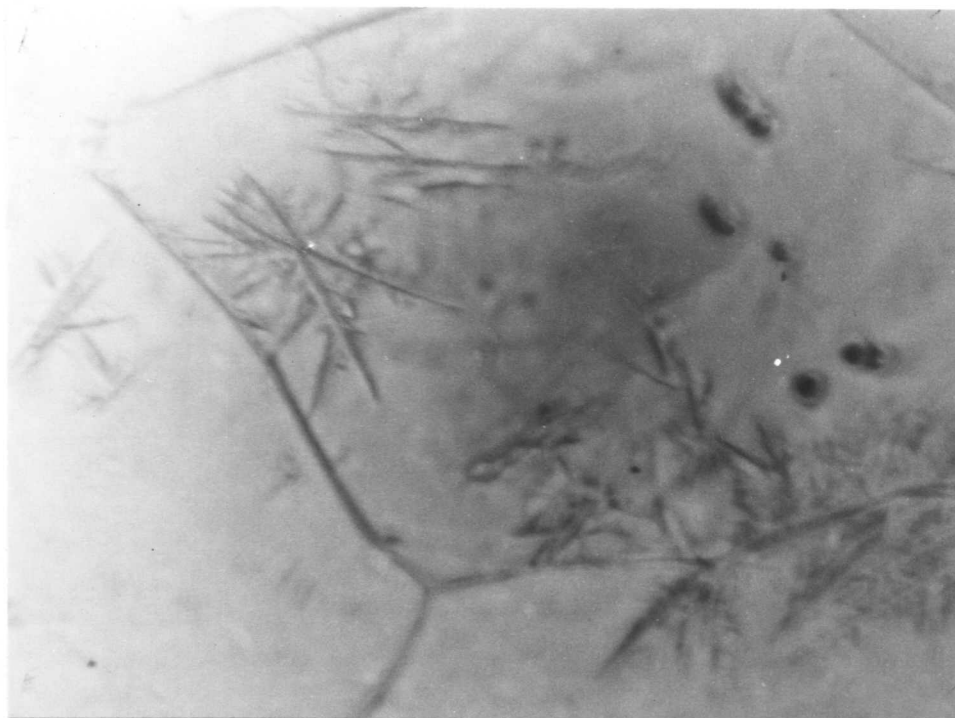
400x Hot-Stage
FIGURE 24. 1.12% C, 5.28% Ni Alloy; 30 min. 1060° C/1180 min.
196° C.



400x Hot-Stage
FIGURE 25. 1.12% C, 5.28% Ni Alloy; 30 min. 1060° C/1567 min.
196° C.



400 \times Hot-Stage
FIGURE 26. 1.12% C, 5.28% Ni Alloy; 30 min 1060° C/1967 min
196° C



400 \times Hot-Stage
FIGURE 27. 1.12% C, 5.28% Ni Alloy; 30 min 1060° C/2210 min
196° C

In order to obtain a fair measure of the growth rate, length versus time plots were made for as many plates as possible on each sample. The number of plates on which it was possible to make measurements varied from four to ten per sample. The growth rate results are summarized in Figures 29 - 33. The results are plotted in the form of $\log \dot{f}$ versus the reciprocal of the absolute temperature in order to obtain activation energies.

4.1.2 Scatter in Growth Rates

It is apparent from Figures 29-33 that considerable scatter is present in the values of \dot{f} . Although the length versus time plots give good straight lines, the slopes of these lines (\dot{f}) are different for different plates growing at the same temperature. The scatter is much too large to be explained on the basis of experimental uncertainty in the length measurements. These variations could arise from two causes: (1) a scatter due to geometry, or (2) a scatter in the actual growth rate. The problem of geometric scatter is treated below.

The most reasonable shape to assume for the bainite plates is a disc. The relation of a growing disc to the free surface is shown in Figure 34. The relation

$$S^2 + f^2 = R^2 \quad (14)$$

can be derived from Figure 32, where S is the perpendicular distance from the center of the disc to the chord formed by the intersection of the free surface and the disc, R , is the radius of the disc, f is the

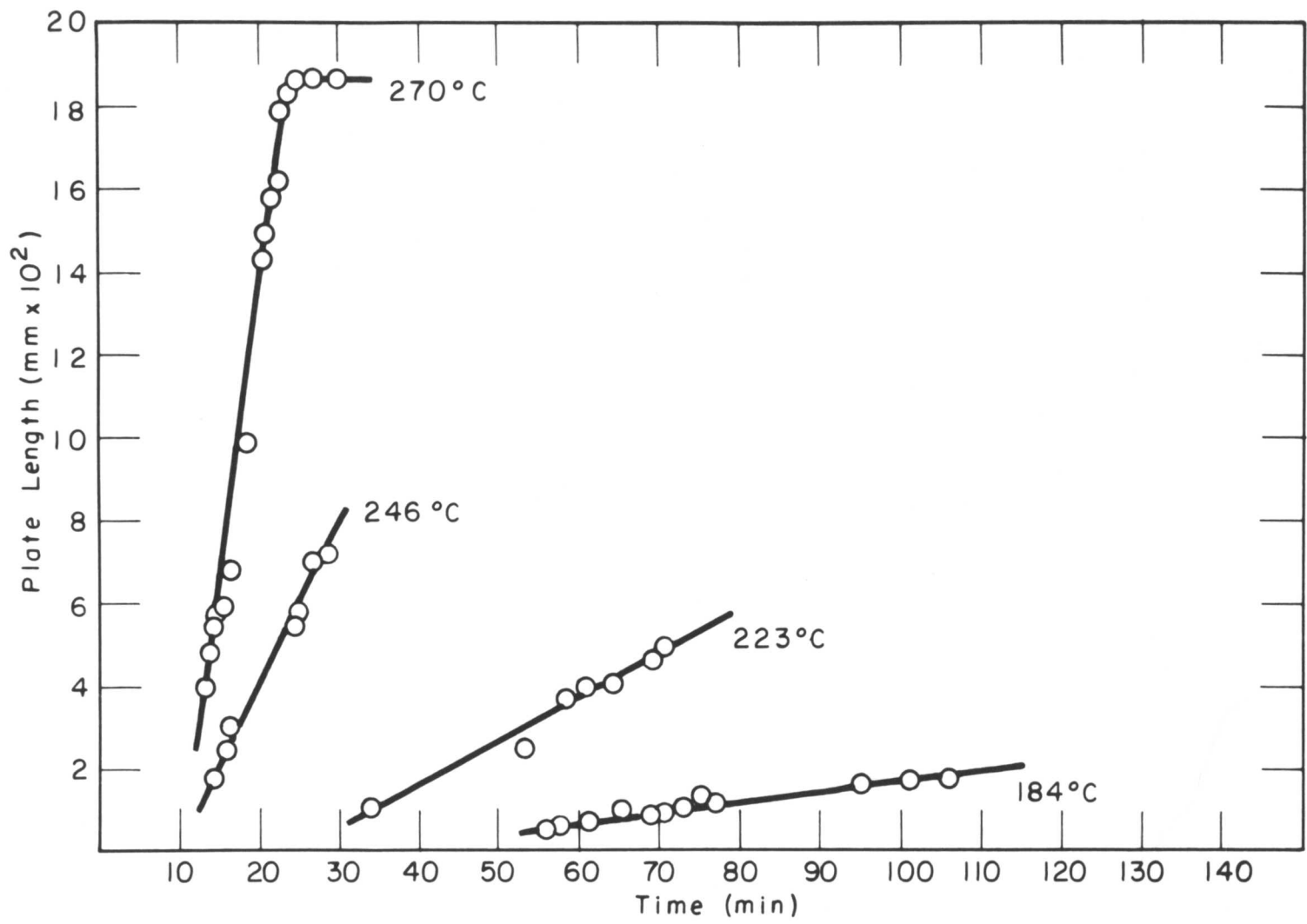
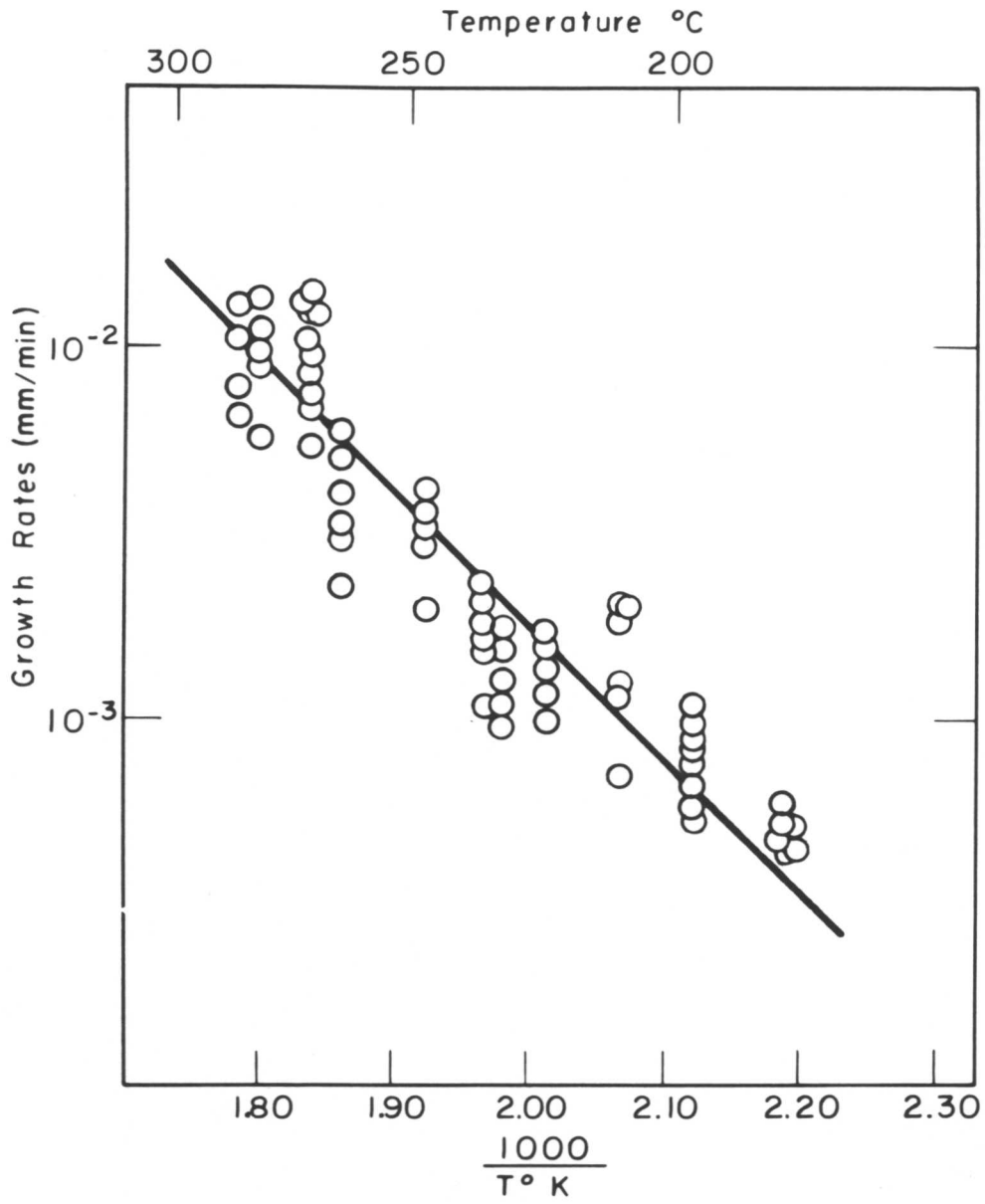
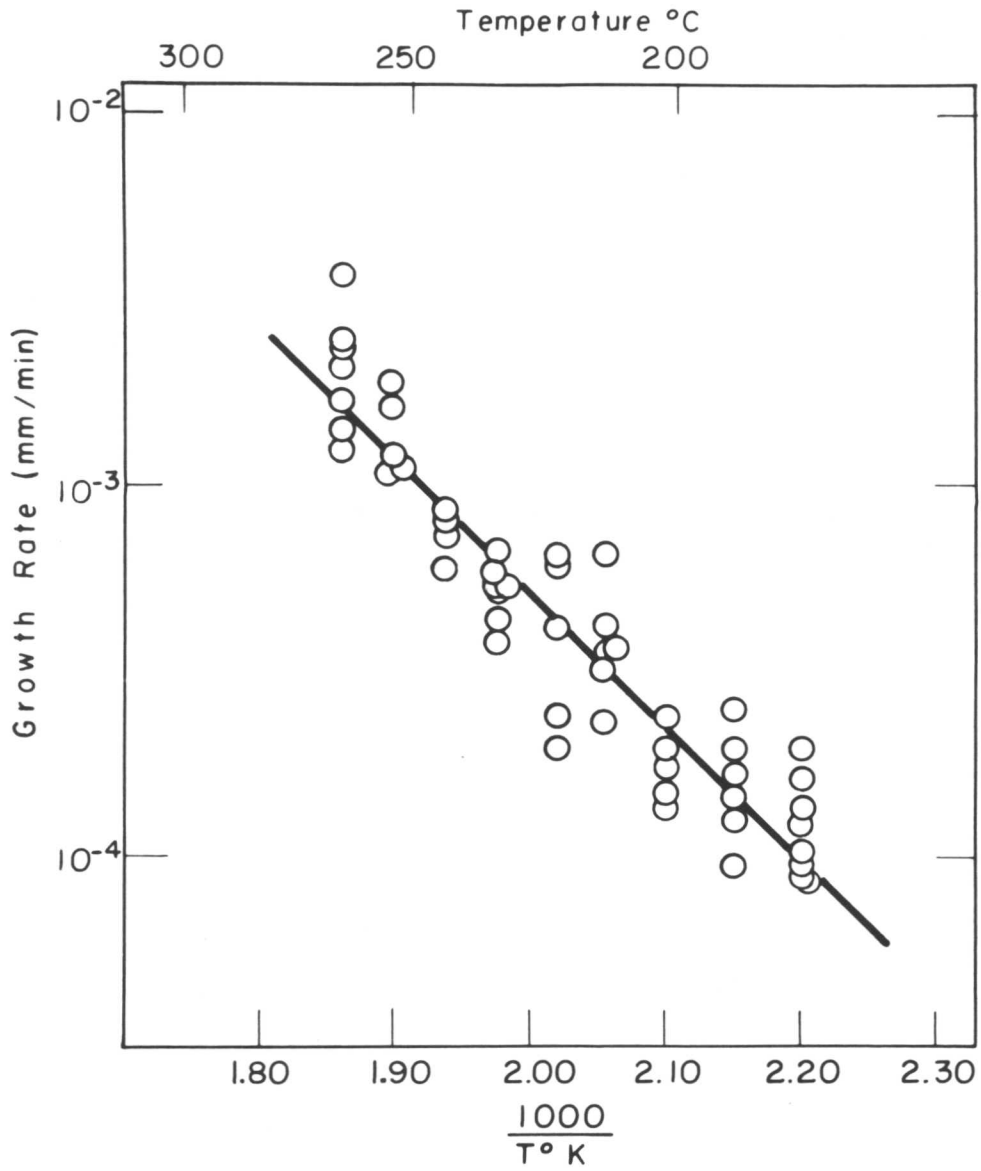


FIG. 28 PLATE LENGTH VERSUS TIME FOR A 1.16 %C, IRON-CARBON ALLOY





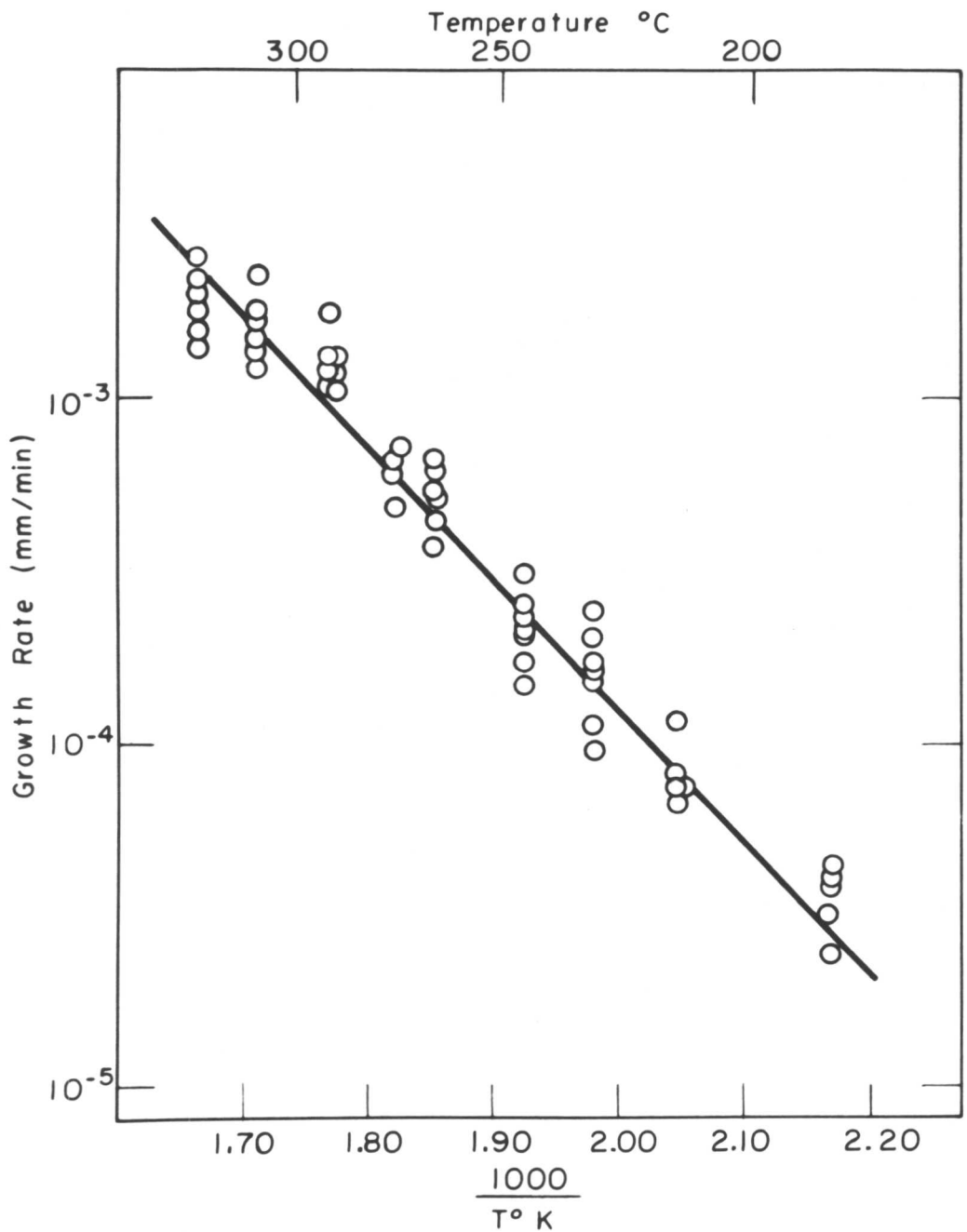


FIG.32 GROWTH RATES FOR A 1.14% C, 2.71% CR, IRON - CARBON - CHROMIUM ALLOY

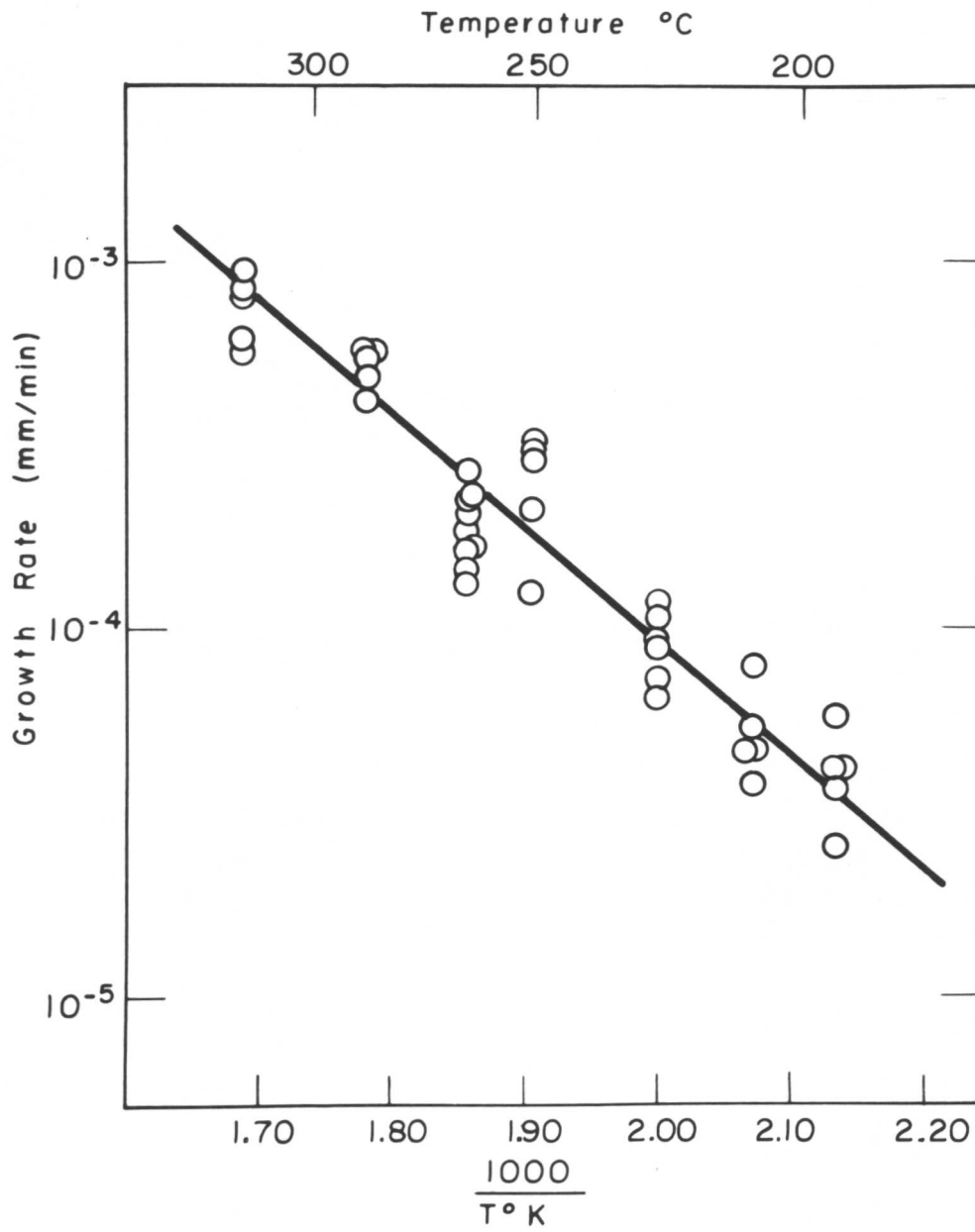


FIG. 33 GROWTH RATES FOR A 1.12% C, 5.28% NI, IRON-CARBON-NICKEL ALLOY

length of the plate measured on the surface, N_D and N_S are the normals to the disc and the surface respectively, θ is the angle between the two normals, and d is the perpendicular distance between the center of the disc and the surface.

Differentiating equation (14) with respect to time gives:

$$\dot{l} = \dot{R} \left(\frac{\sqrt{l^2 + S^2}}{l} \right) \quad (15)$$

The value of S is given by

$$S = \frac{d}{\sin \theta} \quad (16)$$

Now if we assume \dot{R} is a constant it can be seen that \dot{l} will vary with l since S is a constant depending only on the orientation of the disc in space. The ratio \dot{l}/\dot{R} is plotted as a function of l in Figure 35 assuming reasonable values of S . It can be seen that different values of \dot{l} can be obtained, depending on the value of S ; however, for a constant S the value of \dot{l} should decrease with increasing l . Since all the length versus time plots were straight lines (constant \dot{l}) it is evident that most of the values of S must be close to zero, or in other words the centers of the growing plates must be at or near the surface. In this case, it is not possible to explain the scatter in the growth rates by a geometric factor since $\dot{l} = \dot{R}$ if S has a value near zero.

The only possibility left is that the scatter in the growth rates is due to real variations in the radial growth rate \dot{R} . On this basis, the average growth rate can be selected as the most representative of the growth rate

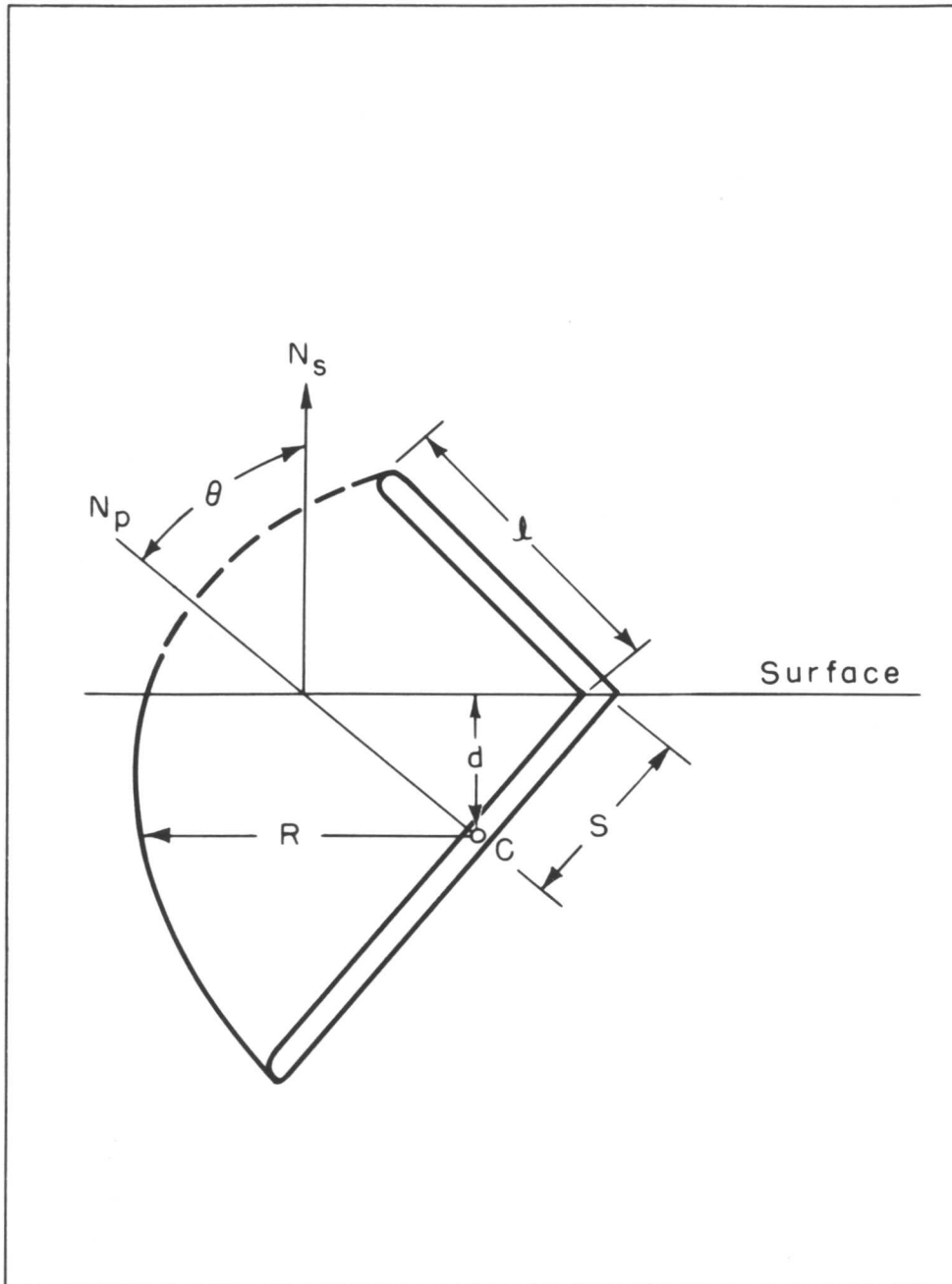


FIG. 34 BAINITE PLATE IN SPACE

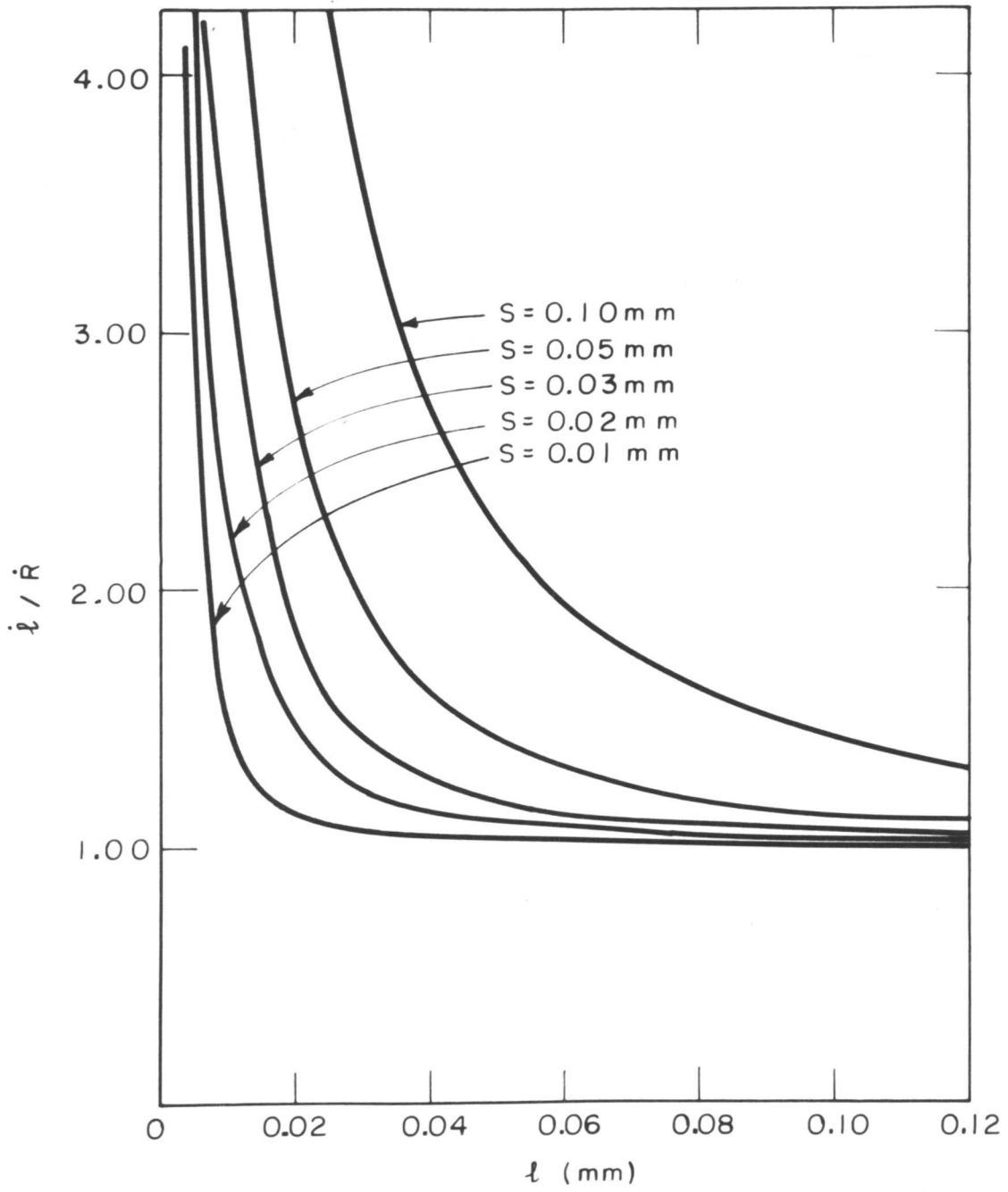


FIG.35 VARIATION OF i/\dot{R} WITH l AND S

at any temperature. The average growth rates for all the alloys are shown in Figures 36 - 40. The line drawn through these points in each case is the least squares line. The least squares lines are also shown in Figures 29 - 33. The bars on the points in Figures 36 - 40 represent the 95 percent confidence limits for the average growth rate assuming the scatter obeys a Gaussian error distribution.

4.1.3 Activation Energies for Growth

From the slopes of the lines of Figures 36 - 40, the activation energies for growth can be calculated converting from common logarithms to natural logarithms, we have:

$$\ln \dot{l} = - \frac{Q_g}{RT} + \ln B \quad (17)$$

where Q_g is the activation energy for growth, T is the absolute temperature, R is the gas constant, and B is a constant. It should be emphasized that the activation energy for growth measured here is only for growth in the direction of the long dimension of the bainitic plate. It was not possible to make accurate width measurements on the hot stage. The values of Q_g and B are given in Table II.

4.1.4 Effect of Composition on the Growth Rate

The effect of carbon content on \dot{l} can be evaluated from the results for the three iron-carbon alloys. These results are summarized in Figure 41. It can be seen that the growth rates are markedly lowered with increasing carbon content. The activation energies for growth do not seem to be significantly affected by changes in carbon content,

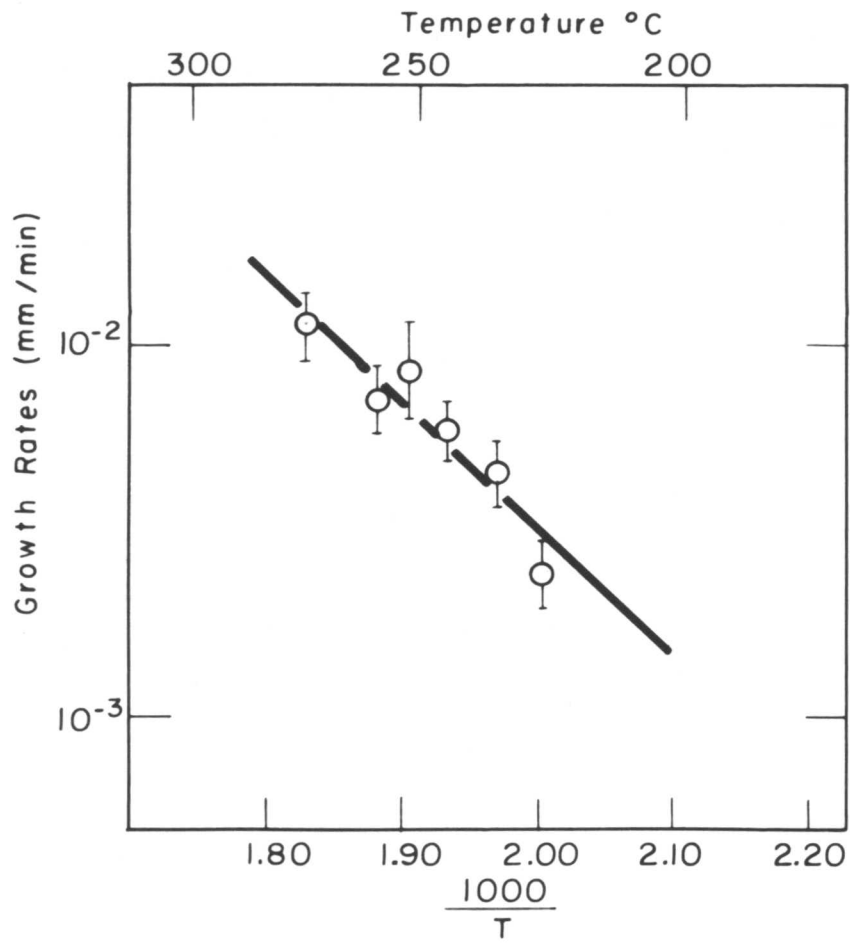


FIG.36 AVERAGE GROWTH RATES FOR A 0.96 %C, IRON-CARBON ALLOY

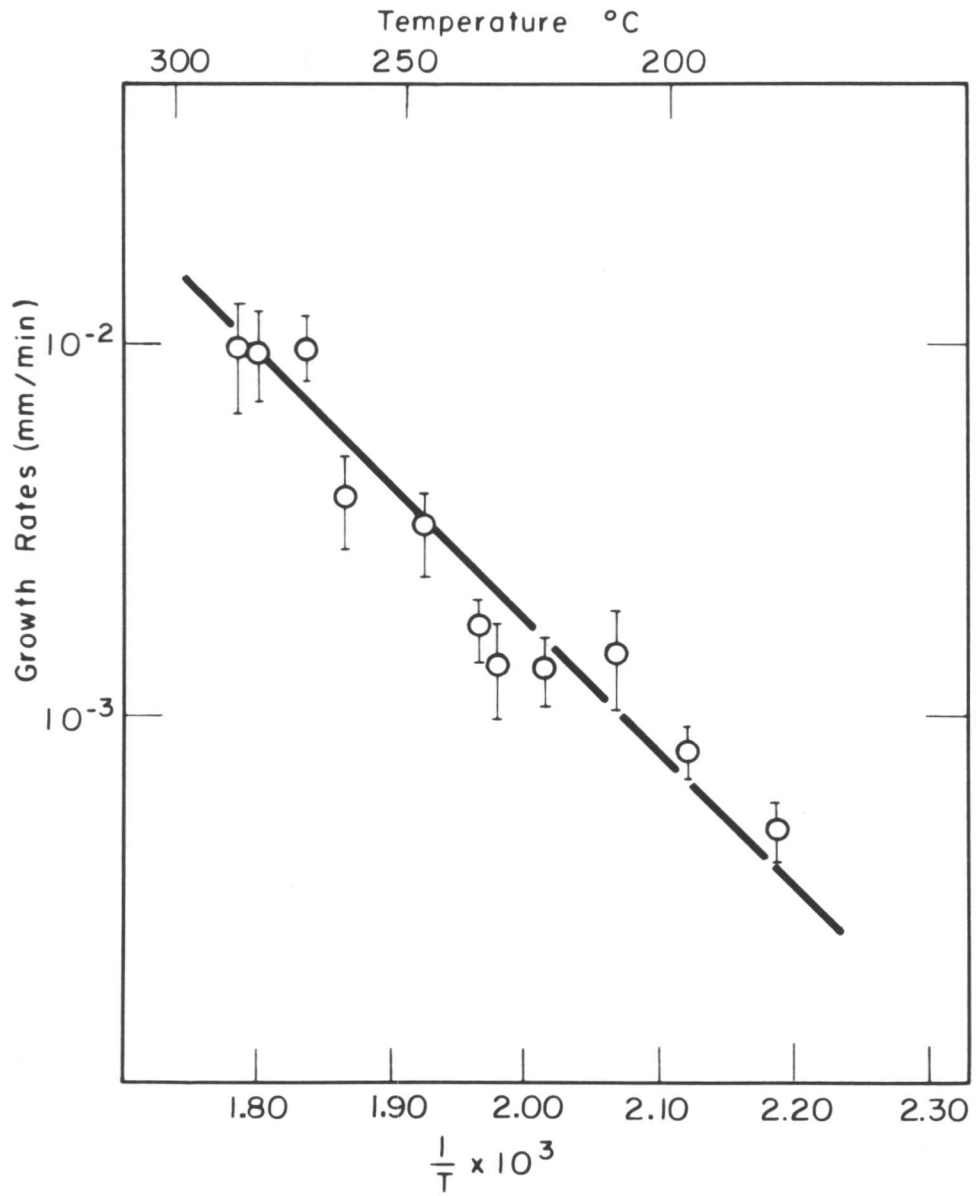


FIG.37 AVERAGE GROWTH RATES FOR A 1.16 % C, IRON - CARBON ALLOY

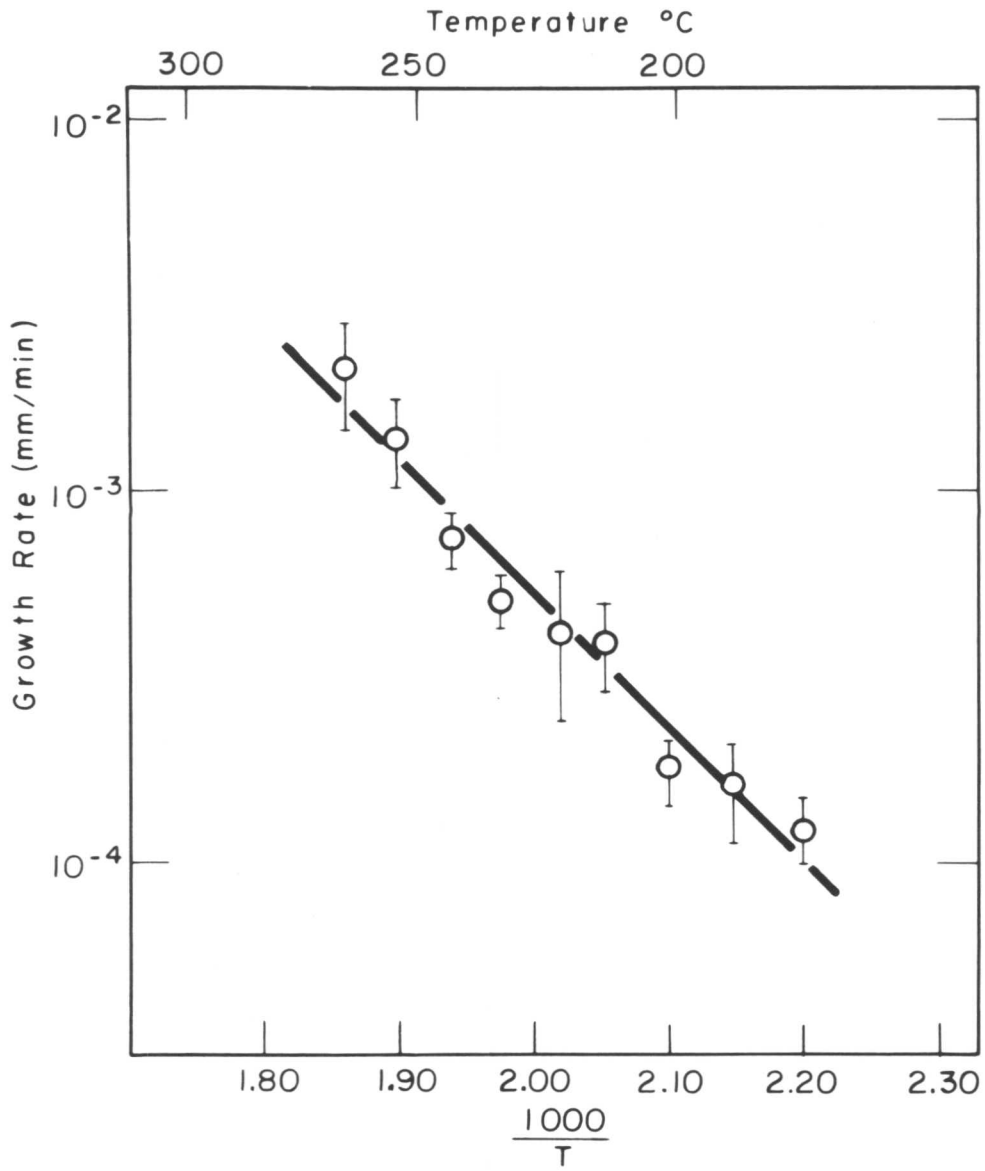


FIG. 38 AVERAGE GROWTH RATES OF A 1.43 %C, IRON-CARBON ALLOY

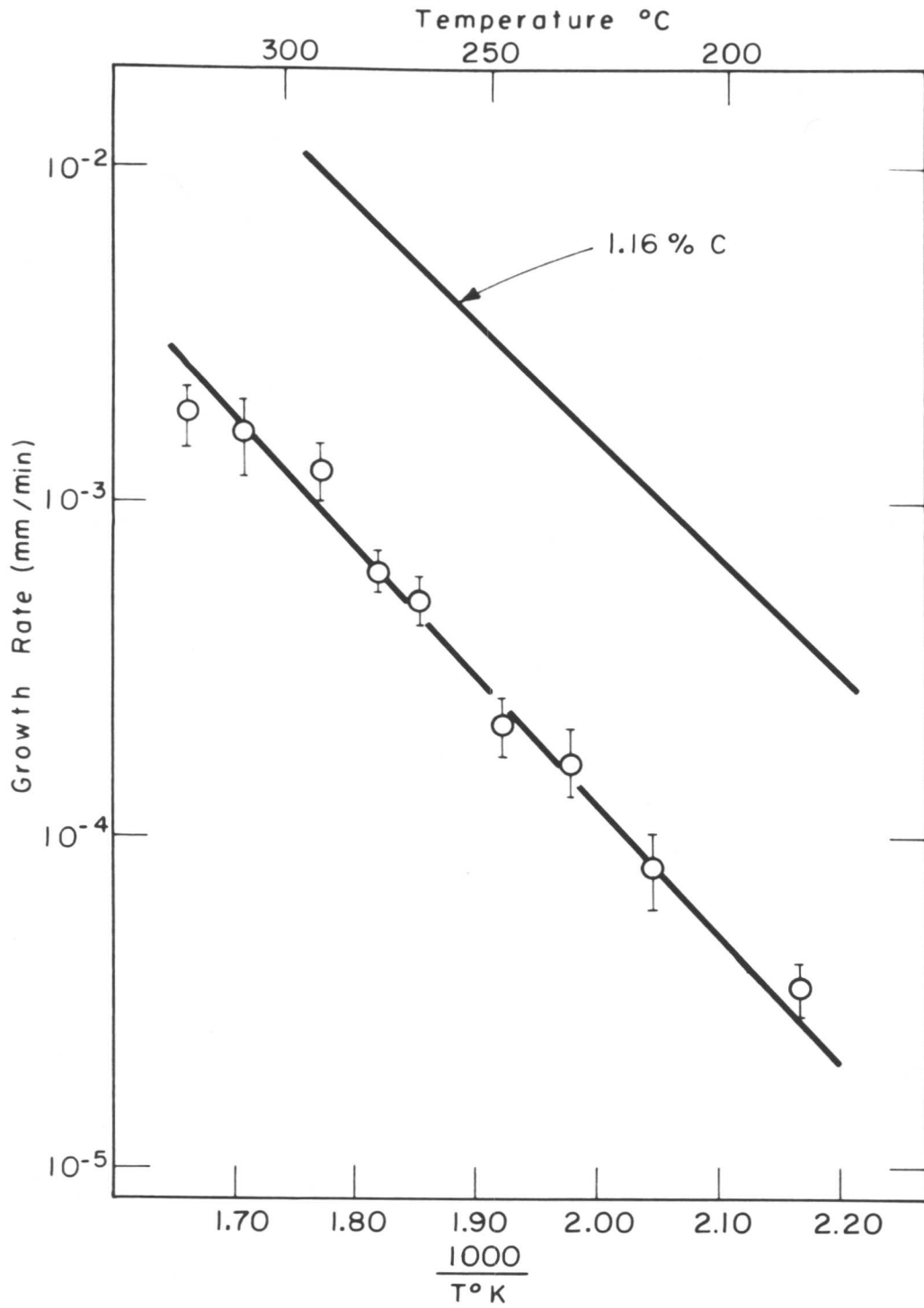


FIG. 39 AVERAGE GROWTH RATES FOR A 1.14 %C, 2.71% Cr, IRON-CARBON-CHROMIUM ALLOY

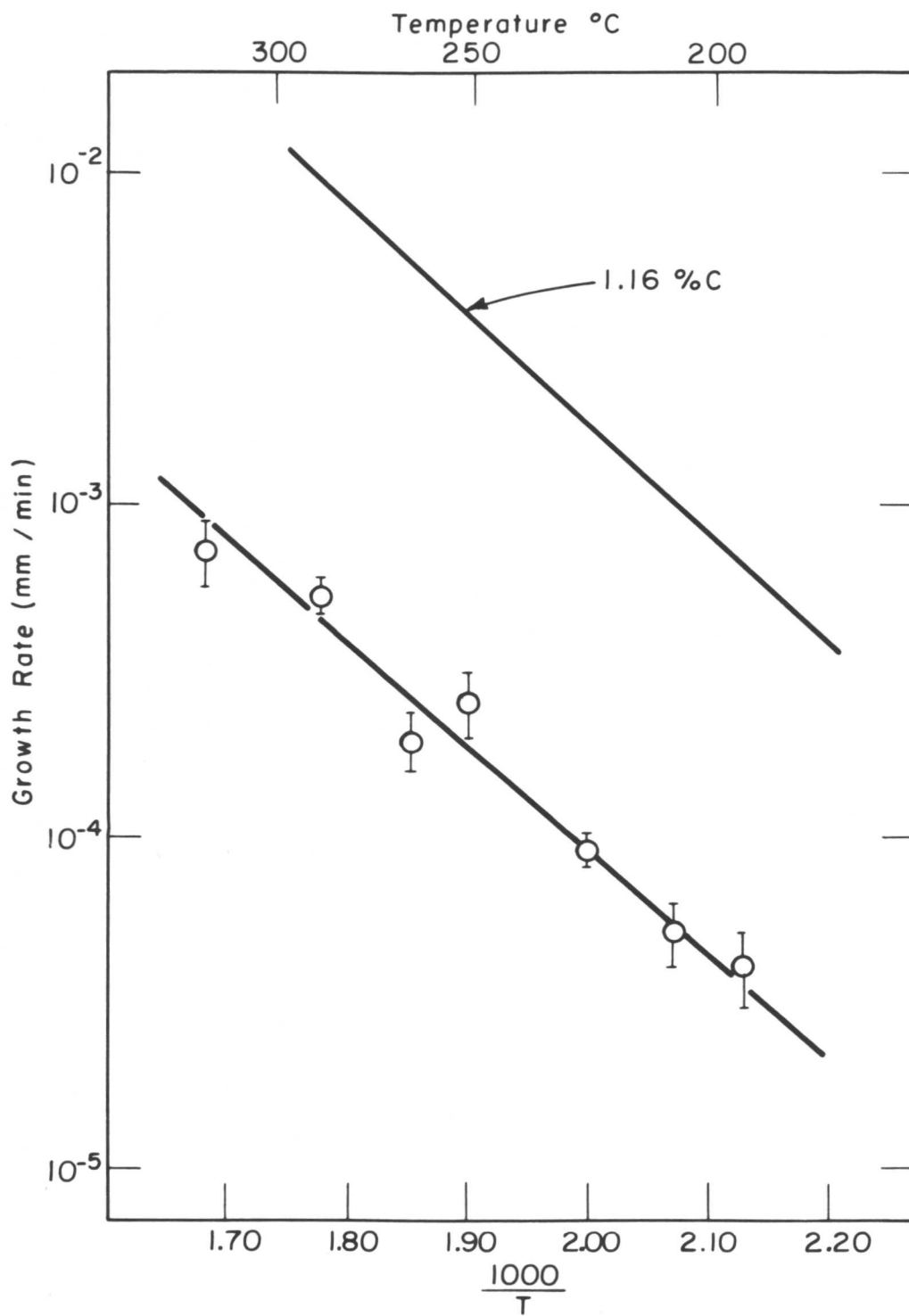


FIG. 40 AVERAGE GROWTH RATES FOR 1.12% C, 5.28% NI, IRON-CARBON-NICKEL ALLOY

TABLE II
Values of Q_1 and B

<u>Composition</u>	<u>Q_1</u>	<u>ln B</u>	<u>B (mm/min)</u>
0.96% C	15800	10.240	2.75×10^4
1.16% C	16400	10.222	2.76×10^4
1.43% C	16600	9.140	9.31×10^3
1.14% C, 2.71% Cr	17600	9.070	8.50×10^3
1.12% C, 5.28% Ni	14300	5.124	1.65×10^2

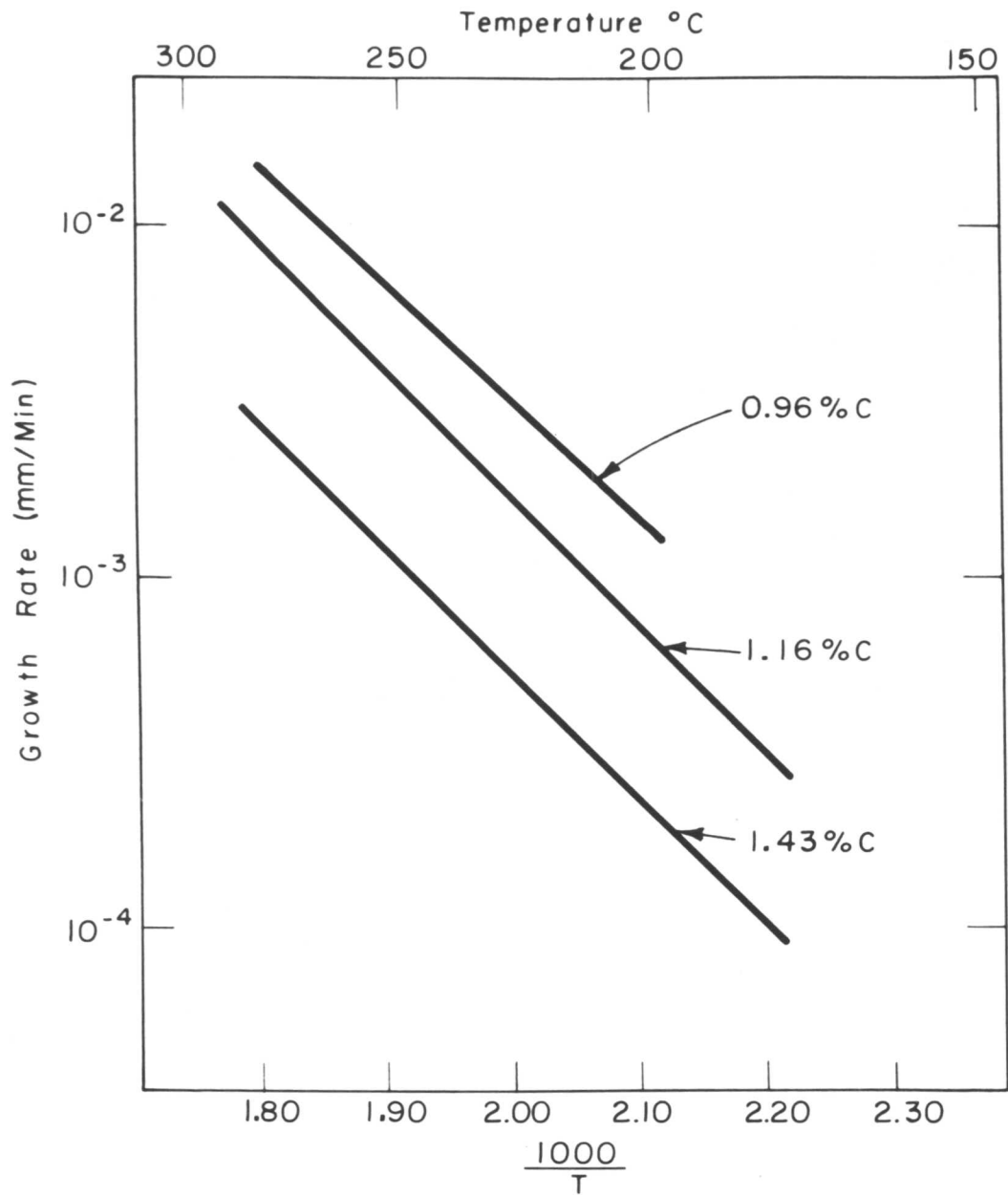


FIG. 41 THE EFFECT OF CARBON ON BAINITIC GROWTH RATES IN HIGH-PURITY IRON-CARBON-ALLOYS

although there is a slight trend toward larger values with increasing carbon contents.

The effect of chromium and nickel on the bainitic growth rates at a constant carbon level of about 1.1 percent can be evaluated from Figures 39 and 40. The line representing the growth rate equation for the 1.16 percent carbon iron-carbon alloy is shown in each figure for comparison with the growth rates for the alloys of the same carbon content but containing either chromium or nickel. It can be seen that additions of either chromium or nickel at a carbon level of 1.1 percent markedly lowers the bainitic growth rates. The activation energies for growth seem to be somewhat raised by chromium and lowered by nickel (See Table II).

4.1.5 Width Measurements

Since the growth rate measurements have only considered growth in the long direction of the bainitic plate, it was felt advisable to make width measurements. This was not possible with the hot-stage microphotographs because of the poor resolution of the width of the plates. In order to obtain some measure of the width, the widths of a number of bainitic units were measured on a series of normal light photomicrographs, e.g. Figures 50 to 56. The lengths of the bainitic units were measured at the same time. The ratio l/w at one temperature and composition, was found to be roughly constant with an average deviation of ± 20 percent from the average value. The

value of l/w did, however decrease sharply with increasing temperature. The results are shown in Figure 42. Since the data for all five alloys fall on the same curve, it would seem that the value of l/w is not very sensitive to compositional changes.

The values of l/w and the measured values of \dot{V} allow one to calculate the volume growth rate of the bainitic areas. This subject is treated in more detail in the discussion section.

4.1.6 Hot-Stage Lengths Compared to Metallographic Lengths

Since there is some question as to whether the length measured by the surface relief actually represents the true plate length, a number of samples were prepared with a reference grating ruled on the surface with microhardness indentations. It was then possible to find the area viewed on the hot stage after the sample had been removed from the stage. In this way, the lengths obtained from the surface relief effects could be compared with the lengths obtained from normal metallography after lightly etching the sample. The appearance of the same area, on the hot stage and after etching, are shown in Figures 43 and 44. The comparison of etched and hot-stage lengths for a number of samples are shown in Figure 45. The line drawn in this figure has a 45° slope, and if the etched and hot-stage lengths were identical all the points should fall on this line. This seems to be the case with a small amount of experimental scatter

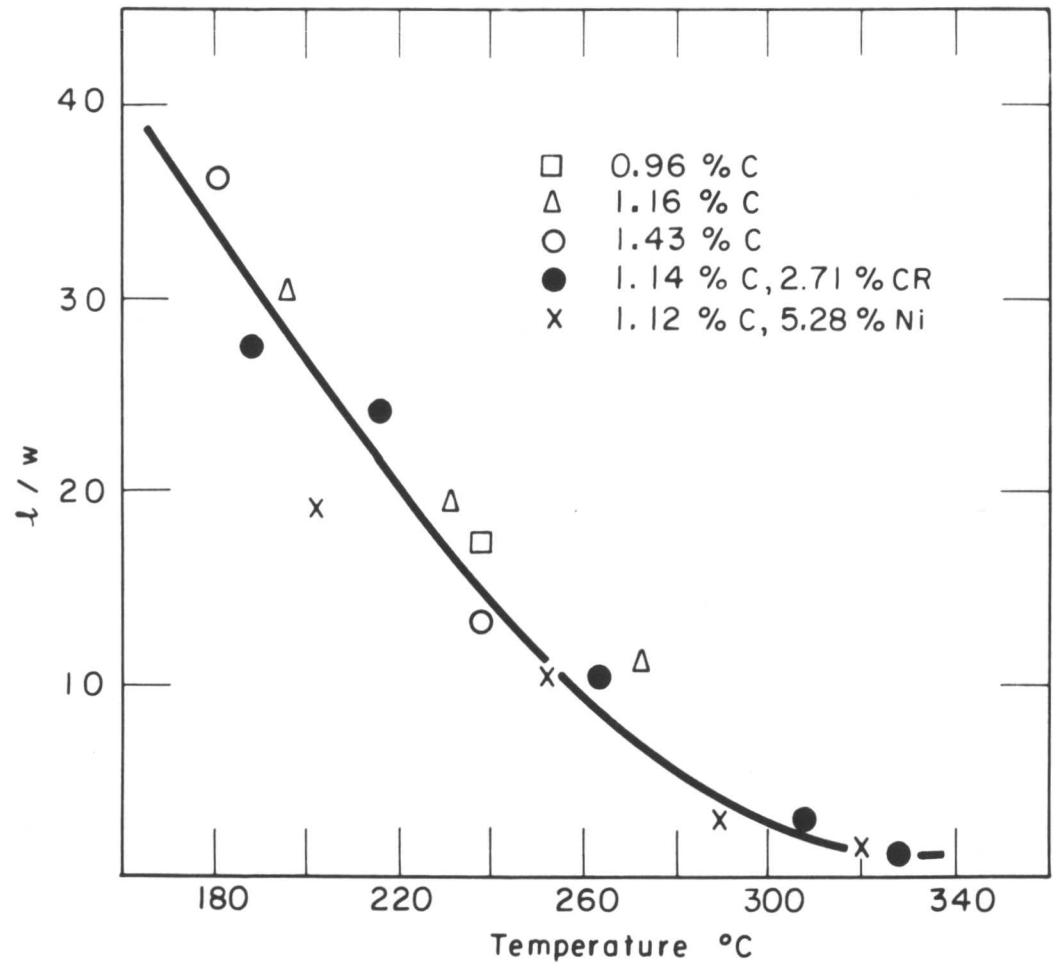
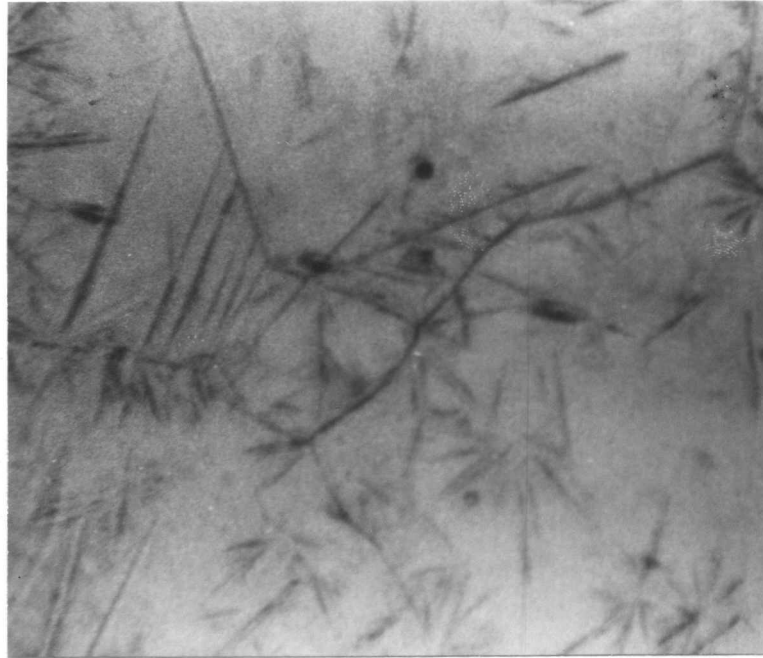


FIG.42 LENGTH-WIDTH RATIOS OF BAINITIC AREAS



250× Hot Stage
FIGURE 43. 1.14% C, 2.71% Cr Alloy; 30 min 1060° C/180 min
260° C. Unetched.



250× 1% Nital
FIGURE 44. 1.14% C, 2.71% Cr Alloy; 30 min 1060° C/180min.
260° C. Etched.

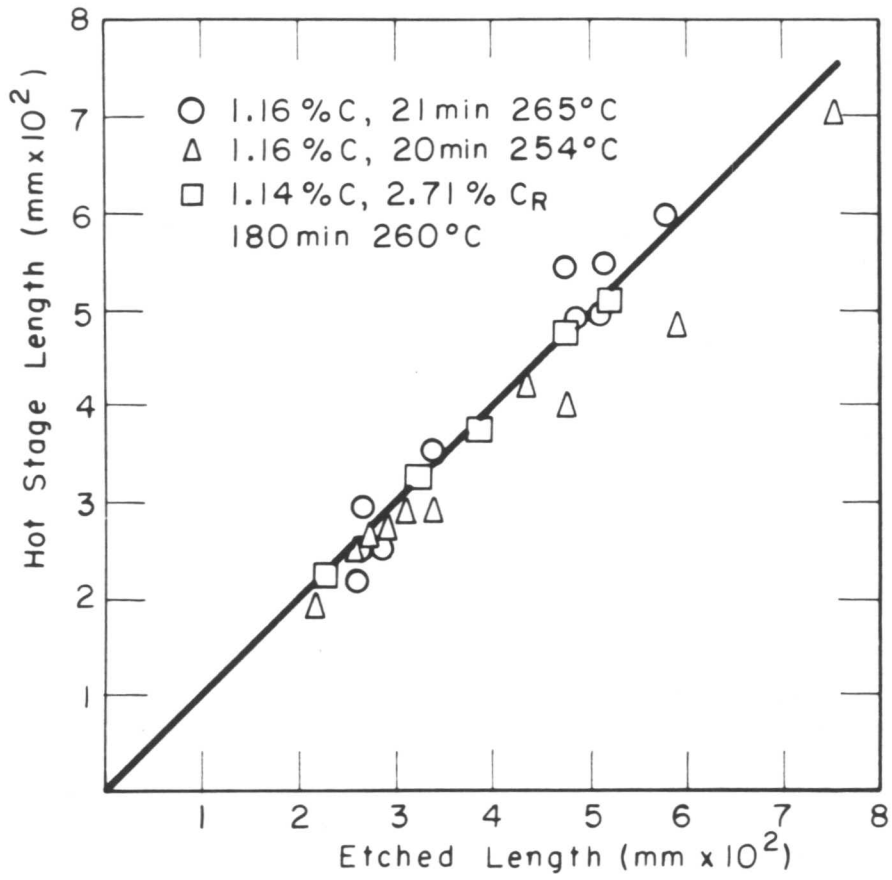


FIG. 45 COMPARISON OF HOT-STAGE AND ETCHED LENGTHS

present. Thus, we can safely assume that the lengths measured on the hot-stage are the true lengths of the bainitic areas.

4.2 M_s Measurements

The M_s temperatures of all the alloys were measured on the hot-stage by quenching to a temperature near M_s and then slowly cooling the sample. The temperature at which martensite first appeared was taken as the M_s temperature. Figures 46 and 47 show the appearance of the surface of a sample above and below M_s. Figure 48 shows the increase in the amount of martensite with decreasing temperature (Compare to Figure 45). The M_s results for the iron-carbon alloys are shown in Figure 49. The curve in Figure 49 is taken from the work of Greninger⁽⁴⁴⁾. The experimental M_s temperatures agree very well with Greninger's data.

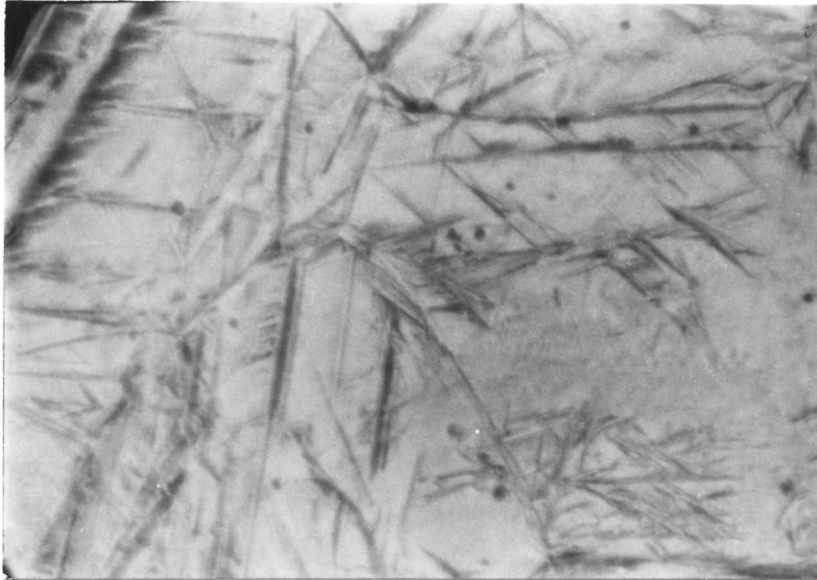
The M_s data for the iron-carbon-chromium and iron-carbon-nickel alloys are shown in Table III.

TABLE III

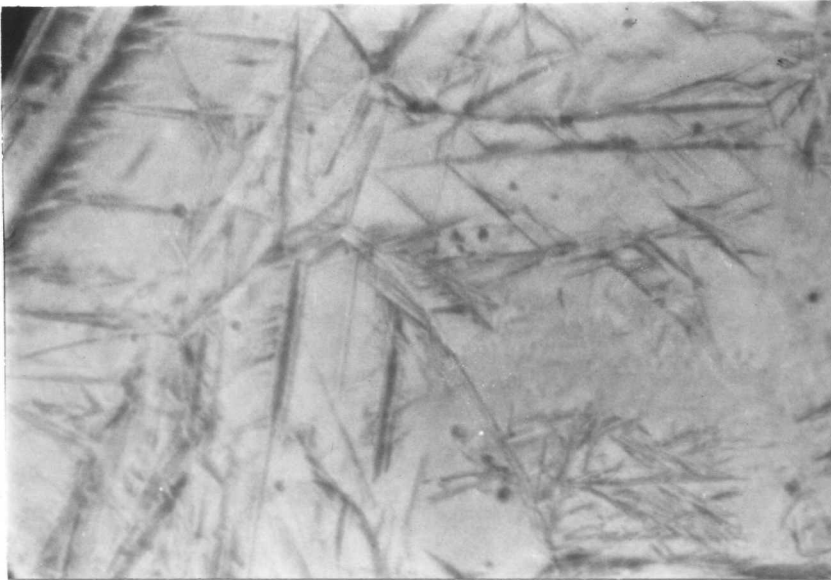
Alloy M_s Temperatures

<u>Composition</u>	<u>Hot Stage M_s</u>	<u>M_s (Exp)</u>	<u>Reference</u>
1.14% C, 2.71% Cr	87 ± 4° C	94° C	Lyman and Troiano ⁽¹⁴⁾
1.12% C, 5.28% Ni	93 ± 3° C	96° C	Howard and Cohen ⁽⁴³⁾

The value of M_s (exp) was taken from the literature with corrections



250X Hot Stage
FIGURE 49. 1.14% C, 2.71% Cr alloy 30 min 1060° C/74° C
(below M_s).



250X

FIGURE 48. 1.14% C, 2.71% Cr alloy 30 min 1060° C/74° C
(below M_s). Hot Stage

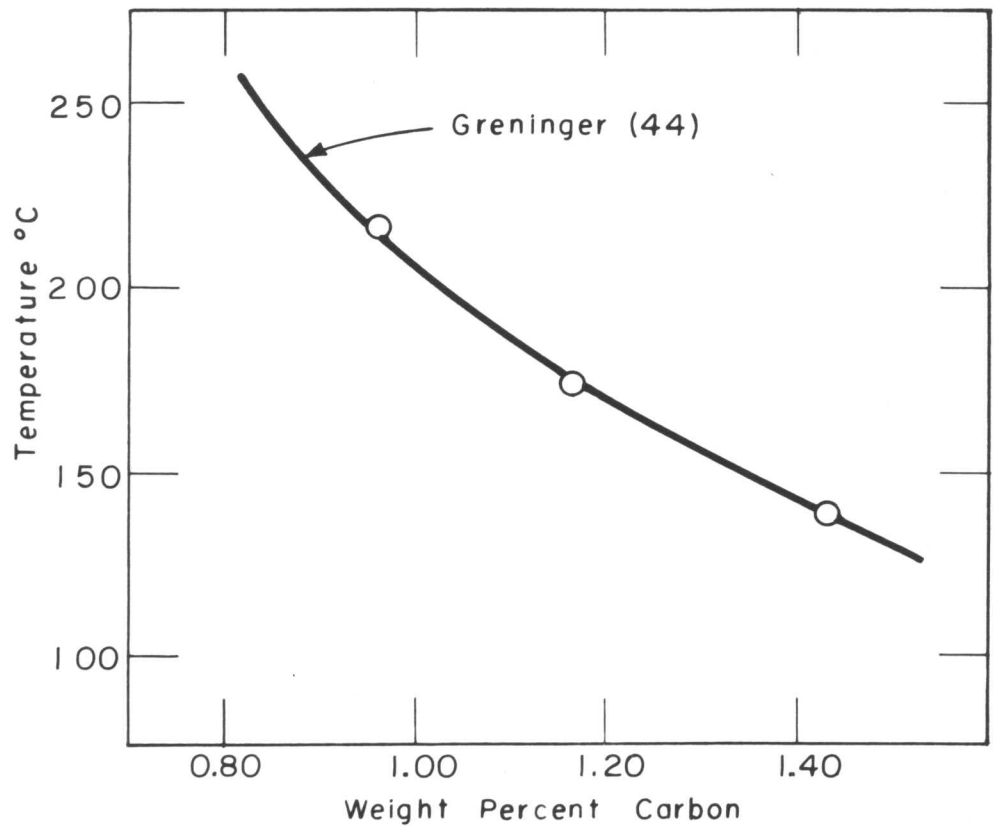


FIG.49 M_s TEMPERATURES FOR IRON-CARBON ALLOYS

being made for small differences in composition using the M_s formula of Payson and Savage⁽⁴⁵⁾. The agreement is quite good, considering the differences in method of determination of M_s .

Thus in addition to determining the M_s by the thermal arrest method, the Greninger-Troiano technique, and by a change in some physical property such as length or resistance, we have another reliable method of determining M_s . On the basis of these results, it would seem that the M_s at the free surface is identical with the volume M_s . It is rather surprising that the surface M_s is the same as the volume M_s , since the presence of the free surface should make the formation of martensite easier and thus raise the M_s .

One difficulty with this technique is that slow cooling is needed on the hot stage to assure thermal equilibrium, and this introduces the possibility of stabilization. The effect of different cooling rates on the M_s has not been investigated in this work.

4.3 Light Metallography

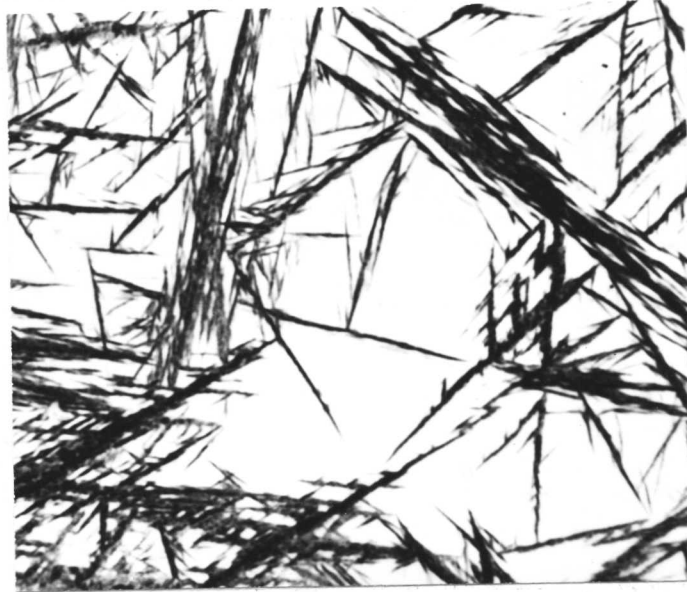
4.3.1 Chemically Etched Structures

In order to determine the general shape of the bainitic area as a function of temperature and composition, a number of samples were examined by normal light metallography. In all the alloys, the lower temperatures favored the more acicular structure, while at higher temperatures a structure very similar to nodular fine pearlite appeared. This behavior is also indicated by the l/w plot of Figure 40.

Typical structures for the iron-carbon alloys are shown in Figures 50 and 51. Contrary to general opinion, the low-temperature bainite did nucleate at grain boundaries in these alloys. This is shown in Figure 52. About the first 20 percent of the transformation seems to nucleate at the grain boundaries. The remaining transformation occurs by nucleation of new plates within the grains. Grain boundary nucleation has also been reported in the 1.43 percent carbon alloy by Werner⁽⁴⁶⁾. At present, it is not clear whether this effect is due to a fine precipitation of carbide formed during the quench at the grain boundaries or to the grain boundary per se.

Since the highest temperature studied in the case of the iron-carbon alloys was only 280° C, no nodular product was observed. However, Lister⁽⁶⁾ has studied the structure of the 1.16 percent carbon alloy over a wider range of temperatures and reports a nodular product at 370° C and higher temperatures.

The structures of the iron-carbon-chromium and iron-carbon-nickel alloys were similar to the iron-carbon alloys. Since a wider range of temperatures could be studied in these alloys, the change from the acicular structure to the nodular product was observed in these alloys. Typical structures are shown in Figures 53 - 56. It is interesting to note that the transition from the acicular structure to the nodular structure is very gradual.



1000X
FIGURE 50. 1.43% C iron-carbon alloy; 30 min. 1060° C/366 min. 161° C. 1% Nital



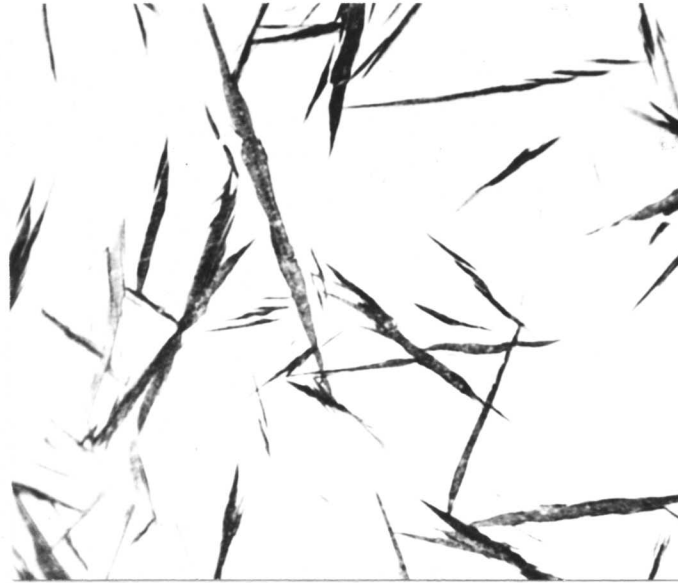
1000X
FIGURE 51. 1.43% C iron-carbon alloy; 30 min. 1060° C/43 min. 238° C. 1% Nital



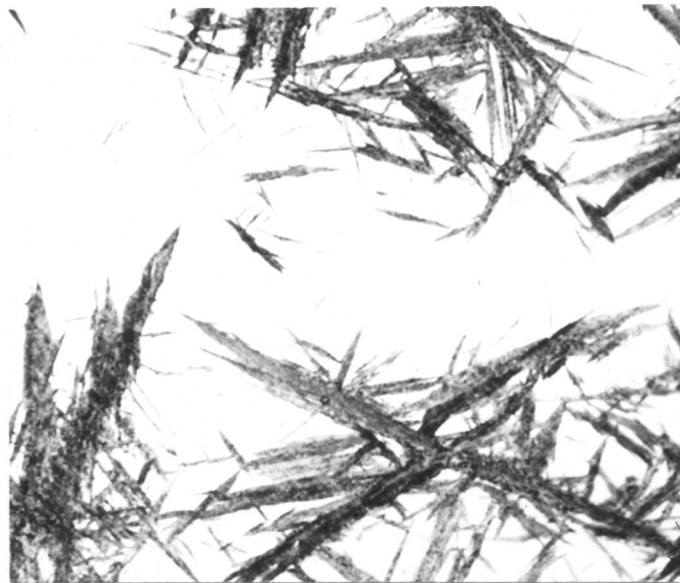
250×

1% Nital

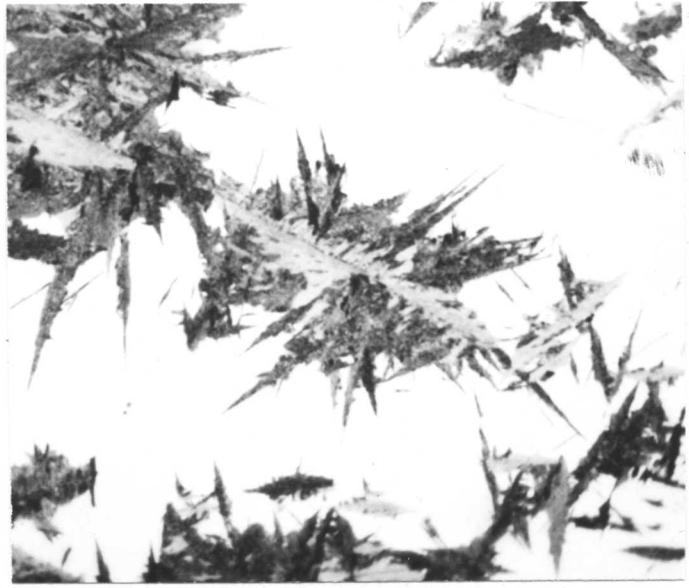
FIGURE 52. 1.43% C iron-carbon alloy; 30 min. 1060° C/366 min. 181° C.



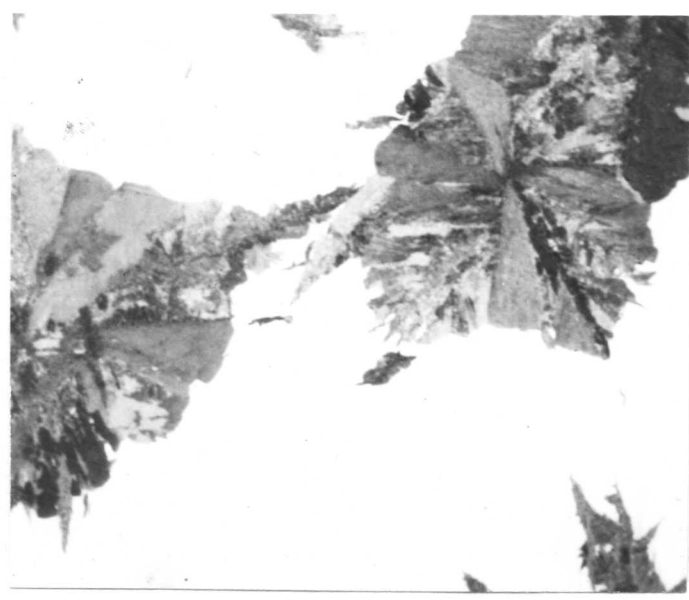
1000x
FIGURE 53. 1.14% C, 2.71% Cr alloy; 30 min. 1060° C/652 min. 215.7° C. 1% Nitral



1000x
FIGURE 54. 1.14% C, 2.71% Cr alloy; 30 min. 1060° C/180 min. 263° C. 1% Nitral



1000X 1% Nital
FIGURE 55. 1.14% C, 2.71% Cr alloy; 30 min. 1060° C/43 min.
307° C.

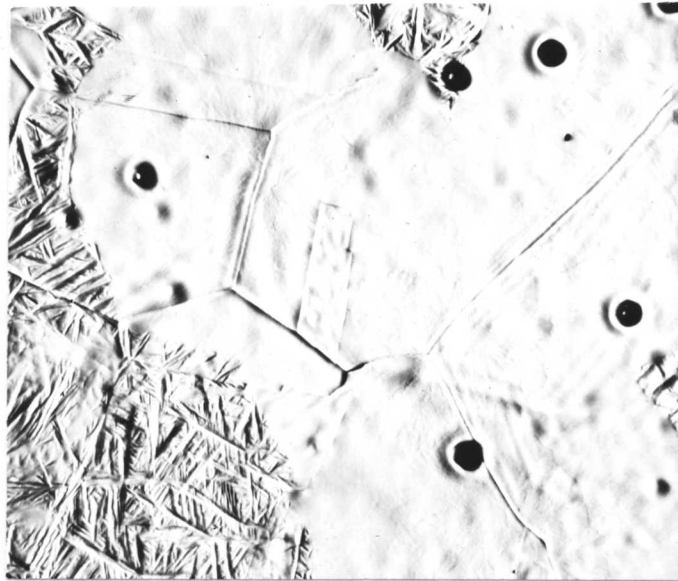


1000X 1% Nital
FIGURE 56. 1.14% C, 2.71% Cr alloy; 30 min. 1060° C/38 min.
328° C.

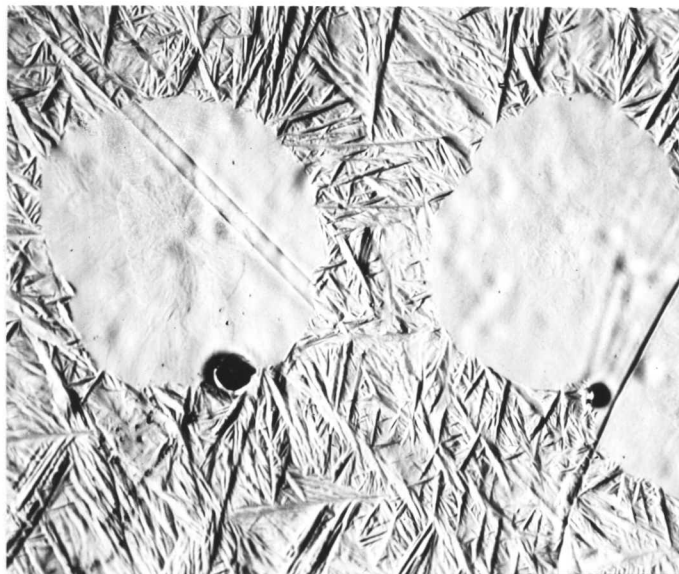
At 216° C the structure is quite acicular, almost needlelike; at 263° C the structure is still acicular, but the bainite areas are star-shaped; at 307° C, the structure is almost nodular but there are still remnants of acicularity at the edges of the bainite areas; finally, at 320° C the structure is almost completely nodular, with little acicularity left.

4.3.2 Thermally Etched Structures

The thermal etching that accompanied the austenitization on the hot-stage yielded some very interesting structures. Not only was it possible to see annealing twins, and former austenite grain boundaries, but also to see evidences of grain boundary migration. A sample of the 0.96 percent carbon iron-carbon alloy, which had not been cooled sufficiently rapidly to prevent the formation of some pearlite, is shown in Figures 57 and 58. The pearlite patches show up as flat, circular areas, while the remaining austenite which was transformed to bainite exhibits the surface upheavals characteristic of bainite. A number of annealing twins are visible in Figures 57 and 58. The austenitic grain boundaries and annealing twins show up in both figures due to thermal etching at the austenitizing temperature; in addition, a series of lines parallel to the final boundary position are visible (see left-hand side of both figures). These parallel lines are former positions of the boundaries where it stopped long enough for thermal etching to occur. This indicates that grain boundary migration



500X Oblique Lighting
FIGURE 57. 0.96% C iron-carbon alloy; 30 min. 1060° C/40 min.
237° C.



500X Oblique Lighting
FIGURE 58. 0.96% C iron-carbon alloy; 30 min. 1060° C/40 min.
237° C.

in the austenite is not continuous but "jerky".

The source of the pits present in these thermally etched structures is not at present clear. They may be thermally etched inclusions or dislocations, or possibly due to gas evolution⁽²⁾.

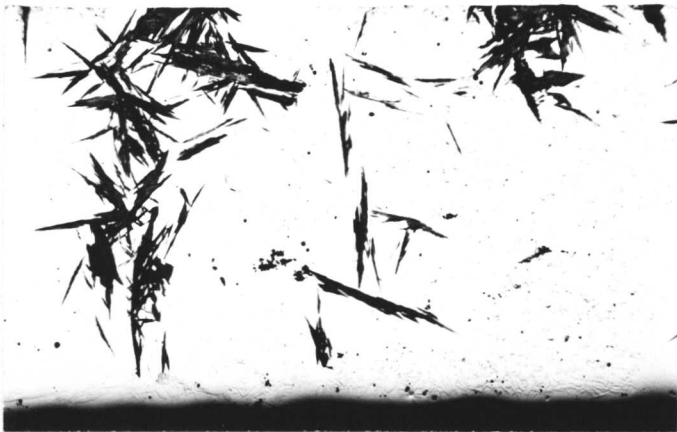
A closer examination of Figures 57 and 58 also reveal a substructure in the pearlite nodules. This appears as another nodule about half the diameter of the larger one. The explanation of this substructure is not known.

4.3.3 Effect of the Free Surface

In order to observe the distribution of plates with respect to the free surface, a number of samples were nickel plated and the cross section metallographically polished. A typical result is shown in Figure 59. There are plates growing down from the surface, which have probably nucleated at or near the surface. In addition, there are a number of plates which have nucleated within the center of the sample. The volume percent transformation does not seem to be much different at the surface than in the interior of the sample. The question as to whether or not the surface influences the rate of transformation cannot be settled by this limited information, but from the evidence available it does not seem that the surface has a very marked effect on the transformation rate.

4.4 Electron Metallography

In order to determine the distribution of carbide particles within



← Copper Foil

← Nickel Plate

250X

1% Nitral

FIGURE 59. 1.16% C iron-carbon alloy; 30 min. 1060° C/23 min. 253° C.

the ferrite phase of bainite, a number of samples were examined by electron microscopy. The details of the sample preparation are given in the experimental procedure section. Some representative electron micrographs are shown in Figures 60 - 65. It can be seen that the carbide distribution becomes coarser as the temperature is raised. In all cases the carbide particles are surrounded by a ferrite sheath, and no carbide precipitation is visible in the austenite or in the interface. The carbides appear to line up roughly parallel to the long axis of the bainite areas at high temperatures, and at some angle to the long axis at lower temperatures. These results are in agreement with other work⁽⁸⁾.

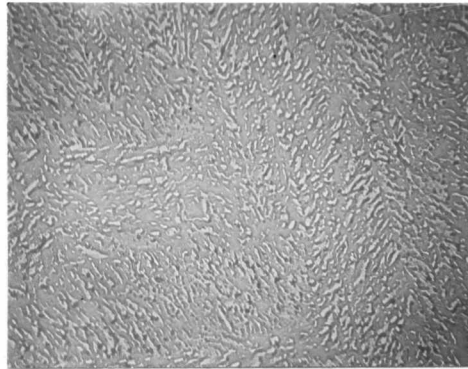
4.5 Electron Diffraction

A number of samples were examined by electron diffraction to determine the nature of the carbide phase formed in bainitic structures at lower temperatures. X-ray diffraction analysis is not practical here due to particle size broadening.

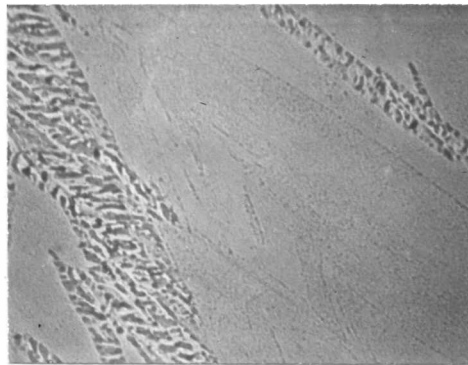
The electron diffraction unit was calibrated with an iron standard, giving the following formula for the d spacings:

$$d = \frac{16.81}{R} \quad (18)$$

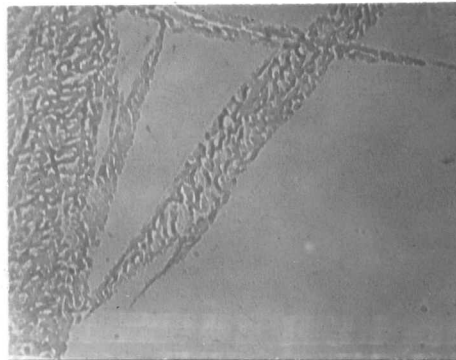
where d is the d spacing in Å for the line whose radius on the film is R mm. The reflection method was used with the sample being etched to make the carbide stand in relief.



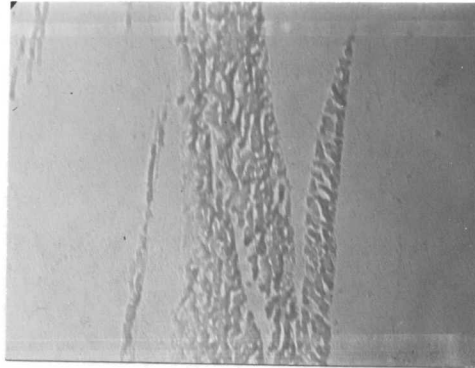
8000X
FIGURE 60. Chromium Shadowed
1.16% C iron-carbon alloy. 30 min.
1060° C/34 min. 30 sec. 270° C.



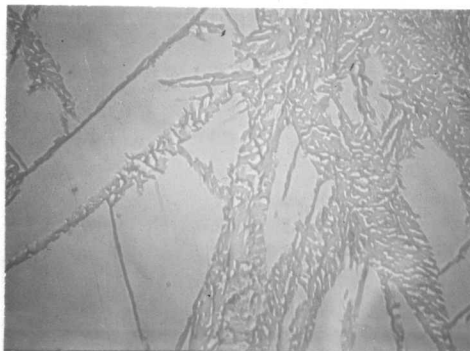
14000X
FIGURE 61. Chromium Shadowed
1.43% C iron-carbon alloy. 30 min.
1060° C/366 min. 181° C.



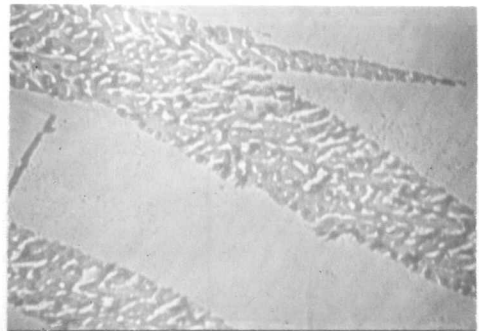
14000X
FIGURE 62. Chromium Shadowed
1.43% C iron-carbon alloy 30 min.
1060° C/43 min. 237.7° C.



14000 \times Chromium Shadowed
FIGURE 63. 1.14% C, 2.71% Cr alloy; 30 min.
1060° C/3017 min. 188° C

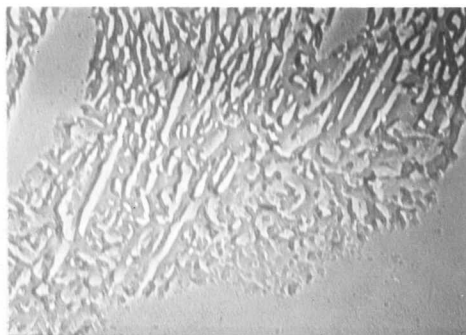


(a) 8000 \times Chromium Shadowed



(b) 14000 \times Chromium Shadowed

FIGURE 64. 1.14% C, 2.71% Cr alloy; 30 min. 1060° C/
180 min. 263° C.



14000 \times Chromium Shadowed
FIGURE 65. 1.14% C, 2.71% Cr alloy; 30 min.
1060° C/38 min. 328° C.

Sharp diffraction patterns were only obtained for samples transformed above 300° C; nevertheless, it was also possible to make measurements on the samples transformed at lower temperatures, even though the lines were broadened. The results are given in Table IV along with the expected d spacings for ϵ -carbide formed in martensite tempered at 120° C and cementite formed in martensite tempered at 250° C, according to Jack⁽⁴⁰⁾. The position of the iron lines are also given for reference.

The number of lines found for samples transformed below 300° C ranged from four to eight. Above 300° C, many more lines appeared in the diffraction patterns. Although the lines for the samples transformed below 300° C agreed roughly with the number to be expected from an ϵ -carbide pattern (seven), the positions of some of the lines could not be explained by an ϵ -carbide structure. For instance, in the 1.43 percent carbon alloy transformed at 181° C, good agreement between the ϵ -carbide lines and the observed lines are found for d spacings of 1.17, 1.23, 1.38, 1.62, 2.10 and 2.39 Å; however, the line at 1.91 Å cannot be explained by either ϵ -carbide, cementite, or iron. This may be a line due to surface oxide or some other form of contamination. However, in most cases the lines present could be fitted to an ϵ -carbide pattern if allowances were made for the error in measurement of the d values from broadened lines (say 3 - 4 percent). Allowances also had to be made for one or two lines to be missing or

043
 410
 1.09mw 411
 1.02 - "
 1.01

	1.09nm	1.06nm	1.09nm		
		0.953w	0.965w	1.03	220
		0.884w	0.899w	0.901	310
		0.809w	0.805w	0.826	222
		0.764w	0.765w	0.765	321
		0.697vw		0.717	400
				0.674	411
				0.653	330
				0.610	420
				0.596	332
		0.597vw		0.570	422
				0.570	510
				0.533	431
				0.516	521
				0.489	440
				0.489	530
					433

* Overlapping ferrite reflections.

** Not reported by Jack, but found by Lagerberg and Lement⁽¹⁷⁾.

added to the patterns. The additional lines could be explained on the basis of cementite or contaminants. It is not clear why some lines are missing from the diffraction patterns.

Above 300° C, a number of new lines appeared in the diffraction patterns. The d values for some of these lines were, however, too low to be indexed as new cementite lines. It is possible that some of these lines are iron lines.

There seems to be strong evidence from these results, that below 300° C, the carbide phase present in bainitic structures is ϵ -carbide. At temperatures above 300° C, a number of new lines appear in the diffraction patterns which cannot be completely indexed as new cementite lines. This agrees in part with the results of Austin and Schwarts⁽¹¹⁾ who found both ϵ -carbide and Fe_3C present in bainitic structures formed at 500° F (260° C) in a eutectoid plain-carbon steel. Further electron diffraction work should be done in order to more fully clarify the nature of the carbide phase forming in bainitic structures at lower temperatures.

5. DISCUSSION OF RESULTS

5.1 Volume Growth Rates

Since the hot-stage length measurements only gave the rate of growth in the long dimension of the bainite region, the width measurements described in Section 4.1.5 were also made. From these two growth measurements, it is possible to calculate volume growth rates if some simple shapes are assumed for the bainite regions. At temperatures below 250° C, the bainite regions are assumed to have a disc shape. At temperatures above 300° C, the bainite regions are assumed to be spherical. The intermediate temperature range (250 - 300° C) is not treated here due to the complex shape of the bainite regions.

For a disc, the volume is given approximately by:

$$V = \frac{1}{2} \pi R^2 w \quad (19)$$

where V is the volume of the disc, R is the radius, and w is the width at the center. Now if we assume that the discs are sectioned close to their centers in the hot stage measurements, $l = R$ and the w values reported in 4.1.5 represent the widths at the centers of the plates. If we let $\frac{l}{w} = A$, where A is independent of time and composition, but dependent on temperature, we obtain:

$$V = \frac{\pi}{2A} l^3 \quad (20)$$

Since the growth rate is constant, $l = kt$ and substitution in (20) gives:

$$V = \left(\frac{\pi}{2A}\right) \dot{i}^3 t^3 \quad (21)$$

The volume growth rate is then given by:

$$\dot{V} = \left(\frac{3\pi}{2A}\right) \dot{i}^3 t^2 \quad (22)$$

The variation of A can be fairly well represented from 180° C to 250° C by the equation:

$$\ln A = \frac{7680}{RT} - 4.93 \quad (23)$$

Substituting (17) and (23) in (21) and (22) gives:

$$V = \left(\frac{137\pi}{2A}\right) t^3 \exp\left(-\frac{(3Q_f + 7680)}{RT}\right) \quad (24)$$

$$\dot{V} = \left(\frac{411\pi B^3}{2}\right) t^2 \exp\left(-\frac{(3Q_f + 7680)}{RT}\right) \quad (25)$$

The values of B and Q_f are given in Table II.

Now if we assume that the bainite region has a spherical shape,

$l/w = 1$, and the volume is given by:

$$V = \frac{4}{3} \pi R^3 \quad (26)$$

Assuming once again that $l = R$, and $\dot{l} = \dot{i}t$, we obtain:

$$V = \frac{4}{3} \pi \dot{i}^3 t^3 \quad (27)$$

and

$$\dot{V} = 4\pi \dot{i}^3 t^2 \quad (28)$$

Using equation (17) for \dot{i} we obtain:

$$V = \left(\frac{4}{3} \pi B^3\right) t^3 \exp\left(-\frac{3Q_f}{RT}\right) \quad (29)$$

$$\dot{V} = (4\pi B^3) t^2 \exp\left(-\frac{3Q_f}{RT}\right) \quad (30)$$

5.2 Comparison of Experimental Data with the Krisement-Wever

Theory

The Krisement-Wever theory has been discussed in some detail in Section 2.7.6. The Krisement-Wever formula for the rate of surface displacement is given by:

$$\dot{X} = \beta \exp\left(-\frac{\bar{A}}{RT}\right) \quad (31)$$

Krisement and Wever did not consider the case of lenticular shaped regions where there are two growth rates, i.e. \dot{i} and \dot{w} . Since Krisement-Wever did not evaluate the proportionality constant in (31), it is not possible to make a quantitative comparison with the experimental data in this work. However, the activation energies for growth can be compared with the value of \bar{A} predicted by Krisement and Wever, i.e. $A_{coh} \leq \bar{A} \leq A_c^Y$. The equations for \dot{i} and \dot{w} are:

$$\dot{i} = B \exp\left(-\frac{Q_f}{RT}\right) \quad (32)$$

$$\dot{w} = \frac{\dot{i}}{A} = 137 B \exp\left[-\frac{(Q_f + 7680)}{RT}\right] \quad (33)$$

The values of B and Q_f are given in Table II. The values of A_c^Y determined by Wells, Bartz and Mehl are shown in Table V.

TABLE V

Activation Energy for Carbon Diffusion in Austenite⁽⁴⁷⁾

<u>Atomic % C</u>	<u>Weight % C</u>	<u>A_c^V (cal/mol)</u>
1.0	0.22	35,800
2.0	0.44	34,500
3.0	0.67	33,300
4.0	0.89	31,800
5.0	1.11	30,200
6.0	1.33	28,500

The value of A_{coh} is not known but is some very small value since martensite is observed to form at $4^\circ K$ ⁽⁴⁸⁾. The value of A_{coh} is certainly less than 3000 cal/mol⁽⁴⁸⁾. The values of Q_f and $Q_w = Q_f + 7680$ cal/mol can be seen to agree with the prediction of Krisement and Wever that the activation energy for growth should lie between A_{coh} and A_c^V . However, the value of Q_f does not show any significant dependence on carbon content as predicted by Krisement and Wever.

Another check on the Krisement-Wever theory can be made since we have the overall activation energies for the bainite transformation in a series of high-purity iron-carbon alloys from the work of Radcliffe⁽⁴⁹⁾ which are shown in Table VI.

TABLE VI
Overall Activation Energies for Bainite⁽⁴⁹⁾

<u>Material</u>	<u>% C</u>	<u>-Q (cal/mol)</u>	
		<u>Above 350° C</u>	<u>Below 350° C</u>
Plain carbon steel	0.65	18,500	7,500
Iron-carbon alloy	0.77	22,000	9,500
Iron-carbon alloy	1.02	29,000	11,500
Iron-carbon alloy	1.2	32,000	13,000

The values which pertain to this work are those for temperatures below 350° C since no studies of the growth rates were made at higher temperatures. The Kricement-Wever formula for the relation between the overall activation energy Q , and the values of A_c^Y and Q_2 is given by

$$Q = \frac{1}{4} (A_c^Y + 3Q_2) \tag{34}$$

The values of Q calculated from the values of A_c^Y of Wells et al⁽⁴⁷⁾ and the values of Q_2 from Table II are shown in Table VII.

TABLE VII
Overall Activation Energies

<u>%C</u>	<u>A_c^Y^(*)</u>	<u>Q (calc.)</u>	<u>Q(exp.)^(**)</u>
0.96	31300	19650	11000
1.16	29800	19700	12700
1.43	27700	19350	14900

(*) Values interpolated from Wells et al⁽⁴⁷⁾.
 (**) Values interpolated from Radcliffe (49).

It can be seen that the calculated values do not agree very well with the experimental values nor do the calculated values of Q depend on the carbon content as suggested by Krisement and Wever. If the values of the activation energy for growth in the width direction ($Q_w = Q_f + 7680$) are used instead of Q_f still poorer agreement would be obtained between the calculated and the observed values.

On the basis of these results, the Krisement-Wever theory is inadequate to explain the bainite growth rates below 350° C. Above 350° C, the Krisement-Wever theory may be more realistic since the observed overall activation energies do approach the value of A_c^Y at temperatures above 350° C and exhibit the correct dependence on carbon content (see Table VI). The fact that Radcliffe finds two different activation energies for the formation of lower and upper bainite may indicate that two different reaction mechanisms are operating. As suggested by Ko and Cottrell⁽²⁾, carbon removal from the austenite may occur by carbide precipitation in the ferrite at low temperatures and by carbide precipitation in the austenite at higher temperatures (where the Krisement-Wever theory may find application).

5.3 Comparison of Experimental Data with the Fisher Growth Model

A growth model assuming carbide precipitation within the ferrite phase was originally suggested by Fisher⁽²⁶⁾ and the expression he derived for the growth rate is given by equation (1). The present

section treats this growth model in more detail. The plane front growth model is shown schematically in Figure 66. The rate of growth of the carbide within the ferrite is given by:

$$\left(\frac{dx}{dt}\right)_c = \frac{(C_{\alpha\gamma} - C_{\alpha c})}{(C_c - C_{\alpha c})} \frac{D_c^{\alpha}}{(x - x_c)} \quad (34)$$

The rate of growth of the ferrite front is given by:

$$\left(\frac{dx}{dt}\right)_\alpha = \frac{(C_{\alpha\gamma} - C_{\alpha c})}{(C_0 - C_{\alpha\gamma})} \frac{D_c^{\alpha}}{(x - x_c)} \quad (35)$$

where x_c is the thickness of the carbide, x is the thickness of the ferrite-carbide aggregate, $C_{\alpha\gamma}$ is the carbon content in the ferrite at the α/γ interface, $C_{\alpha c}$ is the carbon content of the ferrite at the α /carbide interface, C_0 is the carbon content of the parent austenite, $\left(\frac{dx}{dt}\right)_\alpha$ is the rate of advance of the ferrite interface, $\left(\frac{dx}{dt}\right)_c$ is the rate of advance of the carbide interface, and D_c^{α} is the diffusion coefficient for diffusion of carbon in ferrite. In Figure 66, $C_{\gamma\alpha}$ is the carbon content of the austenite at the α/γ interface. The value of $C_{\gamma\alpha}$ is unknown but is assumed to be equal to C_0 in the present discussion. If the value of $C_{\gamma\alpha}$ was that for metastable equilibrium of ferrite and austenite in the absence of carbide, it would have some higher value than C_0 and this is shown by the dashed line in Figure 66.

In order to integrate (35) it is necessary to find a relation between x_c and x . This can be done using a carbon balance, since the carbon originally in the austenite must appear either in the ferrite or in the carbide, thus:

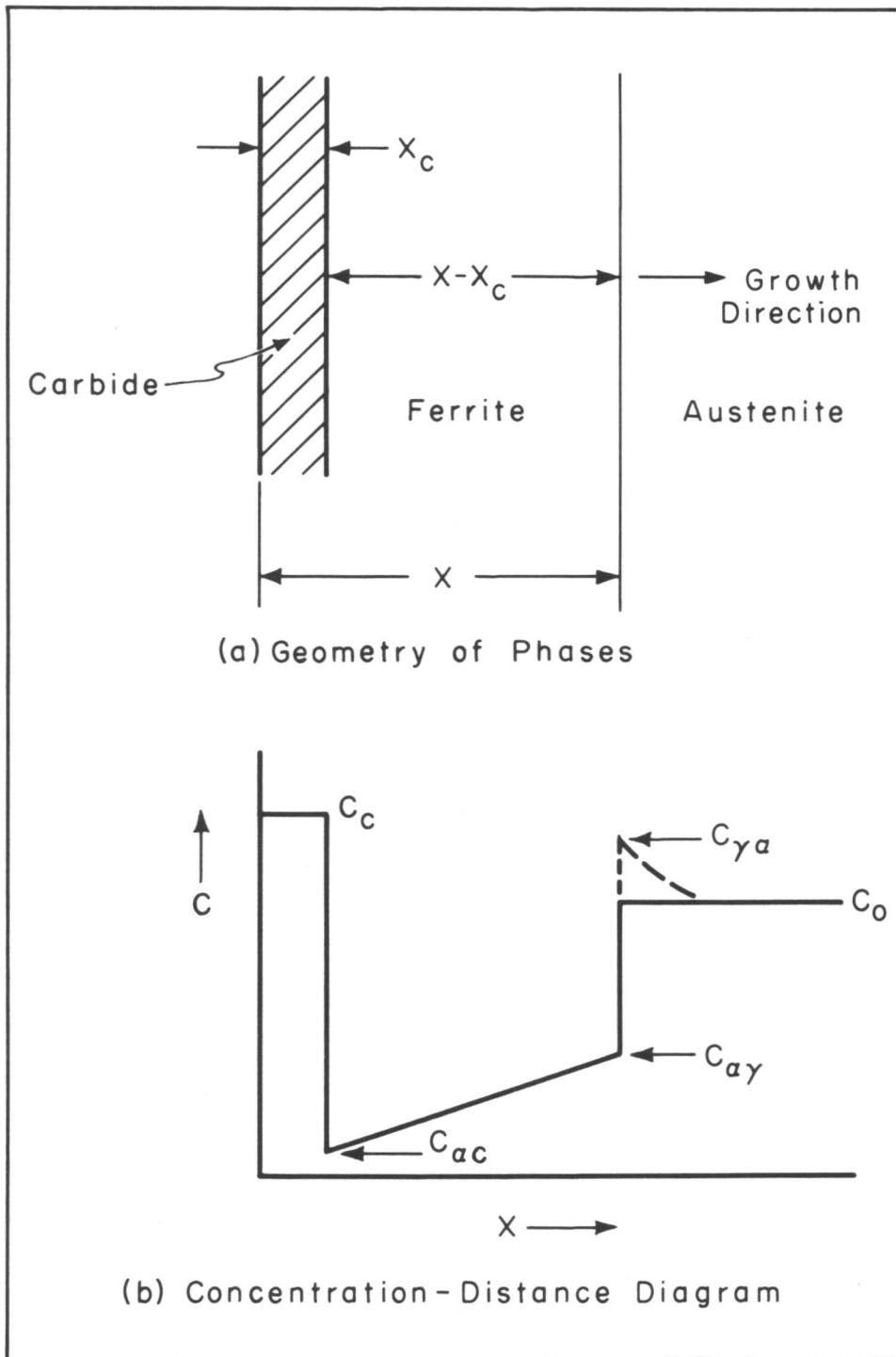


FIG. 66 - GROWTH MODEL FOR BAINITE

$$\int_{x_c}^x A C_e (X') dX' + A X_c C_0 = A X C_0 \quad (36)$$

where $C_e(X')$ is the concentration of carbon in the ferrite at a distance X' , and A is the area of the advancing front. The values of $C_e(X')$ is given by (37) if a linear concentration gradient is assumed in the ferrite.

$$C_e(X') = \frac{(C_{ey} - C_{ec})}{(X - X_c)} (X' - X_c) + C_{ec} \quad (37)$$

If (36) is substituted in (35) and the result integrated, we obtain

$$x_c = \frac{[C_0 - (\frac{C_{ey} + C_{ec}}{2})]}{[C_e - \frac{C_{ey} + C_{ec}}{2}]} X \quad (38)$$

If we assume that $\frac{C_{ey} + C_{ec}}{2} \ll C_0$ and $\frac{C_{ey} + C_{ec}}{2} \ll C_e$, we find:

$$x_c = \frac{C_0}{C_e} X \quad (39)$$

This is simply the result one would obtain by neglecting the carbon content of the ferrite.

Substituting (39) in (35) we obtain:

$$\left(\frac{dx}{dt}\right)_c = \frac{C_e (C_{ey} - C_{ec})}{(C_0 - C_{ey})(C_e - C_0)} \frac{D_c^2}{X} \quad (40)$$

Integrating (40)

$$X = \left[2 \frac{C_e (C_{ey} - C_{ec})}{(C_0 - C_{ey})(C_e - C_0)} \right]^{1/2} (D_c^2 t)^{1/2} \quad (41)$$

The growth rate is then given by:

$$\left(\frac{dx}{dt}\right)_c = \frac{1}{2} \left[2 \frac{C_c (C_{cy} - C_{cc})}{(C_o - C_{cy})(C_c - C_o)} \right]^{1/2} (D_c^s)^{1/2} t^{-1/2} \quad (42)$$

The growth law of (42) of course is only true if the growth of the carbide phase is continuous. In this case, the diffusion distance in the ferrite increases with time, and the parabolic growth law results. However, since carbide precipitation must occur intermittently in the ferrite between the carbide and austenite, this will shorten the diffusion distance for carbon and increase the growth rate. The growth rate for the overall process is something like that shown in Figure 67. The values of x_N and t_N are the values of x and t at which a new carbide particle nucleates in the ferrite region between the austenite and the existing carbide. If the nucleation of these new carbides occurs in a regular fashion, the growth curve shown in Figure 67 results. This is similar to the double-growth mechanism of Krisement and Wever except that the carbide phase is forming in the ferrite. The overall growth rate is given by

$$\frac{dx}{dt} = \frac{x_N}{t_N} \quad (43)$$

The values of x_N and t_N cannot be determined since the nucleation of rate of carbide cannot be experimentally measured. However, the value of x_N can be equated to the value of the average intercarbide spacing \bar{x}_c in the ferrite. From electron micrographs it is possible to

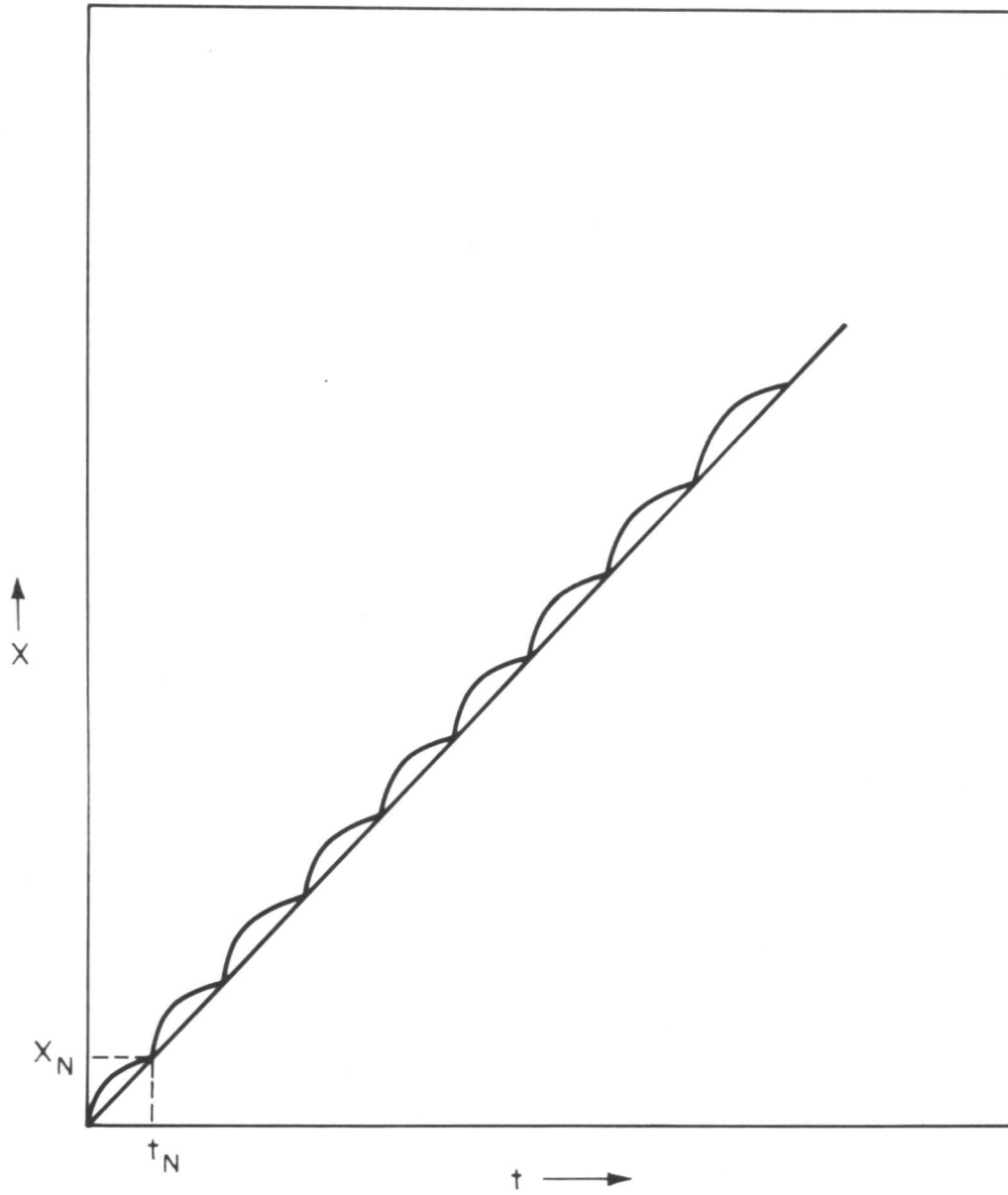


FIG. 67 - SCHEMATIC GROWTH PROCESS FOR BAINITE

determine this quantity. From (41) we obtain:

$$x_N = c (D_c^0 t_N)^{1/2} \quad (44)$$

$$\text{where } c = \left[\frac{2 C_c (C_{cy} - C_{cc})}{(C_0 - C_{cy})(C_c - C_0)} \right]^{1/2}$$

Substituting (44) in (43) and setting $x_N = \bar{x}_c$, we find that

$$\frac{dx}{dt} = \frac{c^2}{\bar{x}_c} D_c^0 \quad (45)$$

The relation between the precipitated carbides and the overall bainite region are shown schematically in Figures 68a and 68b. The two extremes shown are those where the carbides are lined up almost perpendicular to the long axis of the bainite plate (lower bainite) and where the carbides are lined up along the long axis of the bainite region (upper bainite). These diagrams are based on the electron microscope work of the ASTM Committee XI^(9, 10).

Using the results of Wert⁽³⁰⁾ for the value of D_c^0 , i.e.

$$D_c^0 = 0.02 \exp \left(- \frac{20100}{RT} \right), \text{ we obtain:}$$

$$\frac{dx}{dt} = \left(\frac{0.02 c^2}{\bar{x}_c} \right) \exp \left(- \frac{20100}{RT} \right) \quad (46)$$

The value of \bar{x}_c can be evaluated from electron micrographs by the use of lineal analysis. This can only be done for samples transformed above 230° C, since below this temperature the carbides are not resolvable by electron microscopy. The results of such measurements are shown in Table VIII.

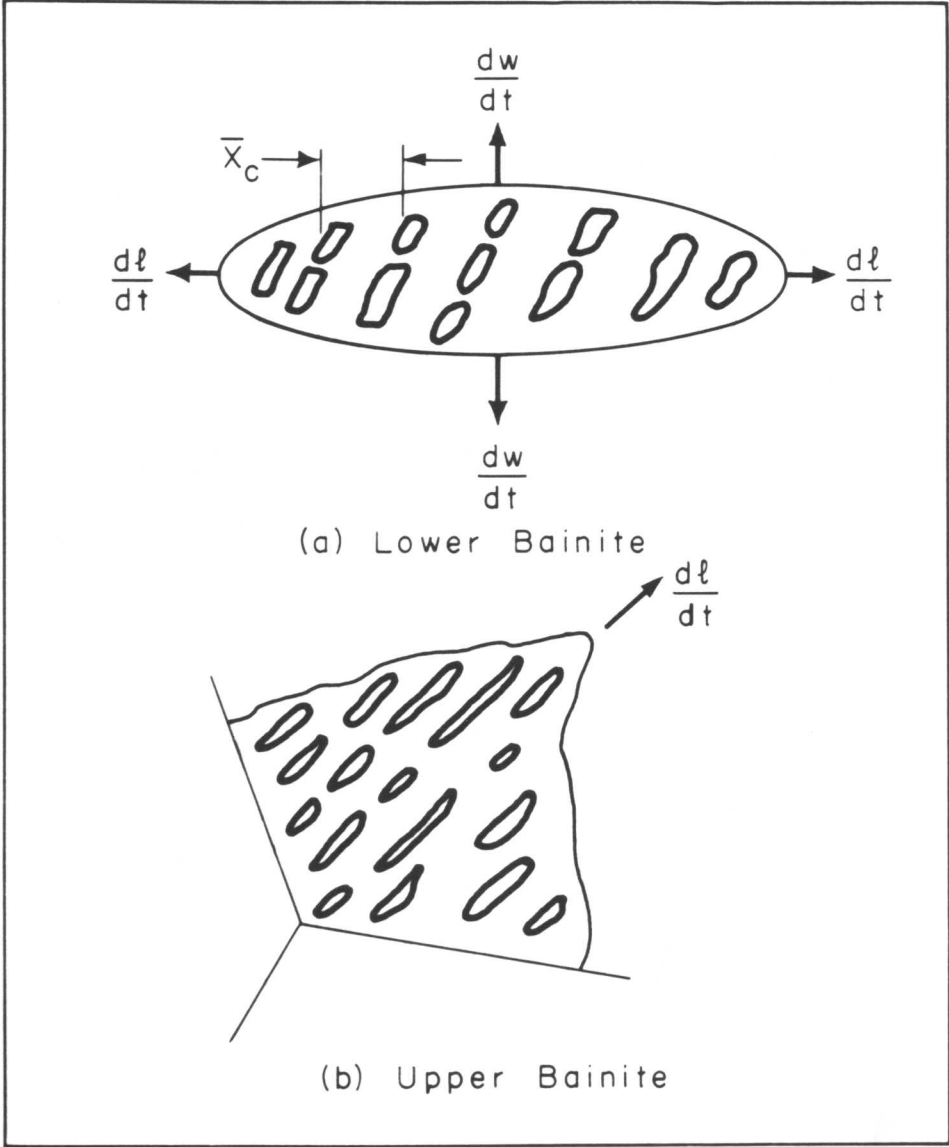


FIG. 68 - SCHEMATIC PICTURE OF CARBIDE DISTRIBUTION IN UPPER AND LOWER BAINITE

TABLE VIII

Intercarbide Spacings

<u>Composition</u>	<u>Isothermal Treatment</u>	<u>\bar{x}_c (cm)</u>
0.96% C	30 min. 237° C	1.97×10^{-5}
1.16% C	34 min. 30 sec. 270° C	2.49×10^{-5}
1.43% C	43 min. 238° C	1.41×10^{-5}
1.14% C, 2.71% Cr	180 min. 263° C	2.98×10^{-5}
1.14% C, 2.71% Cr	38 min. 328° C	2.55×10^{-5}
1.12% C, 5.28% Ni	54 min. 320° C	2.77×10^{-5}

The value of ϵ^2 is more difficult to evaluate since it involves a number of concentration parameters which can only be obtained by extrapolation. The values of C_c and C_o are of course known; C_{cc} can be obtained from the internal friction work of Wert⁽⁵¹⁾. He reports that the concentration of carbon in ferrite in equilibrium with carbide is given by:

$$C_{cc} \text{ (wt\% C)} = 2.55 \exp \left(- \frac{9700}{RT} \right) \quad (47)$$

These measurements were made at temperatures as low as 150° C so they should be reliable at temperatures in the bainite range. The only unknown concentration term left in the expression for ϵ is C_{cy} . This cannot be measured experimentally and can only be obtained by extrapolation of the ferrite/ferrite plus austenite boundary from high temperatures. This extrapolation can be done analytically by

use of Zener's formula⁽³²⁾:

$$C_{\alpha\gamma} = \frac{\Delta F'_m}{RT} \left[1 - \frac{1}{3} \exp\left(\frac{8100}{RT}\right) \right] \quad (\text{atomic percent}) \quad (48)$$

where $\Delta F'_m$ is the free energy change accompanying the transformation of one mol of austenite to one mol of ferrite in the absence of carbon.

The values of $C_{\alpha\gamma}$ calculated from Zener's data⁽³²⁾ is shown in Table IX.

TABLE IX
Calculation of $C_{\alpha\gamma}$

$T \text{ } ^\circ\text{C}$	$T \text{ } ^\circ\text{K}$	$\Delta F/RT$	$C_{\alpha\gamma}$ (atomic %)
100	373	-1.24	6.62×10^{-5}
200	473	-0.830	4.43×10^{-4}
300	573	-0.543	1.33×10^{-3}
400	673	-0.362	2.55×10^{-3}
500	773	-0.222	3.46×10^{-3}
600	873	-0.120	3.45×10^{-3}
700	973	-0.050	2.08×10^{-3}
800	1073	-0.0135	1.10×10^{-3}
910	1183	0	0

In order to put all concentrations in grams of carbon/unit volume, the following relations were used:

$$\text{weight percent C} = 21.5 \text{ atomic percent C} \quad (49)$$

and

$$\frac{\text{grams C}}{\text{cm}^3} = \left(\frac{\text{Wt. \% C}}{100} \right) \rho_x \text{ (g/cm}^3\text{)} \quad (50)$$

where ρ_x = density of the phase for the concentration in question. The densities used were

$$\begin{aligned} \rho_{\alpha\text{-Fe}} &= 7.87 \text{ g/cm}^3 \\ \rho_{\gamma\text{-Fe}} &= 8.22 \text{ g/cm}^3 \\ \rho_{\text{Fe}_3\text{C}} &= 7.74 \text{ g/cm}^3 \end{aligned}$$

The values of C_{cc} and C_{cy} calculated from (47) and (48) are given in Table X.

The value of α^2 calculated from the tabulated values of $(C_{cy} - C_{cc})$, and the values of C_0 and C_c are shown in Table XI.

The variation in α^2 with temperature is shown in Figure 69. Using the values of α^2 from Figure 69, the measured values of \bar{x}_c from Table VIII, and equation (46), we can calculate the value of $\frac{dx}{dt}$ for the iron-carbon alloys. The results are shown in Table XII.

It can be seen that the observed values of the growth rate are higher than the calculated values of $\dot{\bar{x}}$ by a factor of 10-100; however, reasonably good agreement exists between the calculated growth rates and the values of \dot{w} . This seems reasonable since the model is based on a plane front analysis and these are the conditions that exist at the sides of the

TABLE X

T° C	Values of C_{sc} and C_{sy}			
	C_{sy} (weight% C)	C_{sc} (weight% C)	C_{sy} (grams C/cm ³)	C_{sc} (grams C/cm ³)
100	1.42×10^{-3}	4.97×10^{-6}	1.12×10^{-4}	3.91×10^{-7}
200	9.55×10^{-3}	8.20×10^{-5}	7.50×10^{-4}	6.45×10^{-6}
300	2.87×10^{-2}	5.07×10^{-4}	2.25×10^{-3}	3.99×10^{-5}
400	5.50×10^{-2}	1.79×10^{-3}	4.32×10^{-3}	1.40×10^{-4}
500	7.43×10^{-2}	4.53×10^{-3}	5.85×10^{-3}	3.48×10^{-4}
600	7.40×10^{-2}	9.50×10^{-3}	5.82×10^{-3}	7.47×10^{-4}
700	4.48×10^{-2}	1.70×10^{-2}	3.50×10^{-3}	1.34×10^{-3}
800	2.37×10^{-2}	2.32×10^{-2}	1.86×10^{-3}	1.82×10^{-3}

TABLE XI
Calculated Values of α^2

<u>T° C</u>	<u>C_o</u> <u>(weight% C)</u>	<u>C_o</u> <u>(grams C/cm³)</u>	<u>C_c</u> <u>(grams C/cm³)</u>	<u>α^2</u>
100	0.96	0.079	0.517	3.34×10^{-3}
	1.16	0.095	0.517	2.88×10^{-3}
	1.43	0.117	0.517	2.46×10^{-3}
200	0.96	0.079	0.517	2.22×10^{-2}
	1.16	0.095	0.517	1.905×10^{-2}
	1.43	0.117	0.517	1.64×10^{-2}
300	0.96	0.079	0.517	6.70×10^{-2}
	1.16	0.095	0.517	5.72×10^{-2}
	1.43	0.117	0.517	4.92×10^{-2}
400	0.96	0.079	0.517	0.128
	1.16	0.095	0.517	0.109
	1.43	0.117	0.517	0.095

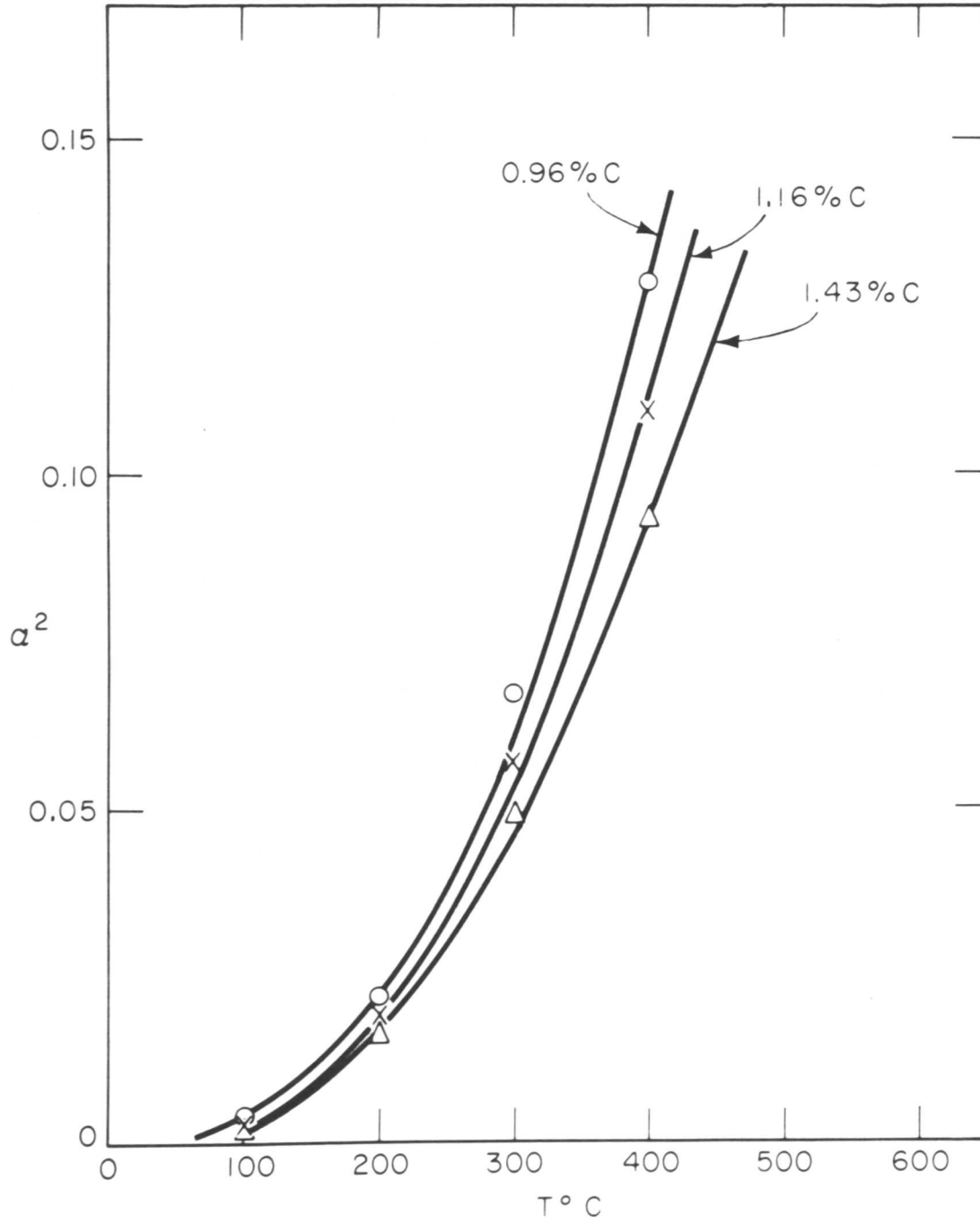


FIG. 69 - VARIATION OF α^2 WITH TEMPERATURE

TABLE XII

Values of $\frac{dx}{dt}$

T° C	C ₀ (weight% C)	e ²	\bar{x} (cm)	$\frac{dx}{dt}$ (calc.) $\frac{\text{mm}}{\text{min}}$	\dot{i} (obs.) $\frac{\text{mm}}{\text{min}}$	\dot{w} (obs.) $\frac{\text{mm}}{\text{min}}$
237° C	0.96% C	0.034	1.97×10^{-5}	5.21×10^{-5}	4.5×10^{-3}	2.8×10^{-6}
270° C	1.16% C	0.030	2.49×10^{-5}	1.17×10^{-4}	0.9×10^{-3}	7.3×10^{-6}
238° C	1.43% C	0.026	1.41×10^{-5}	6.24×10^{-5}	7.5×10^{-4}	6.2×10^{-5}

growing lens-shaped plate. The conditions at the tip are much more complex and it is not obvious how to modify equation (46) to make it applicable at the tip of the plate. The activation energy for growth from equation (46) is 20100 cal/mol if we assume that the temperature dependence of the values of α^2 and \bar{x}_c cancel each other. This does not agree very well with the values of Ω_f (14000 - 18000 cal/mol), but is in reasonable agreement with the values of Ω_w ($\Omega_f + 7600$ cal/mol).

The influence of carbon content on the growth rate can be predicted from the Fisher model since the values of α^2 and \bar{x}_c are the only terms in equation (46) which can be affected by a change in carbon content. Both the value of α^2 and \bar{x}_c decrease with increasing carbon content (see Table XII), however, the value of $\frac{\alpha^2}{\bar{x}_c}$ increases slightly with increasing carbon content and thus the growth rate should also increase with increasing carbon content. This is contrary to what is observed experimentally, since we find that the growth rate is markedly decreased by increasing carbon content (see Figure 41).

Both chromium and nickel decrease the growth rate markedly when added at a constant carbon level (see Figures 39 and 40). Since the addition of alloying elements does not seem to alter the value of \bar{x}_c (see Table VIII), they must affect either D_c^a or α^2 in the Fisher model. No information is available on the effect of alloying elements on D_c^a ; however, since they do not affect D_c^v , it seems reasonable to assume they have no

effect on D_c^0 . In this case the only effect of alloying elements on the growth rate would be their effect on the value of a^2 . Darken et al⁽⁵²⁾ have recently set up a growth model for pearlite which is very similar to the Fisher model for bainite. Their explanation of the influence of alloying elements on the pearlitic growth rate is that they lower the carbon activity gradient in the ferrite (i.e. they change the value of a^2). A similar explanation may be offered for the influence of alloying elements on the growth rate of bainite. Unfortunately, this problem cannot be treated quantitatively at present.

5.4 Modified Fisher Model

As stated in Section 2.7.4, the main drawback of the Fisher model is that it cannot explain the surface upheavals accompanying the formation of bainite. The Krisement-Wever model does this rather neatly by postulating that carbide precipitation in the austenite lowers the carbon content of the austenite until it becomes possible to form martensitic ferrite. Unfortunately, it is not clear that carbide precipitation in the austenite is actually occurring.

It is possible to modify the Fisher model to explain the surface upheavals by postulating, as do Krisement and Wever, that the carbon content of the austenite is lowered at the ferrite/austenite interface. This means that rather than assuming that $C_{\gamma a}$ is equal to C_0 , we postulate that $C_{\gamma a} < C_0$ and in fact is equal to C_Y^* , where C_Y^* is the carbon content of austenite that has an M_s equal to the temperature of

formation of the bainite plate. This lowering of the carbon content of the austenite can occur if carbon diffusion in the ferrite occurs so rapidly that the value of $C_{\alpha\gamma}$ (the carbon content of ferrite in equilibrium with austenite) cannot be maintained. In order to keep the activity of carbon the same in the austenite and ferrite, on either side of the ferrite/austenite interface, the carbon content of the austenite will be lowered by carbon diffusion through the ferrite to the existing carbide. Once the carbon content of the austenite has been lowered to the value of C_{γ}^* , a thin layer of martensite can form. This would explain the surface upheavals. The carbon inherited by the martensitic layer surrounding the bainite plate can diffuse rapidly out into the ferrite or precipitate as carbide. Once the carbon has been removed from this region, the carbon content of the austenite can again be lowered and the whole process repeated. Although this mechanism would involve the diffusion of carbon in austenite (as well as in ferrite), this diffusion may occur over such short distances that the diffusion of carbon in ferrite is still the controlling factor.

With the modified Fisher model, the influence of alloying elements on the growth of bainite assume a new role. The rate of removal of carbon from a small martensitic layer surrounding the plate should be independent of the carbon content of the original austenite since the carbon content of the martensitic layer (C_{γ}^*) is dependent only on temperature and not on the carbon content of the original austenite. Thus the influence

of carbon content on the growth rate can only be explained by the longer time required to lower the value of C_o to C_Y^* for the higher carbon contents. However, if this is true, it is not clear why there should not be a marked acceleration in the growth rate at temperatures just above M_s where

$$C_Y^* = C_o.$$

The influence of alloying elements on the bainitic growth rate in the modified Fisher model can be explained by their influence on the activity gradient of carbon in the ferrite and in addition by their influence on the value of C_Y^* . Since, the addition of alloying elements in general lower the M_s , they will raise the value of C_Y^* . As stated in the discussion of the Fisher Model it is not possible at present to explain the effects of alloying elements quantitatively.

Tsuya⁽²⁰⁾ in Japan has recently studied the heights of the surface upheavals accompanying the formation of bainite as a function of temperature. His results for a 0.47 percent carbon and 0.72 percent carbon nickel-chromium-molybdenum steels are shown in Figure 70. It can be seen that the height of the surface upheavals fall progressively with temperature, with a smooth transition from martensite to pearlite. These results can be explained by the modified Fisher model since according to this model C_Y^* decreases with increasing temperature and it would be expected that the height of a surface upheaval would decrease with decreasing carbon content of the martensite layer. It should be

noted that the heights of the surface upheavals in Figure 70 are independent of the carbon content of the steel. This will be true since the value of C_y^* is independent of the carbon content of the steel. It is interesting to note that Tsuya^(18, 19) has also studied the rate of growth of bainite plates in a forging die steel (0.76 percent carbon, 2.16 percent nickel, 1.14 percent chromium, 0.24 percent molybdenum). He found, as in this work, that the plates grew at a constant rate and the activation energy for growth he reports is 19000 cal/mol. His results are shown in Figures 71a and 71b.

5.5 Electron Diffraction and Electron Microscopy

The results of the electron microscope work are in essential agreement with other work of this nature^(9, 10, 11, 12). The coarseness of the carbide is found to increase with temperature, with a tendency for the carbides to line up along the long axis of the bainite region at higher temperatures. The carbides at both low and high temperatures are surrounded by a ferrite sheath and in no case is carbide precipitation observed to occur within the austenite.

The electron diffraction results are somewhat inconclusive due to the inability to fit all the observed lines to any one carbide structure. However, at temperatures below 260° C, the number of lines and their d values agree roughly with what might be expected from the ϵ -carbide structure Jack⁽⁴⁰⁾ finds in the tempering of martensite at low temperatures. More work will have to be done with electron diffraction in order

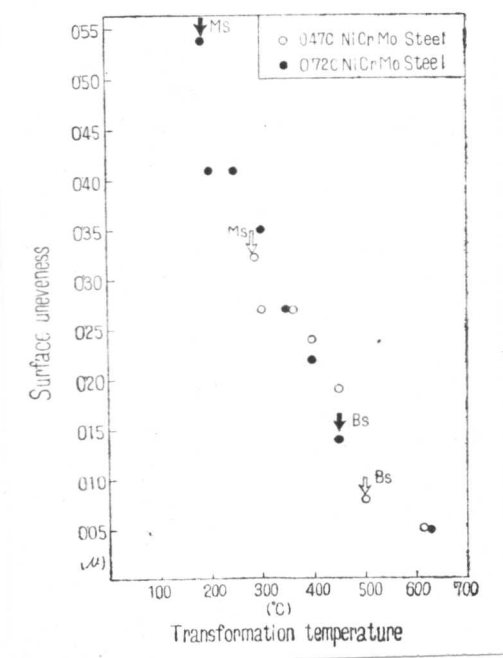


FIGURE 70. Height of the Surface Upheavals Versus Transformation Temperature after Tsuya (20).

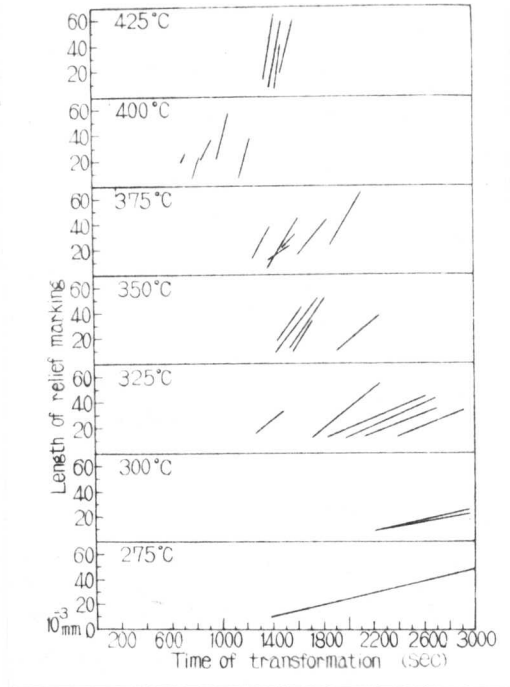
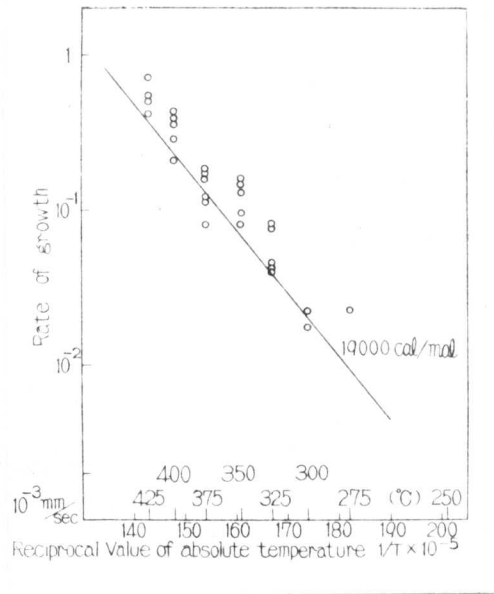


FIGURE 71. (a) Length of relief markings versus time for a 0.76% C Ni-Cr-Mo die steel from Tsuya(19).



(b) Log growth rate versus $\frac{1}{T}$ plot for growth rates given in Figure 71(a) after Tsuya (19).

to more fully clarify the nature of the carbides formed in bainitic structures.

5.6 Summary

It has been shown that at lower temperatures, where the bainite plates have a lenticular shape, two characteristic growth rates exist, one growth rate for the width and one for the length. From these two growth rates it is possible to calculate volume growth rates. At higher temperatures a single growth rate is adequate to explain the rate of growth of the bainite regions.

The experimental data has been compared to the growth theories of Krisement-Wever and of Fisher. The predictions of Krisement-Wever concerning the variation of the activation energy for surface displacement with carbon content and the value of the overall activation energies are not confirmed. The calculated values of the growth rate from the Fisher growth model agree fairly well with the observed width growth rates but not with the length growth rates.

A modified Fisher growth model has been presented which assumes a lowering of the carbon content of the austenite adjacent to the ferrite/austenite interface to allow for the formation of the bainitic ferrite in a martensitic fashion and account for the surface upheavals accompanying the formation of bainite. At present it is not possible to quantitatively compare this model with the experimental data. It is

this martensite-type formation of the ferrite phase of bainite which differentiates bainite from pearlite. The ferrite phase in pearlite is formed by the normal diffusion-controlled growth mechanism and results in no surface upheavals.

6. CONCLUSIONS

1. Bainite plates grow slowly at a constant rate which is temperature dependent. This temperature dependence of the growth rate can be expressed by the equation:

$$\dot{l} = B \exp(-Q_1/RT)$$

where Q_1 has a value between 14000 and 18000 cal/mol.

2. At lower temperatures where the bainite plate has a lenticular shape, there are two characteristic growth rates, one for the length and one for the width. The width growth rate is given approximately by the equation:

$$\dot{w} = 137 B \exp\left(-\frac{Q_1 + 7680}{RT}\right)$$

3. The bainitic growth rate is decreased by increasing the carbon content in iron-carbon alloys. Chromium and nickel additions at a constant carbon level of 1.2 percent carbon also decrease the growth rate.

4. The predictions of the Krisement-Wever theory concerning the variation of the activation energy for surface displacement with carbon content and for the value of the overall activation energy are not confirmed.

5. The calculated growth rates from the Fisher model agree with the observed width growth rates. The length growth rates are greater than the calculated values by a factor of 10 - 100.

6. The Fisher growth model can be modified by assuming that the carbon content of the austenite is lowered adjacent to the ferrite/austenite interface to account for the surface upheavals accompanying the formation of bainite.

7. Examination of bainitic structures with the electron microscope shows no evidence for the precipitation of carbide within the austenite. The coarseness of the carbide phase increases with increasing temperature and at all times the carbides are surrounded by a ferrite sheath.

8. The results of the electron diffraction work indicate the possibility of the formation of ϵ -carbide in bainite structures formed at low temperatures.

7. SUGGESTIONS FOR FUTURE WORK

1. The modified Fisher growth model should be set up in a quantitative fashion so that it can be compared with the present experimental data.

2. A more intensive electron diffraction investigation should be made of the bainite structures formed at low temperatures in order to more fully clarify the nature of the carbide phase forming in these structures.

3. A thorough study of the c/a ratio of the ferrite phase in bainite should be made using the technique of Kurdjumov and Lyssak, in order to settle the question of the carbon content of the ferrite. Both alloy and plain carbon steels should be studied in order to check the results of Kurdjumov.

4. The lattice parameter of the austenite should be studied to determine the carbon content of the austenite, as a function of the holding time in the bainite range. Low, medium, and high-carbon steels should be studied to check the work of Entin in Russia. At the same time, the microstructures should be examined to see if the reported change of carbon content of the austenite is due solely to the bainite reaction or due to complicating side reactions such as the separate formation of carbide in the bainite range.

BIBLIOGRAPHY

1. E. S. Davenport and E. C. Bain: "The Transformation of Austenite at Constant Sub-Critical Temperatures," *Trans. AIME* 90 (1930) 117.
2. T. Ko and S. A. Cottrell: "The Formation of Bainite," *J. of the Iron and Steel Institute* 172 (1952) 307.
3. V. G. Paranjpe and D. D. Kaushal: "Bainite Reaction in Steels," *Trans. Indian Inst. of Metals* 5 (1951) 147.
4. R. E. Hehemann and A. R. Troiano: "The Bainite Transformation," *Metal Progress* 70 (1956) 97.
5. L. Habraken: *Essai de synthese sur la transformation bainitique des aciers*, "Travaux du Centre National de Recherches Metallurgiques No. 19 (November 1957).
6. A. B. Greninger and A. R. Troiano: "Crystallography of the Austenite Decomposition," *Trans. AIME* 140 (1940) 307.
7. G. V. Smith and R. F. Mehl: "Lattice Relationships in Decomposition of Austenite to Pearlite, Bainite, and Martensite," *Trans. AIME* 150 (1942) 211.
8. A. Hultgren et al: "Isothermal Transformation of Austenite and Partitioning of Alloying Elements in Low-Alloy Steels," *Kungl. Svenska Vetenskapsakademiens Handlingen Band 4, No. 3* (1953).
9. "Electron Microstructure of Steel," *Proc. ASTM* 50 (1950) 444.
10. "Electron Microstructure of Steel," *Proc. ASTM* 52 (1952) 543.

11. D. Lister: "An Electron Microscope Study of Bainite Formation,"
M.S. Thesis MIT (August 1955).
12. H. Modin and S. Modin: "Pearlite and Bainite Structures in a
Eutectoid Plain-Carbon Steel, an Electron Microscope Investigation,"
Avtryck ur Jernkontorets Annaler 137 (1955) 481.
13. S. M. Kaufman, G. M. Pound and H. I. Aaronson: "Nucleation Sites
of Bainitic Carbides in Alloy Steels," Trans. AIME 209 (1957) 855.
14. T. Lyman and A. R. Troiano: "Influence of Carbon Content upon the
Transformation in 3% Chromium Steels," Trans. ASM 37 (1946) 402.
15. E. P. Klier and T. Lyman: "The Bainite Reaction in Hypo-Eutectoid
Steels," Trans. AIME 158 (1944) 394.
16. A. E. Austin and C. M. Schwartz: "Electron Diffraction Studies of
Iron Carbides in Bainite and Tempered Martensite," Trans. ASTM
52 (1953) 592.
17. G. Lagerberg and B. S. Loment: Morphological and Phase Changes
during Quench-Aging of Ferrite Containing Carbon and Nitrogen,"
to be published (1958).
18. Kazuo Tsuya: "Observations of Bainite Transformation by Hot-
Stage Microscope," J. of Mech. Eng. Lab of Japan 1 (1955) No. 1.
19. Kazuo Tsuya and Tetsutaro Mitsuhashi: "The Surface Relief Effect
due to Bainite Transformation Observed by Hot-Stage Microscope,"
J. of Mech. Eng. Lab. of Japan 1 (1955) No. 2.
20. Kazuo Tsuya: "On the Characteristics of the Bainite Transformation,"
J. Mech. Eng. Lab. of Japan 2 (1956) No. 1.

21. L. M. Pevzner, G. M. Rovenskii and T. D. Kubyshkiva: "Redistribution of Carbon during Transformation in Bainite Range," *Doklady Akademii Nauk SSSR* 85 (1952) No. 4 (Brutcher Translation No. 2976).
22. F. E. Weraer, B. L. Averbach and M. Cohen: "Matrix Phase in Lower Bainite and Tempered Martensite," *Journal of Metals* (Oct. 1956) 1484.
23. R. I. Eatin: "On the Intermediate Transformation of Austenite," *Doklady Akademii Nauk SSSR* 79 (1951) 973.
24. C. Zener: "Kinetics of the Decomposition of Austenite," *Trans. AIME* 167 (1946) 550.
25. R. F. Hehemann and A. R. Troiano: "Stabilization of the Bainite Reaction," *Trans. AIME* 200 (1954) 1272.
26. S. Bhattacharyya and G. L. Kehl: "Isothermal Transformation of Austenite under Externally Applied Stress," *Trans. ASM* 47 (1955) 351.
27. A. Hultgren: "Isothermal Transformation of Austenite," *Trans. ASM* 39 (1947) 915.
28. J. C. Fisher: "Eutectoid Decompositions," *Thermodynamics in Physical Metallurgy* ASM (1949) 201.
29. O. Krisement and F. Wever: "Kalorimetrische Untersuchung einer Zwischenstufen Umwandlung," *Archiv. für das Eisenhüttenwesen* 25 (1954) 489.

30. O. Krisement and F. Wever: "The Bainite Reaction in High-Carbon Steels," Mechanism of Phase Transformations in Solids, Institute of Metals (1955) 253.
31. O. Krisement: "Wachstum Gesetz Geboppelter Auscheidungen," Archiv. für Eisenhüttenwesen 26 (1955) 55.
32. C. Zener: "Equilibrium Relations in Medium Alloy Steels," Trans. AIME 167 (1946) 513.
33. G. Kurdjumov and L. Lyssak: "The Application of Single Crystals to the Study of Tempered Martensite," J. Iron and Steel Inst. 156 (1947) 29.
34. C. S. Roberts, B. L. Averbach and M. Cohen, "The Mechanism and Kinetics of the First Stage of Tempering," Trans. ASM 45 (1953) 576.
35. G. L. Kehl: "Optical Microscopy," Modern Research Techniques in Physical Metallurgy ASM (1953) 1.
36. Unitron Instrument Division of United Scientific Company, Boston, Massachusetts.
37. H. Saller, R. F. Dickerson and R. J. Carlsson: "A Microscope Hot Stage," Metal Progress (May 1955) 105.
38. L. I. Kogan and P. I. Entin: "Concerning the Intermediate Transformation in Austenite," Izvestia Akad. Nauk, SSSR 'Otdel' tekhn. nauk No. 1 (1955).

39. L. I. Kogan and P. I. Entin: "The Redistribution of Carbon during the Transformation of Austenite in the Middle Temperature Range," *Doklady Akademii Nauk SSSR IV* (1957) 360.
40. K. H. Jack: "Structural Transformations in the Tempering of High-Carbon Martensitic Steels," *J. Iron and Steel Inst.* 169 (1951) 26.
41. G. V. Kurdjumov and M. D. Perkas: "About the Mechanism of the Decomposition of Austenite in the Intermediate Region of Temperatures," *Problemy Metall Ovedeniia i fiziki metallov* 2 (1951) 430.
42. Private communication to M. Cohen from G. V. Kurdjumov (1957).
43. R. T. Howard and M. Cohen: "Austenite Transformation above and within the Martensite Range," *Trans. AIME* 176 (1948) 384.
44. A. B. Grenlager: "The Martensite Thermal Arrest in Iron-Carbon Alloys and Plain Carbon Steels," *Trans. ASM* 30 (1942) 1.
45. P. Payson and C. H. Savage: "Martensite Reactions in Alloy Steels," *Trans. ASM* 33 (1944) 261.
46. F. E. Werner, "The Ferrite Phase in Bainite," *Two Weeks Problem MIT* (1955).
47. C. Wells, W. Bats and R. F. Mehl: "Diffusion Coefficient of Carbon in Austenite," *Trans. AIME* 188 (1950) 553.
48. S. A. Kulin and M. Cohen: "On the Martensitic Transformation at

Temperatures Approaching Absolute Zero," Trans. AIME 188
(1950) 1139.

49. S. V. Radcliffe: "Isothermal Transformation Characteristics of High-Purity Iron-Carbon Alloys," Ph. D. Thesis, University of Liverpool (1956).
50. C. A. Wert: "Diffusion Coefficient of Carbon in Alpha Iron," Physical Review 79 (1950) 601.
51. C. A. Wert: "Solid Solubility of Cementite in Alpha Iron," Trans. AIME 188 (1950) 1242.
52. L. Darken, R. M. Fisher, and J. M. Galligan: "The Growth of Pearlite," Paper presented at the Second World Metallurgical Conference (1957).

BIOGRAPHICAL SKETCH

The author was born in Chicago, Illinois on December 17, 1928. He attended public schools there, and received the B.S. degree from Illinois Institute of Technology in June 1950. In June 1951, he received the M.S. degree from the University of Wisconsin. From 1951 - 1952 he was employed by the Westinghouse Electric Corporation, and in September 1952 he entered M.I.T. as a graduate student. The author left M.I.T. and entered the U. S. Army in April 1953. He was stationed at the Watertown Arsenal, Watertown, Massachusetts from September 1953 to February 1955. In 1955, the author returned to M.I.T. as a research assistant in the Department of Metallurgy and in September 1955 was appointed the Union Carbide Fellow.